Study on the higher-order structure of DNA and gene expression

by

Takashi Nishio

Doshisha University

Graduate School of Life and Medical Sciences

November 2021

Doshisha University

Graduate School of Life and Medical Sciences

Abstract

Study on the higher-order structure of DNA and gene expression

by Takashi Nishio

SUPERVISOR: Professor Yohei Oe

In living cells, large DNA molecules of up to several centimeters in length are packed into a confined space and exhibit a hierarchical higher-order structure. It is well known that such genomic DNA drastically changes its conformation throughout the cell cycle. Therefore, changes in the conformation of large DNA expected to play an essential role in the regulation of gene expression.

The persistence length of DNA is 150-200 bp, corresponding to about 50 nm. This means that long and short DNA have drastically different conformational behavior, and thus it is important to study the behavior and biological function of long DNA above the order of 10-100 kbp to clarify the essential role of genomic DNA in living cells.

This study sheds light on the relation between higher-order structure and gene function by adopting single-DNA molecule observation. A cell-free gene expression experiment revealed that polyamines exert biphasic effects, enhancement and inhibition, on gene expression depending on their concentrations. Furthermore, these biphasic effects were strongly correlated with the changes in the higher-order structure of DNA induced by polyamines. At a lower concentration of polyamine, gene expression was enhanced and DNA molecules took a loosely packed flower-like structure. On the other hand, at a higher concentration of polyamine, gene expression was completely inhibited and DNA molecules were tightly packed.

I also investigated the dependence of the activity of gene expression on DNA length by adopting a cell-free gene expression system with DNAs encoding the firefly luciferase gene. The results showed that longer DNA molecules exhibit significantly greater gene expression. Single-DNA molecule observation by atomic force microscopy (AFM) clarified that longer DNA takes a shrunken conformation with a higher segment density in the reaction mixture for gene

expression, in contrast to the stiff conformation of shorter DNA. Even here, it was clear that a shrunken conformation of DNA enhances gene expression activity. This thesis presents a mechanism for the favorable effect of longer DNA on gene expression in terms of an increase in the access of RNA polymerase to the shrunken conformation.

I also investigated the temperature-dependence of the change in the higher-order structure of DNA induced by polyamine. The branched-chain polyamine found in the hyperthermophilic archaeon *Thermococcus kodakarensis* induces a unique nano-loop structure for DNA at 80°C. This nano-loop structure was not caused in the presence of another linear-chain polyamine and it is assumed that this unique higher-order structure of DNA plays an important role in maintaining gene function near the boiling temperature, where this hyper-thermophilic archaeon lives. To clarify the mechanism by which linear- and branched-chain polyamines induced markedly different higher-order structures for DNA, a Monte Carlo simulation was performed. Based on this theoretical consideration, the difference between the effects of linear and branched-chain polyamines will be discussed in terms of electrostatic interaction against to the DNA phosphate group.

Publications

This thesis is based on the following original papers.

[i] **T. Nishio**, Y. Yoshikawa, W. Fukuda, N. Umezawa, T. Higuchi, S. Fujiwara, T. Imanaka, K. Yoshikawa, "Branched-Chain Polyamine Found in Hyperthermophiles Induces Unique Temperature-Dependent Structural Changes in Genome-Size DNA", *ChemPhysChem*, **19**, 2299-2304 (2018).

[ii] Y. Kashiwagi, **T. Nishio**, M. Ichikawa, C-Y. Shew, N. Umezawa, T. Higuchi, K. Sadakane, Y. Yoshikawa, K. Yoshikawa, "Repulsive/attractive interaction among compact DNA molecules as judged through laser trapping: difference between linear- and branched-chain polyamines", *Colloid and Polymer Sci.*, **297**, 397-407 (2018).

[iii] **T. Nishio**, Y. Yoshikawa, C-Y. Shew, N. Umezawa, T. Higuchi, K. Yoshikawa, "Specific effects of antitumor active norspermidine on the structure and function of DNA", *Sci. Rep.*, **9**, 14971/1–12 (2019).

[iv] **T. Nishio**, K. Sugino, Y. Yoshikawa, M. Matsumoto, Y. Oe, K. Sadakane, K. Yoshikawa, "K^+ promotes the favorable effect of polyamine on gene expression better than Na^+", *PLOS ONE.*, **15**, e0238447/1–13 (2020).

[v] **T. Nishio**, Y. Yoshikawa, K. Yoshikawa, S. Sato, "Longer DNA exhibits greater potential for cell-free gene expression", *Sci. Rep.*, **11**, 11739/1–7 (2021).

Acknowledgments

First and foremost, I would like to express my deepest appreciation to my supervisor, Professor Yohei Oe for his invaluable advice and continuous support during my PhD study.

I would also like to extend my deepest gratitude to Associate Professor Shin-ichi Sato and Associate Professor Koichiro Sadakane served as vice examiner in my thesis committee.

I am deeply indebted to Professor Kenichi Yoshikawa and Dr. Yuko Yoshikawa. Their immense knowledge and plentiful experience have encouraged me in all the time of my academic research and daily life.

My sincere thanks also go to Professor Takahiro Kenmotsu for his thoughtful guidance.

I would also like to express my gratitude to all other collaborators for their constructive suggestions and discussion.

Professor Tsunehiko Higuchi from Nagoya City University.

Associate Professor Naoki Umezawa from Nagoya City University.

Professor Chwen-Yang Shew from NewYork City University.

Professor Tadayuki Imanaka from Ritsumeikan University.

Professor Shinsuke Fujiwara from Kwansei Gakuin University.

Professor Michiaki Matsumoto from Doshisha University.

Dr. Wakao Fukuda from Kwansei Gakuin University.

Dr. Masatoshi Ichikawa from Kyoto University.

Dr. Jose Maria Carnerero from Sevilla University.

Mr. Yusuke Kashiwagi

Mr. Kaito Sugino

Mr. Tomoki Kitagawa.

I also wish to thank Ms. Makiko Furumoto, Dr. Satoshi Takatori, Dr. Yue Ma, Dr. Hiroki Sakuta, Dr. Hiroshi Ueno, Ms. Hikari Baba and all other laboratory members. They encouraged and supported me in my lab life.

I deeply thank my parents and sister for their unconditional trust, timely encouragement, and endless patience.

Finally, I thank with love to my wife, Maria. I could not get through this agonizing period without her understanding, love, encouragement.

Table of Contents

List of Figures

on right are the lowest energy conformations for linear polyamine (left), 3334, and branched polyamine (right), 3(3)(3)4, respectively, which were obtained from the energy minimization, and all methyl, methylene and ammonium groups are then coarse-grained into beads of the same radius. Blue beads denote nitrogen atoms, and gray beads denote carbon atoms. Note that the scale bar denotes 0.15 nm, the average bond length between two neighboring atoms in a polyamine. These beads interacting with phosphate charged spheres through screened Coulomb potential if their separation is above 0.31 nm (cf.: Eq. (1)). Below this distance, the potential becomes infinity. These beads are allowed to penetrate the soft DNA cylinder to mimic the space in DNA major and minor grooves. (b) Plot of the reduced charge density distribution along the radius direction (r) for linear (circles) and branched polyamine (squares) when Γ = 1.02 nm (solid symbols) and 1.70 nm (open symbols). Lines are for eye guide, and the error bars are smaller than the symbols. (c) Typical snapshots for linear polyamine and branched polyamine interacting with DNA when Γ = 1.7 nm. Note that blue beads denote ammonium groups, and white beads denote methyl and methylene groups. (d) Plot of the average surface potential Φ_{surf} with Γ in the presence of linear (circles) polyamine and branched (square) polyamine, and in the absence of polyamine (diamond with dashed line). The error bars are smaller than the size of symbols. Lines are for eye guide.·····78

List of Tables

Chapter 1

General Introduction

A DNA molecule consists of two polynucleotide chains that form a double-helix structure [1,2]. Moreover, each nucleotide is composed of one of four kinds of nitrogen-containing bases (cytosine, guanine, adenine, and thymine), a five-carbon sugar called deoxyribose and a phosphate group. The nucleotide sequence is important, since it encodes genetic information to express the appropriate amino acids through transcription and translation. However, cells in organisms can exhibit various structures and functions even though they have the same genome sequence. Therefore, in the field of life science, it is believed that it is important to study gene regulation that is independent of nucleotide sequences to clarify the underlying mechanisms of, for example, canceration, cell differentiation and so on.

Living cells contain large DNA molecules up to several centimeters long which drastically change their conformation depending on their cellular environment. Therefore, it is considered that there is an important relationship between the higher-order structure of DNA and its biological functions. Since DNA has physico-chemical properties as a semi-flexible polymer and polyelectrolyte, a higher-order structure appears only in DNA that is larger than several kbp in size. In this study, I focused on this structural feature of DNA by adopting single-DNA molecular observation and investigated the relationship between the higher-order structure of DNA and its gene function.

Polyamines are small polycationic organic molecules that are found in all living organisms [3-5]. They are involved in many biological functions. For example, polyamines are important in cell proliferation and differentiation, apoptosis, protection from oxidative damage and gene regulation [6-12]. Because of their cationic nature, they can interact with negatively charged macromolecules such as DNA, RNA, and proteins, thereby affecting the structure and function of these macromolecules. It is well known that polyamines induce DNA compaction/condensation [13-19]. Chapter 2 compares the effects of trivalent polyamines, spermidine (SPD) and norspermidine (NSPD), which is a structural homologue of SPD and has antitumor activity, on the structure of DNA and gene expression. Furthermore, Chapter 3 describes a study on the interaction of polyamines with DNA in the presence of alkali metal ion.

Gene expression in living cells is strictly self-regulated to ensure that the correct amounts of proteins are made at the most appropriate times and locations for maintaining cellular homeostasis.

Gene regulation can occur at any point in gene expression, from the start of the transcription phase to the translation phase. Chapters 2 and 3 focus on the change in the higher-order structure of DNA caused by cationic compounds and its effects on cell-free gene expression. On the other hand, Chapter 4 evaluates the efficiency of protein translation, focusing on the effect of the length of DNA templates on cell-free protein synthesis.

Chapters 5 and 6 describe a further study on the change in the higher-order structure of genome-size DNA. Recently, it was reported that a hyperthermophilic archaeon microorganism, *Thermococcus kodakarensis*, synthesizes the unique branched-chain polyamine N^4-bis(aminopropyl)spermidine 3(3)(3)4, which has not been found in other microorganisms [20,21]. *T. kodakarensis* grows at temperatures between 60 and 100°C, with an optimum growth temperature of 85°C [22]. Interestingly, synthesis of the branched-chain polyamine 3(3)(3)4 increases with an increase in the growth temperature [20]. Therefore, this branched-chain polyamine may be a key molecule for survival in high-temperature environments [20]. Thus, Chapter 5 examines the temperature-dependent effect of a pentavalent branched-chain polyamine, 3(3)(3)4, on the DNA structure. Chapter 6 describes an advanced experiment using optical manipulation to clarify the differences in the physico-chemical properties of compacted DNA induced by linear- and branched-chain polyamine. In addition, Chapter 6 also presents theoretical considerations based on a Monte Carlo simulation.

Chapter 7 summarizes the studies in this thesis and provides a perspective for further research.

References

[1] R. E. Franklin & R. G. Gosling. Molecular configuration in sodium thymonucleate. *Nature* **171**, 740-741, (1953).

[2] J. D. Watson & F. H. Crick. Molecular structure of nucleic acids: a structure for deoxyribose nucleic acid. *Nature* **171**, 737-738, (1953).

[3] C. W. Tabor & H. Tabor. Polyamines. *Annual Review of Biochemistry* **53**, 749-790, (1984).

[4] L. Miller-Fleming, V. Olin-Sandoval, K. Campbell & M. Ralser. Remaining Mysteries of Molecular Biology: The Role of Polyamines in the Cell. *J. Mol. Biol.* **427**, 3389-3406, (2015).

[5] *Polyamines* (eds R. Alcázar & A. F. Tiburcio), in *Methods in Molecular Biology* **1694**, (Humana Press, 2018).

[6] M. Saminathan, T. Thomas, A. Shirahata, C. K. Pillai & T. J. Thomas. Polyamine structural effects on the induction and stabilization of liquid crystalline DNA: potential applications to DNA packaging, gene therapy and polyamine therapeutics. *Nucleic Acids Res.* **30**, 3722-3731, (2002).

[7] A. C. Childs, D. J. Mehta & E. W. Gerner. Polyamine-dependent gene expression. *Cell. Mol. Life Sci.* **60**, 1394-1406, (2003).

[8] S. Mandal, A. Mandal, H. E. Johansson, A. V. Orjalo & M. H. Park. Depletion of cellular polyamines, spermidine and spermine, causes a total arrest in translation and growth in mammalian cells. *Proc. Natl. Acad. Sci. U. S. A.* **110**, 2169-2174, (2013).

[9] A. J. Michael. Polyamines in Eukaryotes, Bacteria, and Archaea. *J. Biol. Chem.* **291**, 14896-14903, (2016).

[10] T. J. Thomas, H. A. Tajmir-Riahi & T. Thomas. Polyamine-DNA interactions and development of gene delivery vehicles. *Amino Acids* **48**, 2423-2431, (2016).

[11] A. O. Gevrekci. The roles of polyamines in microorganisms. *World J. Microbiol. Biotechnol.* **33**, 204/1-7, (2017).

[12] A. J. Michael. Polyamine function in archaea and bacteria. *J. Biol. Chem.*, (2018).

[13] L. C. Gosule & J. A. Schellman. Compact form of DNA induced by spermidine. *Nature* **259**, 333-335, (1976).

[14] D. K. Chattoraj, L. C. Gosule & A. Schellman. DNA condensation with polyamines. II. Electron microscopic studies. *J. Mol. Biol.* **121**, 327-337, (1978).

[15] P. G. Arscott, A. Z. Li & V. A. Bloomfield. Condensation of DNA by trivalent cations. 1. Effects of DNA length and topology on the size and shape of condensed particles. *Biopolymers* **30**, 619-630, (1990).

[16] V. A. Bloomfield. Condensation of DNA by multivalent cations: considerations on mechanism. *Biopolymers* **31**, 1471-1481, (1991).

[17] V. A. Bloomfield. DNA condensation. *Curr. Opin. Struct. Biol.* **6**, 334-341, (1996).

[18] K. Yoshikawa & Y. Yoshikawa. Compaction and condensation of DNA. *Pharmaceutical perspectives of nucleic acid-based therapeutics* (eds R. I. Mahato & S. W. Kim) Chapter 8, 137-163 (CRC Press, 2002).

[19] Y. Yoshikawa *et al.* Critical behavior of megabase-size DNA toward the transition into a compact state. *J. Chem. Phys.* **135**, 225101/1-7, (2011).

[20] K. Okada *et al.* Identification of a novel aminopropyltransferase involved in the synthesis of branched-chain polyamines in hyperthermophiles. *J. Bacteriol.* **196**, 1866-1876, (2014).

[21] R. Hidese *et al.* Identification of a novel acetylated form of branched-chain polyamine from a hyperthermophilic archaeon Thermococcus kodakarensis. *Biosci., Biotechnol., Biochem.* **81**, 1845-1849, (2017).

[22] H. Atomi, T. Fukui, T. Kanai, M. Morikawa & T. Imanaka. Description of Thermococcus kodakaraensis sp. nov., a well studied hyperthermophilic archaeon previously reported as Pyrococcus sp. KOD1. *Archaea* **1**, 263-267, (2004).

Chapter 2

Specific effects of antitumor active norspermidine on the structure and function of DNA [iii]

2.1 Introduction

Polyamines are small polycationic organic molecules that are found in all living organisms [1-3]. Intracellular concentrations of polyamines reach millimolar levels [4]. It has been shown that polyamine synthesis increases in actively proliferating cells and tumor cells [5-7]. Polyamines are involved in many biological functions. For example, polyamines are important in cell proliferation and differentiation, apoptosis, protection from oxidative damage and gene regulation [8-14]. Because of their cationic nature, they can interact with negatively charged macromolecules such as DNA, RNA and proteins, thereby affecting the structure and function of these macromolecules. It is well known that polyamines induce DNA compaction/condensation [15-22]. Several *in vitro* studies have investigated the physical process of DNA packaging and the physicochemical and biological properties of compacted DNA [23-28]. Regarding the potential to induce DNA compaction, it is well known that the valence of polyamines is critical [29,30]. The geometric arrangement of amine groups as well as chirality are also important factors in the ability to induce DNA compaction [31]. Atomic force microscopy (AFM) studies have revealed different morphologies of DNA depending on a polyamine concentration and structure [27,32,33]. The changes in DNA conformation caused by polyamines could be related to genetic activity [34-37]. Recently, it was found that polyamines exert biphasic effects, enhancement and inhibition, on gene expression depending on their concentrations [38]. AFM observations showed that the enhancement correlates with a flower-like conformation with parallel ordering of DNA segments. On the other hand, the complete inhibition is caused by folding transition onto a tightly packed DNA conformation.

In this study, we compared the effects of trivalent polyamines, spermidine (SPD) and norspermidine (NSPD), a structural homologue of SPD, on the structure of DNA and gene expression. NSPD has antitumor activity and is found in some species of plants, bacteria and algae, but not in humans [3,39-46]. Although it has been argued that such antitumor activity is due to competition with natural polyamines for cellular uptake and accumulation [41,47], the

difference in their direct effects on DNA is still unclear. We also performed a theoretical study using a Monte Carlo simulation on the underlying mechanism of the different nature of interaction between SPD and NSPD on double-stranded DNA.

2.2 Experimental Results

2.2.1 Activity of Gene Expression

The effects of SPD and NSPD on the activity of gene expression were evaluated through an *in vitro* cell-free luciferase assay. Figure 2.1 shows the relative luminescence intensity as a marker of gene expression activity at various polyamine concentrations, where the intensity is normalized to the control (= 1), i.e., in the absence of polyamine. The results showed that both polyamines have a biphasic effect, enhancement and inhibition, on gene expression depending on their concentrations. The gene activity increased with an increase in the SPD concentration and reached a maximum at around 0.3 mM. As the SPD concentration increased further, the activity gradually decreased and was completely inhibited above 2 mM of SPD. Biphasic effect was also observed with NSPD: the activity reached a maximum at 0.1 mM and complete inhibition was observed above 0.5 mM. It is noted that the maximum level of gene activity with SPD was significantly higher, ca. 5-fold, than that with NSPD.

2.2.2 Higher-order structure of DNA

To clarify whether the above difference in gene expression is due to the effects of polyamines on the higher-order structure of DNA, we investigated polyamine-induced changes in the structure of DNA by AFM and fluorescence microscopy (FM). Figure 2.2 shows typical AFM images of plasmid DNA (4,331 bp) in the presence of SPD or NSPD. At 0.1 mM SPD or NSPD, DNA molecules were randomly dispersed (Fig. 2.2a,d). With an increase in the SPD concentration, a self-assembled flower-like structure appeared, where multiple loops crossed to form multiple nodal points (Fig. 2.2b). As the SPD concentration further increased, multiple DNA molecules formed a larger flower-like structure (Fig. 2.2c). Similar AFM observations of a flower-like structure with SPD were reported by Fan and Hoh [48]. On the other hand, in the presence of NSPD, the multimolecular loops tended to cross at a single point (Fig. 2.2e,f) and formed a smaller flower-like structure. These AFM observations imply that the difference by only one methylene group between SPD and NSPD leads DNA molecules to exhibit different conformations.

Next, we performed direct real-time monitoring of polyamine-induced changes in the conformation of DNA in aqueous solution by FM. Figure 2.3a,b shows representative FM images of thermally fluctuating T4 DNA molecules in the absence or presence of NSPD. Individual DNA

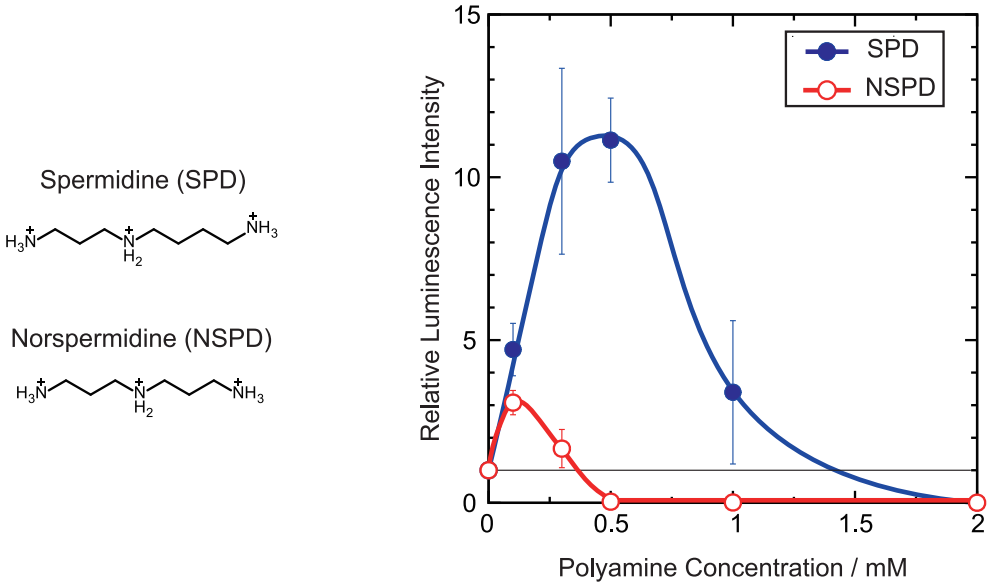

Figure 2.1 Efficiency of gene expression depending on the concentrations of SPD and NSPD. The longitudinal axis is the relative emission intensity of the luciferin-luciferase reaction. The DNA concentration was fixed at 0.3 μM.

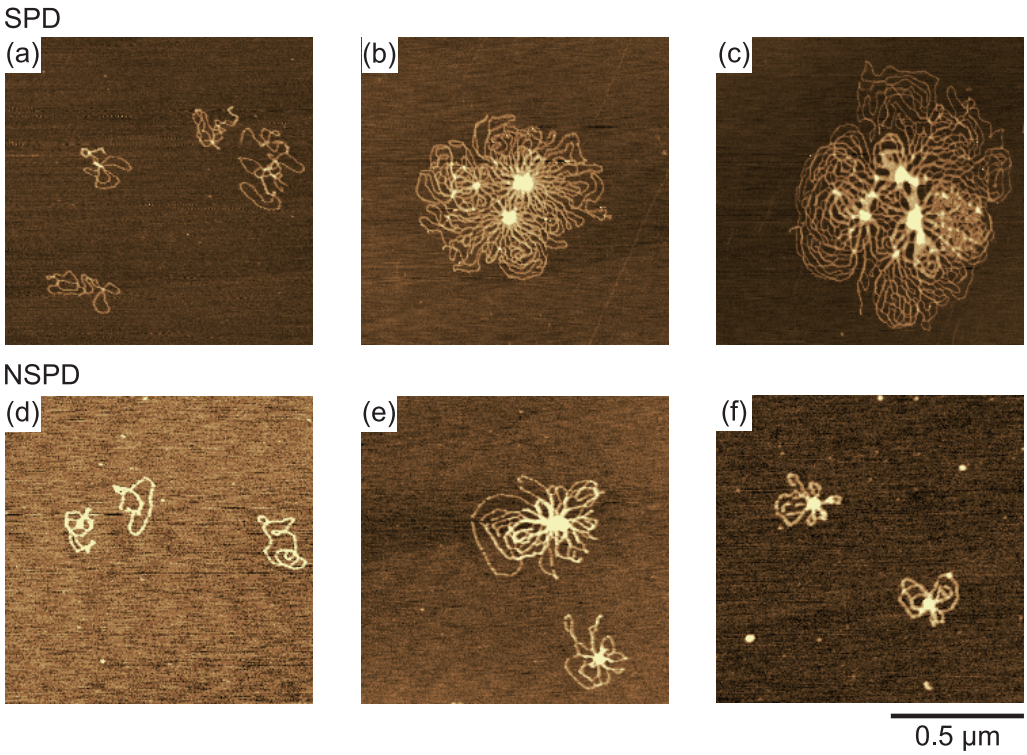

Figure 2.2 AFM images of plasmid DNA (4,331 bp) in the presence of SPD and NSPD. Polyamine concentrations were (a), (d) 0.1 mM, (b), (e) 0.5 mM, and (c), (f) 1 mM. The DNA concentration was 0.3 μM in nucleotide units.

molecules were observed as an elongated random coil and exhibited translational and intramolecular Brownian motion in aqueous solution (Fig. 2.3a). Upon the addition of NSPD to the DNA solution, individual DNA molecules exhibited a structural transition from a coil state to a compact globule state (Fig. 2.3b). Figure 2.3c shows histograms of the long-axis length L of DNA as a function of the concentration of polyamines together with an assignment of the conformational characteristics in FM images. Both NSPD and SPD caused shrinkage of DNA molecules with an increase in their concentrations. The potency for inducing DNA shrinkage was slightly greater for NSPD.

2.2.3 Evaluation of binding equilibrium by ^{1}H NMR

To evaluate the binding affinity of these polyamines for DNA, we performed ^{1}H NMR titration experiments using CT DNA. Figure 2.4 shows the ^{1}H NMR signals of SPD and NSPD in 10 mM Tris-DCl buffer (pD 7.5). The spectrum of SPD was composed of three resonances at around δ = 3.20-3.00, 2.15-2.00 and 1.85-1.70 ppm, and the spectrum of NSPD was composed of two at around δ = 3.20-3.00 and 2.15-2.00 ppm. Peak assignments are summarized in Fig. 2.4. DNA signals were not observed in the ^{1}H NMR spectra of mixtures of the polyamines and DNA because of the significant decrease in T_2, transverse relaxation time, for the protons on the high-molecular-weight CT DNA [49]. Upon addition of CT DNA, the intensity of the signals observed for SPD and NSPD generally decreased as the DNA concentration increased. This trend indicates that the DNA-bound fraction of polyamines is not detectable in the ^{1}H NMR spectrum. In the case of SPD, the chemical shift and the widths of the signals remained essentially constant, similar to our previous results with chiral spermine analogs [31].

Based on the experimental data on the change in ^{1}H NMR signal intensity, we evaluated the binding equilibrium constant of polyamines to DNA. The longitudinal axis in Fig. 2.5 shows the inverse of the ^{1}H NMR intensity evaluated by integration of the observed signals. All of the ^{1}H signals are well-separated, as shown in Fig. 2.4. Thus, the signal intensities in Fig. 2.5 were calculated based on the summation of all of the integrated values for the spectra of SPD and NSPD. The right panel in Fig. 2.5 also shows each binding equilibrium constant, K, evaluated from the slope of the graph. At a DNA concentration lower than 0.5 mM, the binding constants K_2 of SPD and NSPD are 0.36 and 0.34 mM^{-1}, respectively, which are almost identical. At a DNA concentration higher than 0.5 mM, however, the binding constants K_1 of SPD and NSPD differed, and were calculated to be 0.04 and 0.18 mM^{-1}, respectively. This result indicates that NSPD binds to DNA more strongly than SPD at a higher DNA concentration, i.e., under the condition that the polyamine concentration is low with respect to that of DNA.

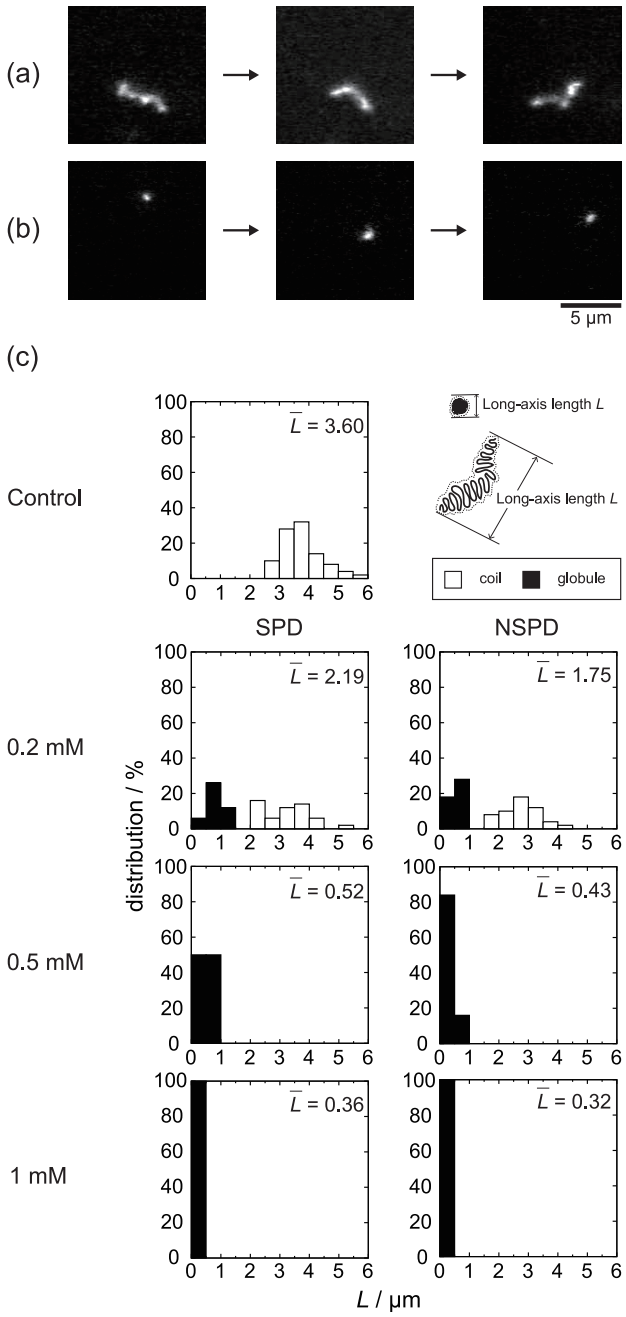

Figure 2.3 Typical FM image of a single T4 DNA molecule undergoing the Brownian motion in solution; (a) in the absence and, (b) in the presence of 1 mM NSPD. The time difference between neighbouring frames is 1 s. (c) Distribution of the long-axis length L of T4 DNA in solution at different concentrations of SPD and NSPD. The DNA concentration was fixed at 0.1 μM in nucleotide units. $\bar{L}$ (μm) is the ensemble average for 50 DNA molecules.

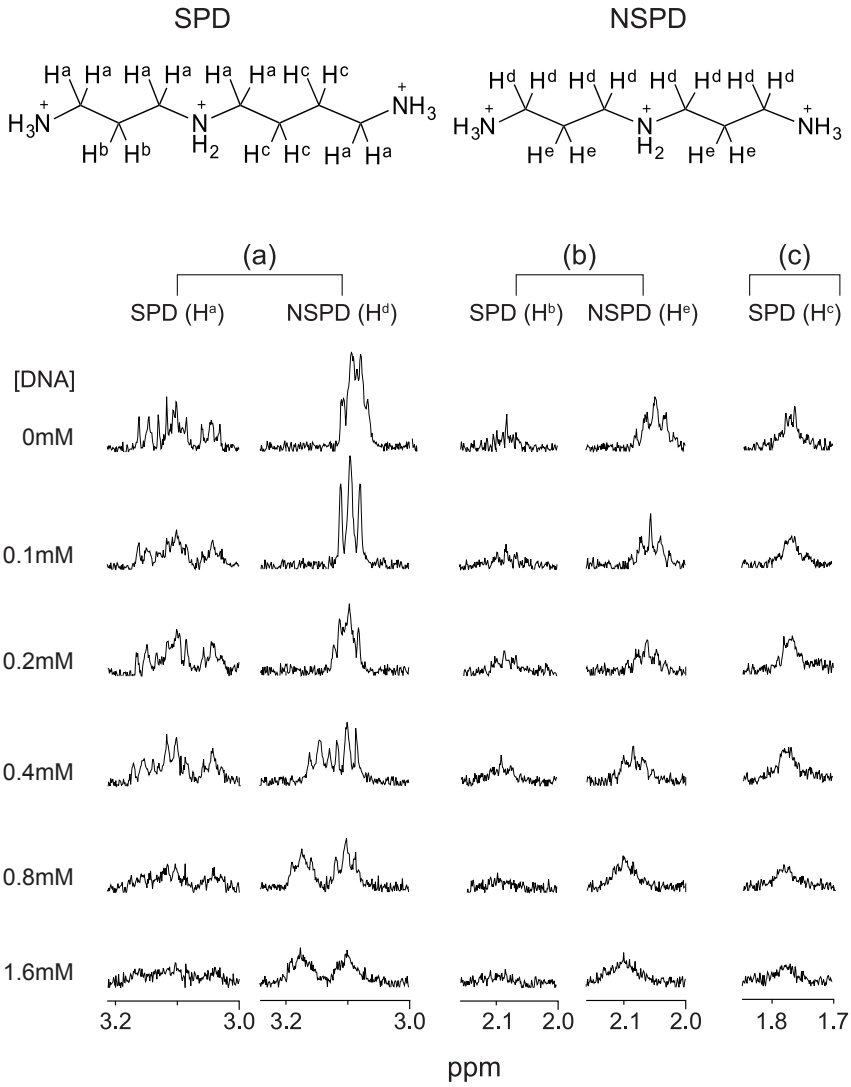

Figure 2.4 ^{1}H NMR spectra for methylene groups of SPD and NSPD at different concentrations of CT DNA. The polyamine concentration was fixed at 0.1 mM. (a) δ = 3.20-3.00 ppm, (b) 2.15-2.00 ppm, and (c) 1.85-1.70 ppm.

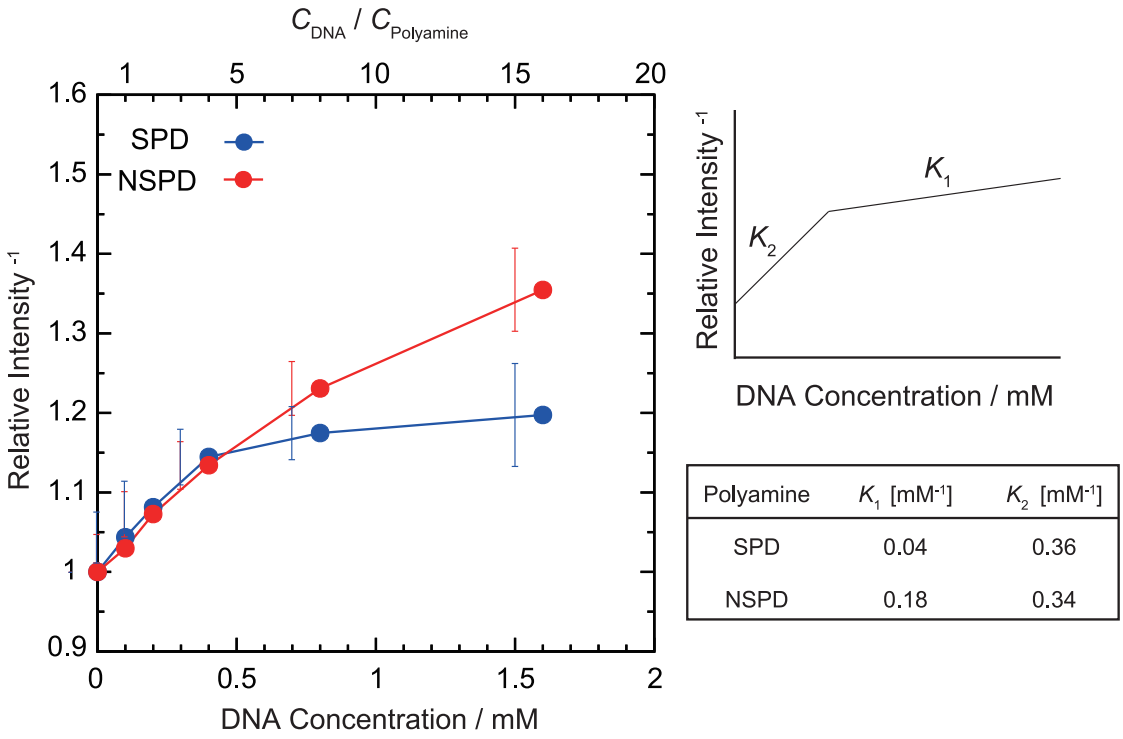

Polyamine	K_1 [mM^{-1}]	K_2 [mM^{-1}]
SPD	0.04	0.36
NSPD	0.18	0.34

Figure 2.5 Left: Change in the intensity of ^{1}H NMR signals depending on the concentration of CT DNA. The longitudinal axis is the inverse of the ^{1}H NMR intensity evaluated through the integration of the observed signals, where all of the ^{1}H signals are well-separated as shown in Fig. 4. The signal intensities in the graph were calculated based on the sum of all of the integrated values for the spectra of SPD and NSPD, so as to minimize the experimental error. Right: Schematic illustration showing how to evaluate the binding equilibrium constant, *K*, from the slope of the graph.

2.2.3 Summary of experimental observations

We found that the biphasic effects, enhancement and inhibition on gene expression, are induced by both polyamines (Fig. 2.1). Moreover, it was revealed that SPD significantly promotes gene expression, while NSPD has a weaker effect (Fig. 2.1). AFM observations indicated clear differences between SPD and NSPD on the morphology of DNA; SPD tends to induce a larger flower-like structure than NSPD (Fig. 2.2), suggesting that DNA segments tend to align in a parallel manner. FM observations demonstrated that NSPD induces shrinkage/compaction with a higher potency than SPD (Fig. 2.3). This trend in the effect on the DNA conformation corresponds to the inhibitory effect on gene expression; NSPD suppresses gene expression at a lower concentration than SPD (Fig. 2.1). In addition, through NMR measurements, it became clear that the binding constant of NSPD to DNA is evidently larger than that of SPD under the condition that the polyamine concentration is relatively low (Fig. 2.5).

2.3 Discussion

In order to capture the essential feature on the manner of interaction of SPD and NSPD with DNA, we have adapted rather simple modelling for both polyamines and DNA. SPD and NSPD are represented as linear beaded chains as shown in Fig. 2.6a. Figure 2.6b shows a typical snapshot of NSPD and SPD interacting with a DNA segment, respectively, for electrostatic interaction of strength Γ = 1.36 nm (between an ammonium and a phosphate), together with the geometrical parameters defined in the present modeling for the coarse-grained model used in our numerical calculation. Note that the Mote Carlo simulation was carried out at T = 298 K to incorporate the effect of thermal fluctuation into the simulation. Detailed definition of Γ is given in Eq. (2.5) of the section 2.5.6. For NSPD, the model has 9 monomers, and the three ammonium groups are placed in positions #1, #5, and #9 (Fig. 2.6a). In contrast, for SPD, a total of 10 monomers are connected linearly, and the ammonium groups are labeled as #1, #5, and #10 based on their position in the chain molecule (Fig. 2.6a). The details of numerical modeling together with parametrization are summarized in the section 2.5.6. Figure 2.6c shows schematics corresponding to the atomistic model. Both NSPD and SPD distribute close to the soft DNA boundary and polyamines tend to tilt by an angle of roughly 45° relative to the DNA axis. Inspection of both the detailed atomistic and coarse-grained models suggests that, for NSPD, the three ammoniums near the DNA soft boundary point in the same direction, which would induce a strong electrostatic attraction between NSPD and DNA. In contrast, for SPD, two ammoniums (#1 and #5) are distributed around the soft DNA boundary facing the phosphate groups, but due to its steric structure, the #10 ammonium points in a direction different from the other two ammoniums, and is located outside of the soft DNA boundary, which should weaken the interaction between SPD and DNA.

To explore the manner of interaction of these polyamines with DNA in more detail, we calculate the two-variable density distribution function $\rho_5(r, \cos\theta)$; where the variables, r and θ, are the radial distance of the #5 ammonium and the angle of the vector measured from the #1 to #5 ammonium groups, respectively (cf. Eq. (2.7) in the section 2.5.6 and Fig. 2.6). We then transform $\rho_5(r, \cos\theta)$ into the conditional free energy $F(r, \cos\theta)/k_BT = -\ln[\rho_5(r, \cos\theta)]$. The two-variable profile of the free energy provides visual insights into the differences between the translational and rotational degrees of freedom of a trivalent polyamine around a DNA. Figure 2.7a,b plot the free energy landscape of $F(r, \cos\theta)/k_BT$ for SPD and NSPD, respectively, when Γ = 1.36 nm. The polyamines show similar profiles in the plot of $F(r, \cos\theta)/k_BT$. First, in the area where the radial distance of the #5 ammonium r is around 1.3 nm or less, two distinct regions can be seen: (i) red and yellow regions, corresponding to lower-energy configurations, and (ii) green and blue regions, corresponding to higher-energy configurations. The lower free-energy area

occurs roughly at |cos θ| between 0.5 and 1, and the higher free-energy area is approximated at |cos θ| between 0 and 0.5. Namely, both SPD and NSPD display a preferential orientation, and the lowest free-energy configuration is found at the red-color region with $\theta = \pm$ 40-50° (similar to the snapshot of SPD and NSPD in Fig. 2.6). Secondly, for $r > 1.3$ nm, the free energy increases steadily as r is increased. The detailed landscape also suggests that, at and beyond $r = \sim 1.3$ nm, both SPD and NSPD start to exhibit similar preference in all orientations, i.e., polyamines experience full rotation degrees of freedom. This is indeed an entropically favorable process. At $r = \sim 1.3$ nm, the polyamine may retain significant electrostatic attraction to DNA and gain enough rotational entropy simultaneously. Based on the landscape of $F(r, \cos\theta)/k_BT$, it becomes possible to distinguish the strong binding regime from the weak binding regime at r near 1.3 nm. In contrast to SPD, the area of lower energy configurations (red and yellow regions) of NSPD is more expanded and the free energy landscape can be deeper.

To elucidate the quantitative difference between NSPD and SPD, we compute the conditional free energy difference: $\Delta F(r, \cos\theta)/k_BT = F_{SPD}(r, \cos\theta) - F_{NSPD}(r, \cos\theta)$. Figure 2.7c plots the profile of $\Delta F(r, \cos\theta)/k_BT$ for $\Gamma = 1.36$ nm and $R_{cyl} = 2.59$ nm. The hills in the landscape reflect configurations for which SPD has a higher free energy than NSPD, whereas in the valleys, SPD has a lower free energy than NSPD. The landscape is not totally symmetric at $\cos\theta = 0$ and π because SPD has an extra methylene group and is basically asymmetric. The hills emerge near $r = 1$ nm within a narrow range of $\cos\theta$, indicating that NSPD is preferentially located at around and within the soft DNA boundary with a specifically narrow range of preferential angles. This finding is consistent with the snapshots in Fig. 2.6 in which the three ammoniums in NSPD can orient themselves to face towards the charged phosphate groups. Moreover, the valleys in the free energy difference landscape are found to be away from the soft DNA surface at around $r = 1.7$-1.8 nm, a sign that SPD, in contrast to NSPD, tends to distance itself from the DNA surface. From these findings, it becomes evident that the extra methylene in SPD may weaken its electrostatic attraction with DNA, but enhances the spatial (translational and rotational) entropy of SPD around a DNA segment.

Our simulation model consists of one polyamine and one DNA segment, which corresponds to an experimental condition with lower concentrations of polyamines with respect to the phosphate groups in DNA; i.e., the line marked as K_1 on the right side of the schematic plot in Fig. 2.5. To compute the binding constant corresponding to K_1 deduced from the NMR measurement, in the simulation we monitor those binding events exclusively when all of the three ammoniums in polyamine simultaneously bind to the phosphates in DNA. To account for binding, the distance between the central nitrogen atom of an ammonium ion and the central phosphorous atom in a phosphate ion needs to be defined to differentiate binding from non-binding for these two types of ions. If we take the radii of ammonium and phosphate as 0.137 nm and 0.258 nm [50,51],

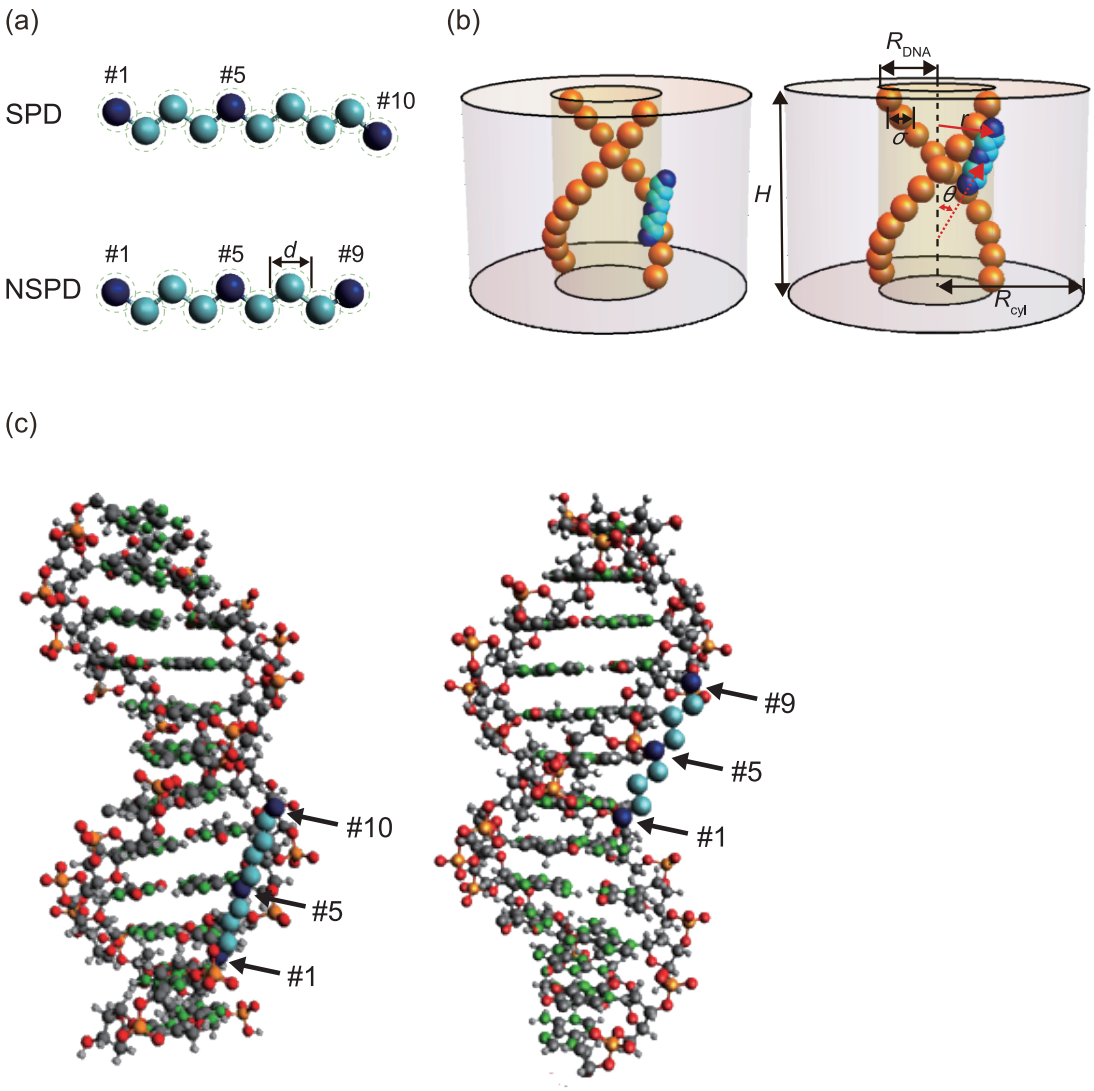

Figure 2.6 Simulation model for rigid SPD and NSPD in (a) and typical snapshots in the simulation for SPD and NSPD interacting with double-stranded DNA in (b) and (c) when the strength of electrostatic interaction Γ = 1.36 nm. For the numerical simulation in (b), pairs of charged spheres to mimic phosphate groups are placed in a soft cylinder of length H (= 3.4 nm) and radius R_{DNA} (= 1.0 nm) under a periodic boundary condition. The pictures in (c) represent the atomistic detail of the coarse-grained model. Hydrogen atoms are omitted for clarity. The positions of the three ammoniums in SPD and NSPD are indicated by #. In our model, a polyamine is allowed to partially penetrate into the DNA interior, which mimics minor and major grooves. The adjacent pairs of negatively charged moieties in the DNA model are separated by 0.34 nm.

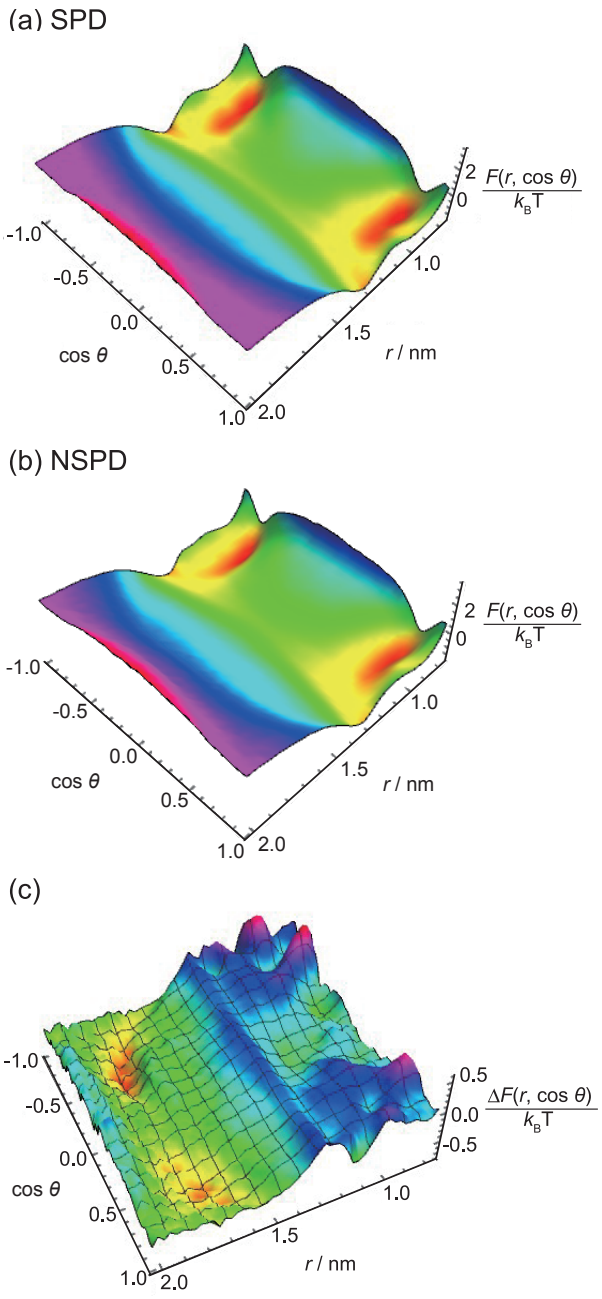

Figure 2.7 Plot of the free energy landscape $F(r, \cos\theta)/k_BT$ of SPD and NSPD when $\Gamma = 1.36$ nm and $R_{cell} = 2.59$ nm in (a) and (b), respectively, and the free energy difference between SPD and NSPD: $\Delta F(r, \cos\theta)/k_BT = F_{SPD}(r, \cos\theta) - F_{NSPD}(r, \cos\theta)$ in (c).

respectively, as well as the hydrogen bonding length (N-H-O-P) between the hydrogen in ammonium and the oxygen in phosphate as 0.174 nm [52], the maximum length between an ammonium ion and a phosphate ion under the binding state can be estimated to be 0.569 nm. Note that 0.258 nm is actually the value for sulfate ion, which is considered to be similar to a phosphate ion in actual atomistic modeling [51]. By considering the angle of hydrogen bonding between ammonium and phosphate, the length between an ammonium ion and a phosphate ion (NH-O-P) may vary from 0.404 nm, 0.453 nm to 0569 nm (corresponding to 90°, 105° to 180°). In this work, we assume that a length 0.453 nm is the maximum length that allows binding between an ammonium and a phosphate. Thus, we can now calculate the binding constant K_i between polyamine and phosphate as follows:

$$K_i = [Polyamine - Phosphate]/[Polyamine][Phosphate] \quad (2.1)$$

where *i* denotes SPD or NSPD. [*Polyamine*], [*Phosphate*], and [*Polyamine-Phosphate*] are the concentrations of free polyamine, free phosphate, and binding between them, respectively. The concentration ratio, [*Polyamine-Phosphate*]/[*Phosphate*], is determined from the bound and free polyamine as in Eq. (2.2).

$$[Polyamine - Phosphate]/[Polyamine] = (N(binding)/V_b)/\big(N(nonbinding)/V_f\big) \quad (2.2)$$

where *N*(*binding*) and *N*(*nonbinding*) are the average probability of a polyamine bound to and free from DNA, respectively, and *N*(*binding*) + *N*(*nonbinding*) = 1. *N*(*binding*) is calculated from the fraction of the events in which all of the three ammonium groups of polyamine simultaneously bind to DNA during the simulation. Thus, *N*(*nonbinding*) includes the other fractions of which any of the ammonium group(s) in a polyamine are free from binding to the phosphate group. Further details about *N*(*binding*) are given in section 2.5.6. R_{cut} is chosen to be 1.3 nm. V_b and V_f denote the volumes where bound and free polyamines are located, respectively, and are estimated based on the free energy diagrams in Figure 2.7 by adapting the following Eq. (2.3) and (2.4) with $\mu = \cos\theta$:

$$V_b = \left[2\pi H \int_{R_{cut}}^{R_{DNA}-\frac{\sigma}{2}} r dr\right][2\int_{0.5}^{1} d\mu \int_{0}^{2\pi} d\phi\Big] \quad (2.3)$$

$$V_f = \left[2\pi H \int_{R_{cut}}^{R_{DNA}-\frac{\sigma}{2}} r dr\right][2\int_{0}^{0.5} d\mu \int_{0}^{2\pi} d\phi\Big] + 4\pi H \int_{R_{cut}}^{R_{cyl}} r dr \quad (2.4)$$

Since our investigation is directed to a low polyamine-to-phosphate concentration ratio, we approximate the free phosphate concentration [*Phosphate*] in Eq. (2.1) to be the same as the overall phosphate concentration in the simulation. Note that when the three ammoniums bind to DNA phosphates, the orientation of the polyamine falls in the range of 40-80 degrees that coincide with the free energy minimum valleys in Fig. 2.7a,b.

Figure 2.8 plots the calculated binding constant K for NSPD and SPD as a function of Γ for two different sizes of cylindrical simulation cell with R_{cyl} = 5.182 and 2.591 nm. Here, it is noted that K_{NSPD} is always greater than K_{SPD} for any given Γ and R_{cyl}. The binding constant ratio K_{NSPD}/K_{SPD} on the data in Fig. 2.8 is around 2, being slightly smaller than the experimental estimation (around 4). This small difference is attributable to the neglect of the contribution from translational entropy of counter ions [20,29] and from the hydration effect including the ionization balance of the free ammonium groups. Nevertheless, it is regarded that the simulation reproduces the essentials on the difference of binding nature between SPD and NSPD in our experiments. The weaker binding of SPD implies larger surviving negative charge on double-stranded DNA, which caused larger repulsive interaction between DNA segments. This effect may promote the parallel alignment of DNA chains, as indicated in our AFM observations in Fig. 2.2, i.e., generation of flower like structure with SPD. It has been suggested that self-avoiding effect of DNA segments in a lightly shrunken DNA chain promote parallel ordering, under the similar mechanism of stabilization with liquid crystalline ordering [38].

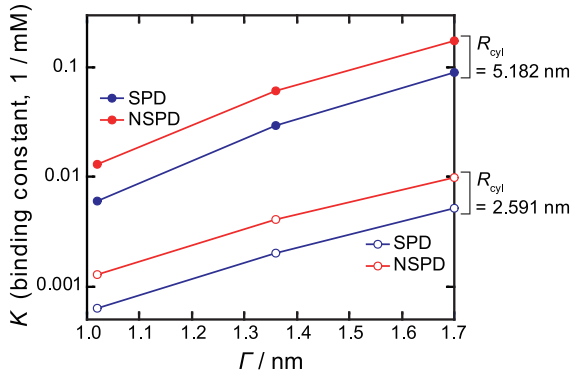

Figure 2.8 Plot of the binding constants K for both NSPD and SPD with DNA as a function of Γ when R_{cyl} = 5.182 and 2.591 nm. Γ is a parameter to represent the strength of Columbic interaction (see section 2.5.6).

Summarizing the above mentioned numerical study, it has become clear that NSPD has preferential configurations in which NSPD binds strongly with DNA, but SPD gains translational and rotational degrees of freedom (entropy-favored) while it is located away from DNA. In other words, SPD plays an essential role in reducing electrostatic attraction between polyamine and DNA (by decreasing the linear charge density of a polyamine). As the result, SPD exhibits weaker

binding with DNA than does NSPD. By analyzing the state in which three ammoniums bind simultaneously to DNA phosphates, the binding constant of polyamines with DNA was estimated. The results revealed that the binding constant ratio between NSPD and SPD deduced theoretically is consistent with the trend observed in the NMR experiment. Such scheme of the specific feature of the interaction between DNA and polyamines will provide a useful insight for the development of both fundamental and application studies on polyamines [15-22,53-58].

2.4 Conclusions

Both experimental and theoretical results clearly show that the difference by only one methylene group between SPD and NSPD causes marked differences in the binding affinity and DNA structure, which leads to significant differences in the gene expression profile *in vitro*. This means that the replacement of SPD by NSPD results in a significant loss of genetic activity; NSPD induces weaker enhancement at low concentrations and stronger inhibition at high concentrations. These findings shed light on the underlying mechanism why SPD and NSPD exhibit markedly different activity *in vivo*. For example, Porter and Bergeron reported that NSPD causes a loss of biological activity in cultured L1210 leukemia cells [41]. Silvia et al. also evaluated the cytotoxic effects of NSD and its Pd(II) complex on human breast cancer cell lines and demonstrated that these compounds cause growth inhibition and cell death [47].

From a methodological point of view, combinatorial study with structural and functional analysis as adapted in the present study would be useful to obtain the essential features of the ligand-DNA interaction. Studies along such direction are expected to contribute for the design of novel polyamines as the candidate of potent antitumor active drug [59].

2.5 Materials and Methods

2.5.1 Materials

Spermidine trihydrochloride (SPD) was purchased from Nacalai Tesque (Kyoto, Japan). Bis(3-aminopropyl)amine (NSPD) was purchased from Sigma-Aldrich (St. Louis, MO, USA). The fluorescent cyanine dye YOYO-1 (1,10-(4,4,8,8-tetramethyl-4,8-diazaundecamethylene)bis[4-[(3-methylbenzo-1,3-oxazol-2-yl)methylidene]-l,4-dihydroquinolinium] tetraiodide) was purchased from Molecular Probes, Inc. (Eugene, OR, USA). The antioxidant 2-mercaptoethanol (2-ME) and calf thymus DNA (CT DNA: 8-15 kbp) were purchased from Wako Pure Chemical Industries (Osaka, Japan). T4 GT7 phage DNA (contour length: 57 μm, 166 kbp) was purchased from Nippon Gene (Toyama, Japan). Plasmid DNA (Luciferase T7 Control DNA, 4,331 bp) containing a T7 RNA polymerase promotor sequence was purchased from Promega (Madison,

WI, USA). Other chemicals obtained from commercial sources were of analytical grade.

2.5.2 Luciferase assay for gene expression

A cell-free luciferase assay with a TnT T7 Quick Coupled Transcription/Translation System (Promega) was carried out according to the manufacturer's instructions as follows. Plasmid DNA with the promotor region of T7 RNA polymerase was used as the DNA template. The DNA concentration was 0.3 μM in nucleotide units. The reaction mixture was incubated for 90 min at 30°C on a Dry Thermo Unit (TAITEC, Saitama, Japan). Luciferase expression was evaluated following the addition of luciferase substrate (Luciferase Assay Reagent, Promega) by detecting the emission around 565 nm using a luminometer (MICROTEC Co., Chiba, Japan)

2.5.3 AFM observations

For AFM imaging using an SPM-9700 (Shimadzu, Kyoto, Japan), 0.3 μM plasmid DNA (4,331bp) was dissolved in 10 mM Tris-HCl buffer solution at pH 7.5 with various concentrations of polyamines. The DNA solution was incubated for more than 10 min and then transferred onto a freshly cleaved mica surface. Subsequently, the sample was rinsed with ultra-pure water, dried with nitrogen gas and imaged by AFM. All measurements were performed in air using the tapping mode. The cantilever, OMCL-AC200TS-C3 (Olympus, Tokyo, Japan), was 200 μm long with a spring constant of 9-20 N/m. The scanning rate was 0.4 Hz and images were captured using the height mode in a 512×512 pixel format. The obtained images were plane-fitted and flattened by the computer program supplied with the imaging module.

2.5.4 FM observations

To visualize individual DNA molecules in solution by FM, a large DNA, T4 GT7 DNA was used. DNA was dissolved in a 10 mM Tris-HCl buffer and 4%(v/v) 2-ME at pH 7.5 in the presence of various concentrations of polyamines (0-1,000 μM). Measurements were conducted at a low DNA concentration (0.1 μM in nucleotide units). YOYO-1 (0.05 μM) was added to the DNA solution and single-molecule observations were performed with an inverted fluorescence microscope (Axiovert 135, Carl Zeiss, Oberkochen, Germany) equipped with a 100× oil-immersion objective lens and fluorescent illumination from a mercury lamp (100 W) via a filter set (Zeiss-10, excitation BP 450-490; beam splitter FT 510; emission BP 515-565). Images were recorded onto a DVD at 30 frames per second with a high-sensitivity EBCCD (Electron Bombarded Charge-Coupled Device) camera (Hamamatsu Photonics, Shizuoka, Japan) and analyzed with the image-processing software ImageJ (National Institute of Mental Health, MD, USA). Based on the observation of time-successive images, the distribution of the long-axis length of DNA in solution was evaluated, and 50 DNA molecules were measured at each

experimental condition.

2.5.5 NMR titration experiments

The binding abilities of NSPD and SPD to CT DNA were investigated via ^{1}H-NMR titration experiments by using a JEOL JNM-ECZ500R. All experiments were carried out in 10 mM Tris-DCl buffer (pD 7.5) and 3-(trimethylsilyl)-2,2',3,3'-tetradeuteropropionic acid (TMSP-d_4) was used as an internal reference. A presaturation technique was used for suppression of a water peak. Both polyamine samples were prepared at a concentration of 100 μM in 10 mM Tris-DCl buffer (pD 7.5). The CT DNA titrant sample (stock solution) was prepared at a concentration of 20 mM in D_2O. Polyamine sample (0.6 mL) was introduced into the NMR tube, and increasing amounts of the titrant DNA solution were added. A progressive disappearance of the proton signals of the polyamine was observed, indicating a significant decrease of T_2, lateral relaxation time of the ^{1}H signals, caused by the binding of polyamines to CT DNA.

2.5.6 Monte Carlo simulation

The SPD and NSPD conformations shown in Fig. 2.6 correspond to the lowest-energy conformer for each molecule, and can be obtained by using the energy minimization scheme of Avogadro software under UFF (Universal Force Field) [60]. To address the excluded volume of ammonium and methylene groups, each of these groups is modeled as a hard sphere of diameter d = 0.39 nm in Fig. 2.6a, similar to the coarse-grained polyethylene model [61]. Each of the three ammonium groups in SPD and NSPD is assigned +1 unit charge.

To model a DNA segment in the coarse-grained model, we adapt a charged DNA segment of one pitch of about 3.4 nm [22]. Figure 2.6 shows the model DNA segment consisting of 10 pairs of charged spheres (-1 unit charge for each sphere) around a soft cylinder of length H = 3.4 nm and radius R_{DNA} = 1 nm. The charged spheres represent the phosphate groups of typical dimeter σ = 0.476 nm. The two charged spheres of each pair are 180° apart around the DNA cylinder (R_{DNA} = 1 nm). The first pair starts at an axial location z = 0.17 nm above the bottom of the cylinder corresponding to the DNA segment (z = 0), and the remaining pairs are oriented 36°and elevated 0.34 nm sequentially. The final pair ends at a height 0.17 nm below the top of the cylinder of the DNA segment (z = 3.4 nm).

In the investigated DNA model, 20 charged sites on the DNA segment are grouped into 10 pairs. The two charged spheres in each pair are separated by 180° around the cylinder and their separation is set at 2 nm, close to the width of a DNA molecule. These 10 pairs of charged groups are arranged from the bottom to the top of the cylinder by rotating 36° for each pair, and any two adjacent pairs are separated by 0.34 nm. The top and bottom pairs are 0.17 nm away from the ends of the cylindrical cell.

The above DNA segment will replicate itself in a one-dimensional periodic boundary condition along the axis of the DNA segment in a Monte Carlos simulation, and by implementing a one-dimensional Ewald summation [35], all the DNA images form an infinitely long DNA chain as in the traditional cell model [62]. Our simulation considers a rigid cylindrical cell with radius R_{cell} = 2.59 and 5.18 nm. The monomers (charged ammonium or neutral methylene) of a polyamine are not allowed to cross the rigid boundary of the simulation cell, and a monomer in the polyamine molecule can reach up to the radial position at R_{cell} - d/2 (d: diameter of an ammonium or a methylene monomer). Nevertheless, monomers can penetrate the soft cylinder of the model DNA core (R_{DNA} = 1 nm) up to R_{DNA} - σ /2 (σ : diameter of a coarse-grained phosphate group), similar to the empty space around the major and minor grooves of DNA that involve binding processes.

In our Monte Carlo simulation, we choose translation and rotation motion randomly with equal probability to sample configurations of the polyamine with temperature at T = 298 K. Also, the step sizes for the above two types of sampling schemes are adjusted to achieve an acceptance ratio around 50-60% under the Metropolis algorithm [63]. For each parameter set, a total of 9 $\times 10^8$ moves are conducted in the simulation, and the first 10^8 moves are discarded to ensure convergence in calculations.

The electrostatic interaction between the monomers of a polyamine and a phosphate group is treated at the level of the primitive model with the screened Coulomb potential to incorporate water, counterions and coions implicitly into the interaction potential, given by

$$\begin{aligned} V(r)/k_{\mathrm{B}}T &= \infty && \text{if } r < r_{\mathrm{c}} \\ &= \Gamma q_i Q_j \exp(-\kappa r)/r && \text{if } r \geq r_{\mathrm{c}} \end{aligned} \tag{2.5}$$

where k_B is the Boltzmann constant; T is the temperature; r is the separation between a monomer in a polyamine and the coarse-grained phosphate group in the DNA; i is the i-th monomer in the polyamine with charge q_i (0 for a methylene group; + 1 for an ammonium group); j is the j-th phosphate group in DNA with charge Q_j ; Γ is the interaction strength; κ is the inverse Debye screening length; and r_c is approximated to be 0.31 nm, a typically closest distance between a charged amine and a phosphate group in DNA [51]. In this work, Γ ranges from 0.68 to 1.7 nm, about 1 to 2.4 Bjerrum lengths at 25°C to mimic the low dielectric regime around DNA with low water content, and the inverse Debye screening length κ is chosen to be 2.4 nm^{-1}. This inverse Debye screening length is set to reflect the low-water and low-electrolyte region close to the DNA surface.

In this work, we are particularly interested in the density distribution function of charged monomers (i.e., ammonium groups) in polyamine. We compute the reduced density distribution

function of the i-th ammonium group $\rho_i(r)$ (defined in Fig. 2.6) as a function of its radial distance r measured from the center of the DNA axis for different Γ. To compute $\rho_i(r)$, the cylindrical simulation cell is divided into 100 layers along the radial direction, and then the average number of the charged monomer i in the k-th layer $B_k(r)$ (histogram) is calculated. $\rho_i(r)$ is obtained by

$$\rho_i(r) = V_{\text{cyl}} B_i(r)/v_i(r) \tag{2.6}$$

where $v_i(r)$ is the volume of the i-th layer, and V_{cyl} is the total volume of the cylindrical simulation cell to keep the density distribution function dimensionless. Moreover, the calculation of $\rho_i(r)$ is further extended to the two-variable density distribution function $\rho_5(r, \cos\theta)$ for the ammonium group at the middle of the polyamine (#5 defined in Fig. 2.6) where θ is the angle between the direction of the DNA axis and the unit vector drawn from the ammonium at position #1 to that at position #5 (shown in Fig. 2.6), given by

$$\rho_5(r, \cos\theta) = V_{\text{cyl}} B_5(r, \cos\theta)/(v_i(r)\Delta\mu) \tag{2.7}$$

where $\mu = \cos\theta$ and $\Delta\mu$ is the interval of μ in the simulation. In the calculation, we divide the range of μ (between -1 and 1) into 50 intervals with $\Delta\mu = 0.04$, and the radial distance r (between $R_{\text{DNA}} - \sigma/2$ and $R_{\text{cell}} - d/2$) into 50 intervals with a total of 2,500 intervals in the histogram $B_5(r, \cos\theta)$.

References

[1] C. W. Tabor & H. Tabor. Polyamines. *Annual Review of Biochemistry* **53**, 749-790, (1984).

[2] L. Miller-Fleming, V. Olin-Sandoval, K. Campbell & M. Ralser. Remaining Mysteries of Molecular Biology: The Role of Polyamines in the Cell. *J. Mol. Biol.* **427**, 3389-3406, (2015).

[3] *Polyamines* (eds R. Alcázar & A. F. Tiburcio), in *Methods in Molecular Biology* **1694**, (Humana Press, 2018).

[4] K. Igarashi & K. Kashiwagi. Modulation of cellular function by polyamines. *International Journal of Biochemistry & Cell Biology* **42**, 39-51, (2010).

[5] T. Thomas & T. J. Thomas. Polyamines in cell growth and cell death: molecular mechanisms and therapeutic applications. *Cell. Mol. Life Sci.* **58**, 244-258, (2001).

[6] B. Desforges *et al.* An intercellular polyamine transfer via gap junctions regulates proliferation and response to stress in epithelial cells. *Mol Biol Cell* **24**, 1529-1543, (2013).

[7] A. K. Handa, T. Fatima & A. K. Mattoo. Polyamines: Bio-Molecules with Diverse Functions in Plant and Human Health and Disease. *Front Chem* **6**, 10/1-18, (2018).

[8] M. Saminathan, T. Thomas, A. Shirahata, C. K. Pillai & T. J. Thomas. Polyamine structural effects on the induction and stabilization of liquid crystalline DNA: potential applications to DNA packaging, gene therapy and polyamine therapeutics. *Nucleic Acids Res.* **30**, 3722-3731, (2002).

[9] A. C. Childs, D. J. Mehta & E. W. Gerner. Polyamine-dependent gene expression. *Cell. Mol. Life Sci.* **60**, 1394-1406, (2003).

[10] S. Mandal, A. Mandal, H. E. Johansson, A. V. Orjalo & M. H. Park. Depletion of cellular polyamines, spermidine and spermine, causes a total arrest in translation and growth in mammalian cells. *Proc. Natl. Acad. Sci. U. S. A.* **110**, 2169-2174, (2013).

[11] A. J. Michael. Polyamines in Eukaryotes, Bacteria, and Archaea. *J. Biol. Chem.* **291**, 14896-14903, (2016).

[12] T. J. Thomas, H. A. Tajmir-Riahi & T. Thomas. Polyamine-DNA interactions and development of gene delivery vehicles. *Amino Acids* **48**, 2423-2431, (2016).

[13] A. O. Gevrekci. The roles of polyamines in microorganisms. *World J. Microbiol. Biotechnol.* **33**, 204/1-7, (2017).

[14] A. J. Michael. Polyamine function in archaea and bacteria. *J. Biol. Chem.* **293**, 18693-18701, (2018).

[15] L. C. Gosule & J. A. Schellman. Compact form of DNA induced by spermidine. *Nature* **259**, 333-335, (1976).

[16] D. K. Chattoraj, L. C. Gosule & A. Schellman. DNA condensation with polyamines. II. Electron microscopic studies. *J. Mol. Biol.* **121**, 327-337, (1978).

[17] P. G. Arscott, A. Z. Li & V. A. Bloomfield. Condensation of DNA by trivalent cations. 1. Effects of DNA length and topology on the size and shape of condensed particles. *Biopolymers* **30**, 619-630, (1990).

[18] V. A. Bloomfield. Condensation of DNA by multivalent cations: considerations on mechanism. *Biopolymers* **31**, 1471-1481, (1991).

[19] V. A. Bloomfield. DNA condensation. *Curr. Opin. Struct. Biol.* **6**, 334-341, (1996).

[20] K. Yoshikawa & Y. Yoshikawa. Compaction and condensation of DNA. *Pharmaceutical perspectives of nucleic acid-based therapeutics* (eds R. I. Mahato & S. W. Kim) Chapter 8, 137-163 (CRC Press, 2002).

[21] Y. Yoshikawa *et al.* Critical behavior of megabase-size DNA toward the transition into a compact state. *J. Chem. Phys.* **135**, 225101/1-7, (2011).

[22] Y. Kashiwagi *et al.* Repulsive/attractive interaction among compact DNA molecules as judged through laser trapping: difference between linear- and branched-chain polyamines.

Colloid. Polym. Sci. **297**, 397-407, (2018).

[23] T. Sakaue & K. Yoshikawa. Folding/unfolding kinetics on a semiflexible polymer chain. *J. Chem. Phys.* **117**, 6323-6330, (2002).

[24] N. V. Hud & I. D. Vilfan. Toroidal DNA condensates: unraveling the fine structure and the role of nucleation in determining size. *Annu. Rev. Biophys. Biomol. Struct.* **34**, 295-318, (2005).

[25] A. Estévez-Torres & D. Baigl. DNA compaction: fundamentals and applications. *Soft Matter* **7**, 6746-6756, (2011).

[26] V. B. Teif & K. Bohinc. Condensed DNA: condensing the concepts. *Prog. Biophys. Mol. Biol.* **105**, 208-222, (2011).

[27] A. Venancio-Marques, A. Bergen, C. Rossi-Gendron, S. Rudiuk & D. Baigl. Photosensitive polyamines for high-performance photocontrol of DNA higher-order structure. *ACS Nano* **8**, 3654-3663, (2014).

[28] R. Everaers & H. Schiessel. The physics of chromatin. *J. Phys.: Condens. Matter* **27**, 060301/1-2, (2015).

[29] M. Takahashi, K. Yoshikawa, V. Vasilevskaya & A. Khokhlov. Discrete coil－ globule transition of single duplex DNAs induced by polyamines. *J. Phys. Chem. B* **101**, 9396-9401, (1997).

[30] J. DeRouchey, V. A. Parsegian & D. C. Rau. Cation charge dependence of the forces driving DNA assembly. *Biophys. J.* **99**, 2608-2615, (2010).

[31] Y. Yoshikawa *et al.* Effective chiral discrimination of tetravalent polyamines on the compaction of single DNA molecules. *Angew. Chem. Int. Ed. Engl.* **52**, 3712-3716, (2013).

[32] A. Muramatsu *et al.* Naturally occurring branched-chain polyamines induce a crosslinked meshwork structure in a giant DNA. *J. Chem. Phys.* **145**, 235103/1-7, (2016).

[33] T. Nishio *et al.* Branched‐Chain Polyamine Found in Hyperthermophiles Induces Unique Temperature‐Dependent Structural Changes in Genome‐Size DNA. *ChemPhysChem* **19**, 2299-2304, (2018).

[34] J. Pelta, Jr., D. Durand, J. Doucet & F. Livolant. DNA mesophases induced by spermidine: structural properties and biological implications. *Biophys. J.* **71**, 48-63, (1996).

[35] H. Takemoto, T. Ohyama & A. Tohsaki. Direct sum of Coulomb potential without ambiguities of conditionally convergent series. *Progress of theoretical physics* **109**, 563-573, (2003).

[36] F. Luckel, K. Kubo, K. Tsumoto & K. Yoshikawa. Enhancement and inhibition of DNA transcriptional activity by spermine: a marked difference between linear and circular templates. *FEBS Lett.* **579**, 5119-5122, (2005).

[37] A. Yamada, K. Kubo, T. Nakai, K. Yoshikawa & K. Tsumoto. All-or-none switching of transcriptional activity on single DNA molecules caused by a discrete conformational transition. *Appl. Phys. Lett.* **86**, 223901/1-3, (2005).

[38] A. Kanemura *et al.* Opposite effect of polyamines on *In vitro* gene expression: Enhancement at low concentrations but inhibition at high concentrations. *PLoS One* **13**, e0193595/1-11, (2018).

[39] S. Yamamoto, S. Shinoda & M. Makita. Occurrence of norspermidine in some species of genera Vibrio and Beneckea. *Biochemical biophysical research communications* **87**, 1102-1108, (1979).

[40] K. Hamana & S. Matsuzaki. Widespread occurrence of norspermidine and norspermine in eukaryotic algae. *J. Biochem.* **91**, 1321-1328, (1982).

[41] N. J. Prakash, T. L. Bowlin, G. F. Davis, P. S. Sunkara & A. Sjoerdsma. Antitumor activity of norspermidine, a structural homologue of the natural polyamine spermidine. *Anticancer Res.* **8**, 563-568, (1988).

[42] B. Rodriguez-Garay, G. C. Phillips & G. D. Kuehn. Detection of norspermidine and norspermine in Medicago sativa L.(alfalfa). *J. Plant Physiol.* **89**, 525-529, (1989).

[43] M. L. Edwards *et al.* Polyamine analogs with antitumor activity. *J. Med. Chem.* **33**, 1369-1375, (1990).

[44] K. Hamana, M. Niitsu & K. Samejima. Unusual polyamines in aquatic plants: the occurrence of homospermidine, norspermidine, thermospermine, norspermine, aminopropylhomospermidine, bis (aminopropyl) ethanediamine, and methylspermidine. *Can. J. Bot.* **76**, 130-133, (1998).

[45] L. Covassin *et al.* Synthesis of spermidine and norspermidine dimers as high affinity polyamine transport inhibitors. *Bioorganic medicinal chemistry letters* **9**, 1709-1714, (1999).

[46] T. M. Silva *et al.* Norspermidine and novel Pd(II) and Pt(II) polynuclear complexes of norspermidine as potential antineoplastic agents against breast cancer. *PLoS One* **8**, e55651/1-15, (2013).

[47] C. W. Porter & R. J. Bergeron. Spermidine requirement for cell proliferation in eukaryotic cells: structural specificity and quantitation. *Science* **219**, 1083-1085, (1983).

[48] Y. Fang & J. H. Hoh. Early intermediates in spermidine-induced DNA condensation on the surface of mica. *Journal of the American Chemical Society* **120**, 8903-8909, (1998).

[49] K. S. Srivenugopal, D. E. Wemmer & D. R. Morris. Aggregation of DNA by analogs of spermidine: enzymatic and structural studies. *Nucleic Acids Res.* **15**, 2563-2580, (1987).

[50] H. Jenkins & K. Thakur. Reappraisal of thermochemical radii for complex ions. *J. Chem. Educ.* **56**, 576-577, (1979).

[51] J. Yoo & A. Aksimentiev. Improved Parameterization of Amine-Carboxylate and Amine-Phosphate Interactions for Molecular Dynamics Simulations Using the CHARMM and AMBER Force Fields. *Journal of Chemical Theory and Computation* **12**, 430-443, (2016).

[52] M. Meot-Ner. The ionic hydrogen bond. *Chem. Rev.* **105**, 213-284, (2005).

[53] N. Korolev. A molecular dynamics simulation study of oriented DNA with polyamine and sodium counterions: diffusion and averaged binding of water and cations. *Nucleic Acids Res.* **31**, 5971-5981, (2003).

[54] L. Dai, Y. Mu, L. Nordenskiold & J. R. van der Maarel. Molecular dynamics simulation of multivalent-ion mediated attraction between DNA molecules. *Phys. Rev. Lett.* **100**, 118301/1-4, (2008).

[55] Q. Shao, S. Goyal, L. Finzi & D. Dunlap. Physiological levels of salt and polyamines favor writhe and limit twist in DNA. *Macromolecules* **45**, 3188-3196, (2012).

[56] A. Kabir, M. Hossain & G. S. Kumar. Thermodynamics of the DNA binding of biogenic polyamines: Calorimetric and spectroscopic investigations. *J. Chem. Phys.* **57**, 445-453, (2013).

[57] A. Kabir & G. Suresh Kumar. Binding of the biogenic polyamines to deoxyribonucleic acids of varying base composition: base specificity and the associated energetics of the interaction. *PLoS One* **8**, e70510/1-13, (2013).

[58] E. Bignon *et al.* Molecular Dynamics Insights into Polyamine-DNA Binding Modes: Implications for Cross‐Link Selectivity. *Chem. Eur. J.* **23**, 12845-12852, (2017).

[59] J. Yoo & A. Aksimentiev. The structure and intermolecular forces of DNA condensates. *Nucleic Acids Res.* **44**, 2036-2046, (2016).

[60] M. D. Hanwell *et al.* Avogadro: an advanced semantic chemical editor, visualization, and analysis platform. *J. Cheminformatics* **4**, 17/1-17, (2012).

[61] K. Schweizer & J. Curro. PRISM theory of the structure, thermodynamics, and phase transitions of polymer liquids and alloys. *Atomistic Modeling of Physical Properties* (eds L. Moonnerie & U. W. Suter), in *Advanced in Polymer Science* **116**, 319-377 (Springer, 1994).

[62] C. F. Anderson & M. T. Record. Ion distributions around DNA and other cylindrical polyions: theoretical descriptions and physical implications. *Annual review of biophysics and biophysical chemistry* **19**, 423-463, (1990).

[63] M. P. Allen & D. J. Tildesley. *Computer simulation of liquids*, (Oxford university press, 2017).

Chapter 3

K^+ promotes the favorable effect of polyamine on gene expression better than Na^+ [iv]

3.1 Introduction

Why do living organisms on Earth generally prefer potassium-rich intracellular fluids? Sodium is much more abundant than potassium in sea water [1]. On the contrary, the significantly greater content of potassium ion in the medium of living cells, compared to sodium ion, is a longstanding puzzle. Potassium ion is the major intracellular cation, and exhibits a high specificity over other monovalent cations such as Na^+. The ionic imbalance of Na^+ and K^+ inside and outside the cell is the major factor to determine the membrane potential [2]. It has been argued that K^+ plays a key role in homeostatic mechanisms such as maintenance of intercellular pH and osmolarity [3-5]. Over the past couple of decades, the generation of a quadruplex structure with guanine-rich sequences, G-quadruplex (G4), has attracted attention from both biological and physicochemical perspectives. G4 is predominantly found in functional regions of the human genome and transcriptome, including replication initiation sites, human telomeres, oncogene promoter regions and untranslated regions [6]. It has been confirmed that K^+ stabilizes G4 structures much more strongly than Na^+ [7-13]. K^+ has also been shown to affect the structure and function of ribosomes [14]. A similar effect of K^+ was reported in an experiment involving RNA polymerase; i.e., with *E. Coli* polymerase the initial reaction velocity is about doubled in the presence of 0.2 M KCl and the synthesis of RNA proceeds for several hours [15]. On the other hand, there is no significant difference between the effects of K^+ and Na^+ on the double helix DNA [16-19]. Korolev et al. reported a theoretical model to interpret how monovalent alkali cations cause different effect on the stability of nucleosome, the assembly between DNA and positively-charged histone octamer, by taking into account the effect that Na^+ has a little bit larger affinity than K^+ [20].

Recently, we have reported that polyamines can either enhance or inhibit gene expression depending on their concentration [21,22]. In our study on the effects of polyamine on gene expression, we observed that, in the presence of polyamine, K^+ enhances gene expression *in vitro* much more strongly than Na^+. To shed light on this difference in the effects of K^+ and Na^+, we measured the effects of K^+ and Na^+ on the binding of polyamine to DNA. As the results, it

becomes clear that Na^+ exhibit apparently larger inhibitory effect of polyamine binding to DNA than K^+. Such observation will be discussed in terms of the greater interfering effect of Na^+ vs. K^+ on the binding of polyamine to the phosphate groups of DNA. We will argue that the enhanced gene expression with K^+ is attributable to its smaller inhibitory effect on polyamine binding. In addition, we discuss the competitive effects of K^+/Na^+ on polyamine binding to DNA together with the promotion of gene expression with K^+, in relation to the intrinsic effect of a K^+-rich environment in the cell cytoplasm as the general situation in living organisms.

3.2 Results

To study the effects of Na^+ and K^+ on gene expression, a cell-free luciferase assay was performed (Fig. 3.1). Figure 3.1a shows the relative luminescence intensity as a marker of protein synthesis depending on the concentration of SPD. A biphasic effect is observed; i.e., enhancement and inhibition of gene expression at low and higher concentrations, respectively. This biphasic effect of SPD corresponds well to the observations in recent studies [21,22]. Figure 3.1b,c show the relative luminescence intensity depending on the mole fraction of Na^+ or K^+, ΔC, added to the reaction buffer at different concentrations of SPD. The upper part of each graph depicts the total concentration C of Na^+ or K^+, the concentrations C^0 of Na^+ and K^+ contained in the original reaction buffer are 18 mM and 33 mM, respectively (see Materials and Methods).

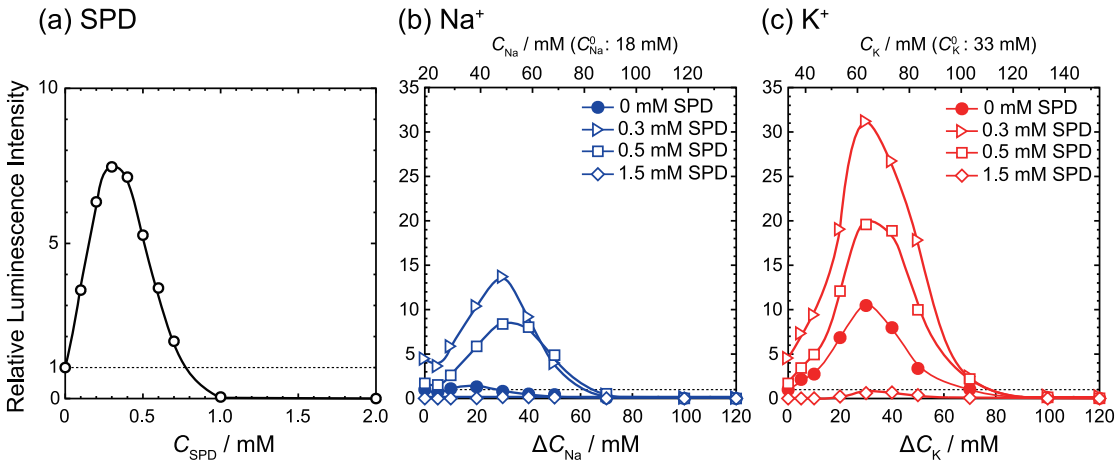

Figure 3.1 Efficiency of gene expression vs. concentrations of (a) SPD, (b) Na^+ and (c) K^+. C^0 is the concentration of Na^+ and K^+ contained in the original reaction buffer; $C = C^0 + \Delta C$. The intensity is normalized to the control condition (= 1), where $\Delta C = 0$ in the absence of SPD. The DNA concentration was fixed at 0.3 μM.

The addition of Na^+ or K^+ to the solution tends to increase the luminescence intensity, and K^+ has a greater enhancing effect, except in experiments with 1.5 mM SPD. The complete inhibition at

1.5 mM SPD is attributable to the transition of the higher-order structure to a tightly packed state, as suggested previously [21,22]. The enhancement of gene expression in the presence of K^+ has been confirmed at different SPD concentrations as revealed in Fig. 3.2.

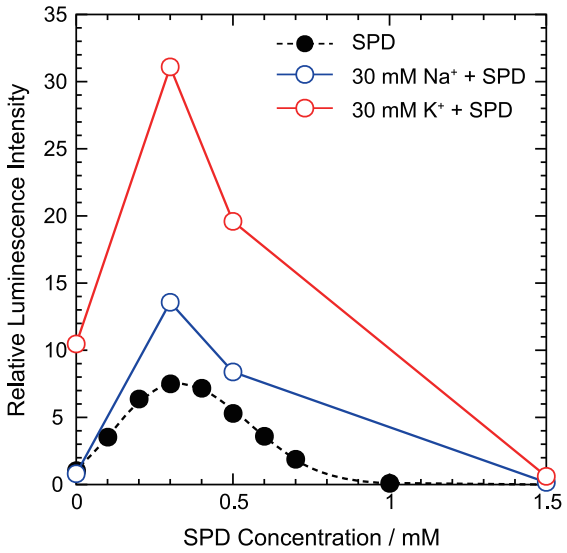

Figure 3.2 Gene expression efficiency depending on SPD concentration. Closed circle: without addition of Na^+ and K^+. Blue open circle: with addition of 30 mM Na^+ (ΔC_{Na}) to the reaction buffer. Red open circle: with addition of 30 mM K^+ (ΔC_K) to the reaction buffer. The concentrations of Na^+ and K^+ contained in the original rabbit reticulocyte lysate-based reaction buffer is 18 mM and 33 mM, respectively. DNA concentration was fixed at 0.3 μM.

To shed light on the effects of Na^+ and K^+ on the higher-order structure of DNA in the presence of different concentrations of SPD, we performed real-time single-molecule observation of T4 DNA fluctuating in aqueous solution by using fluorescence microscopy (FM). Figure 3.3 exemplifies the FM images of single T4 DNA molecules exhibiting translational and intramolecular Brownian motion in aqueous solution. In the absence of SPD, DNA molecules exhibit an elongated random coil conformation (Fig. 3.3a). In the presence of 0.3 mM SPD, a compact globule conformation is observed (Fig. 3.3b). With the addition of 30 mM NaCl to the solution of 0.3 mM SPD, the compact DNA molecule unfolds into an elongated coil conformation (Fig. 3.3c). This retarding effect of K^+/Na^+ on the folding transition, or coil-globule transition, corresponds to our past observation [23]. As will be discussed later, the weaker binding of K^+ to the phosphate group of DNA compared to that of Na^+ means that K^+ will have a weaker inhibitory effect to cause the folding transition.

Figure 3.4 shows histograms of the long-axis length L of DNA at different concentrations of SPD and at different Na^+ and K^+ concentrations, where L was evaluated from the FM images of

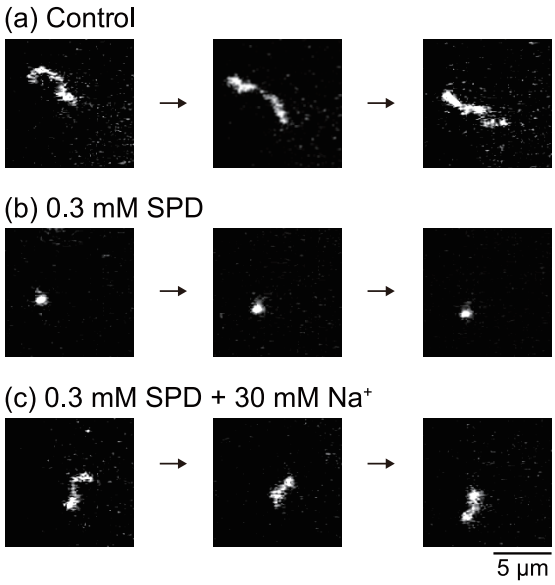

Figure 3.3 Examples of FM images of a single T4 DNA molecule undergoing Brownian motion in solution. (a) In the absence of any condensation agent such as SPD, Na^+ or K^+. (b) In the presence of 0.3 mM SPD. (c) In the presence of 0.3 mM SPD and 30 mM ΔC_{Na}. The total observation time for (a)-(c) is 3 s.

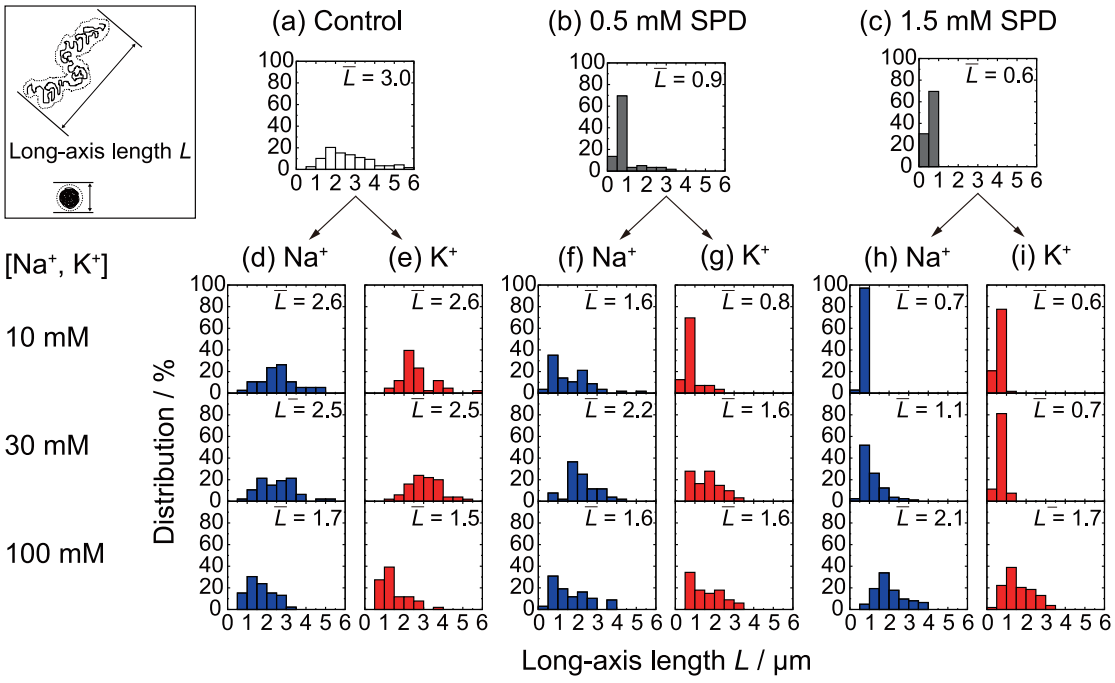

Figure 3.4 Histograms for the long-axis length L of T4 DNA at different concentrations of C_{Na} or C_K with 0 - 1.5 mM SPD.

T4 DNA molecules. The long-axis length is represented as a histogram, reflecting the effect of thermal fluctuation of intrachain Brownian motion. Figure 3.4a-c reveal the process of the folding transition from an elongated coil to a compact state, i.e., coil-globule transition. In the absence of SPD, Fig. 3.4a shows the elongated state with rather significant fluctuation. With 0.5 mM SPD, the elongated and compact states coexist (Fig. 3.4b). Finally, with 1.5 mM SPD, all of the DNA molecules are in the compact state. Figure 3.4d-i show the changes in the long-axis length L in the absence of SPD at different concentrations of Na^+ and K^+. The histograms in Fig. 3.4d,e indicate that DNA molecules tend to shrink slightly, while maintaining the elongated coil state, with an increase in the concentrations of Na^+ and K^+. On the other hand, Fig. 3.4f-i show that both Na^+ and K^+ ions tend to unfold compact DNA molecules into the elongated coil state. This inhibitory effect of monovalent cations has been reported in other recent studies and has been interpreted in terms of the competitive effect on the change in the translational entropy of the counter ions [23,24]. Interestingly, Na^+ definitely has greater potency for inducing the unfolding transition of DNA in the presence of polyamines.

To evaluate the effect of SPD on the binding affinity of Na^+ and K^+ for DNA, we performed ^1H NMR titration experiments. Figure 3.5a,b show the ^1H NMR signals of SPD in 10 mM Tris-DCl buffer (pD 7.5) observed at 400 MHz. As shown in Fig. 3.5a, the signals of SPD appear at three different chemical shifts: around δ = 3.20-3.00, 2.15-2.00 and 1.85-1.70 ppm. The assignments of the signals are given in Fig. 3.5a,b. The top signals in Fig. 3.5b indicate that the intensity of the signals in solutions containing DNA are apparently smaller than those in the absence of DNA as shown in Fig. 3.5a. Such a decrease in signal intensity is attributable to the binding of SPD to DNA, i.e., ^1H signal of the bound fraction of SPD to DNA is invisible because of a significant decrease of the transverse relaxation time, T_2 [22,25,26]. With increases in the Na^+ and K^+ concentrations, the depressed intensity caused by DNA tends to recover. Such an increase in signal intensity upon the addition of Na^+ and K^+ indicates that the degree of dissociation of SPD from DNA increases with an increase in the concentration of monovalent cations [22].

To evaluate the change in the binding affinity of SPD in the presence of Na^+ and K^+, Fig. 3.5c shows the intensity of the ^1H NMR signal of SPD plotted as a function of the Na^+ or K^+ concentration. The signal intensities in Fig. 3.5c were calculated based on the sum of all of the integrated values for the spectra of SPD. The graph shows that Na^+ has a greater effect than K^+ to suppress the binding degree of SPD to DNA molecules. Figure 3.5d shows the log-log plot of the data in Fig. 3.5c, revealing almost linear dependences. The slope of the graphs is nearly 1/3, reflecting the effect of the relative magnitudes of the plus-charge between the monovalent cation (Na^+ and K^+) and trivalent cation (SPD), as will be discussed in the following section.

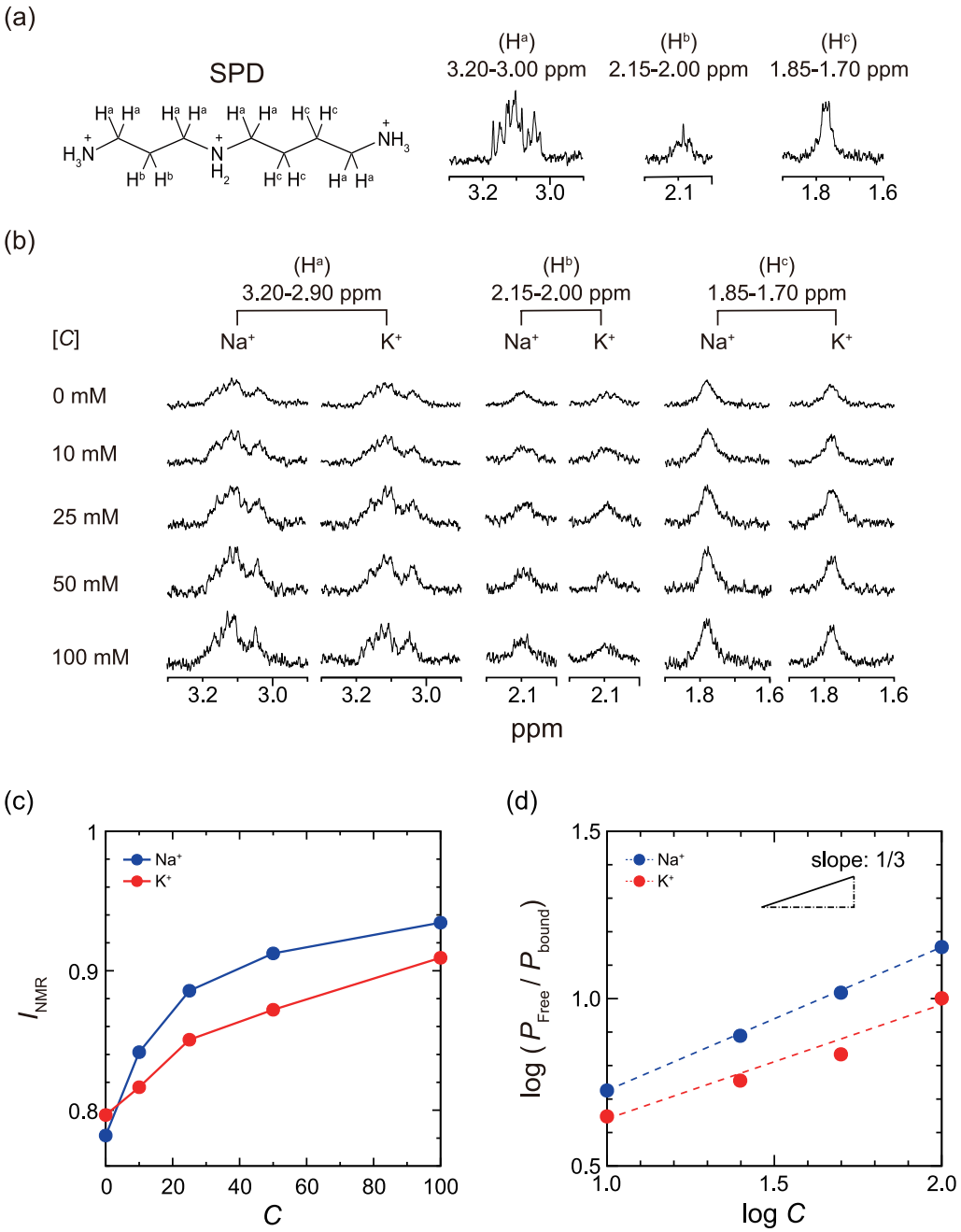

Figure 3.5 Evaluation of the binding affinity of Na^+ and K^+ for DNA through ^1H NMR measurements. (a) ^1H NMR signals of 0.1 mM SPD in D_2O solution. (b) ^1H NMR signals of 0.1 mM SPD with different concentrations of Na^+ or K^+ in the presence of 1.6 mM CT DNA. (c) Changes in the integrated intensity of ^1H NMR signals, I_{NMR}, depending on the concentrations C. The intensities in the graph were evaluated from the sum of all integrated values for the signals of SPD. (d) Log-log plot; proportion of unbound SPD to bound SPD, P_{Free}/P_{Bound}, vs. the salt concentrations C. P_{Free} and P_{Bound} are evaluated from the relationship; $P_{Free} = I_{NMR}$ and $P_{Bound} = 1 - I_{NMR}$, respectively.

3.3 Discussion

In summary, the following points have become clear in the present study: 1) K^+ enhances gene-expression in the presence of SPD more strongly than Na^+, based on *in vitro* experiments with a Luciferase assay on cell extracts; 2) Na^+ suppresses the folding transition of DNA caused by SPD more effectively than K^+, under a relatively high concentration of SPD with respect to the negatively charged phosphate moiety of DNA; and 3) Na^+ releases SPD from the binding state to DNA more strongly than K^+, under a low concentration of SPD with respect to that of the phosphate groups of DNA.

In the present study, we focused on the competitive/cooperative effect of a polyamine, SPD, and monovalent cations, Na^+ and K^+, on the DNA structure and genetic activity, since polyamines and monovalent cations naturally coexist in intracellular fluids in living cells. As has been reported previously, Na^+ tends to bind to the phosphate groups of double-strand DNA somewhat stronger than K^+ [27,28]. The results of our study reveal that this difference in binding ability between Na^+ and K^+ to the phosphate groups causes an apparent difference in the interaction of polyamine with DNA, as shown in Fig. 3.5. As for the change in the higher-order structure of DNA, it has been revealed that individual DNA molecules undergo a discrete transition from an elongated state to a compact folded state with an increase in polyamines, such as SPD and spermine [21,23,29,30]. The observation of the conformation of single DNA molecules, as reflected in the histogram in Fig. 3.4, indicates the coexistence of elongated and compact states for intermediate concentrations of SPD. Thus, an examination of Fig. 3.4 with respect to the relative ratio between the elongated and compact states indicates that Na^+ has a greater effect than K^+ to suppress the formation of the compact state through the decrease of SPD binding to DNA.

It has become evident that Na^+ inhibits DNA compaction by SPD more strongly than K^+, based on single-DNA observations in the present study and in a past report [23]. This experimental trend is easily explained in terms of the greater interfering effect of Na^+ vs. K^+ on the binding of SPD to the phosphate groups of DNA by inducing the charge neutralization of DNA, as indicated in Fig. 3.5. On the other hand, Na^+ has higher potential than K^+ for DNA compaction under a crowded environment in the absence of a polycation such as a polyamine [24]. It is well known that DNA undergoes polymer- and salt-induced (PSI) condensation, Ψ-condensation [31-33]. As reported by Zinchenko et al., for the folding transition of a giant DNA molecule under crowded conditions with polymers from an elongated coil to a compact globule, it has been confirmed that the stronger binding of a monovalent cation as with Na^+ preferentially causes the compact state, because of the enhancement of the charge neutralization of DNA [24]. In addition, in Fig. 3.5d, the slope is almost 1/3 for the log-log relationship between the monovalent cation concentration and free, or unbound, SPD. This relationship reflects the charge ratio between the monovalent

cation and SPD, and is attributable to the competition for the negatively charged phosphate groups of DNA. In relation to the issue of the interaction of polyamine to DNA, Deng, et al. reported that polyamine binds preferentially to DNA phosphate but that binding to major groove of DNA tends to increase with increasing polyamine concentrations [34]. Although such an observation seems to be informative, no experimental data were available for the polyamine concentrations to cause the change of the higher-order structure of DNA, i.e., DNA compaction, because of the experimental difficulty due to the occurrence of precipitation. As will be discussed later, the change of binding position either to phosphate or to electro-negative sites of bases in DNA is expected as an important parameter to describe the different competitive effect of Na^+ and K^+ on the interaction of polyamine to DNA.

As noted in the Introduction, the relative binding activities of Na^+ and K^+ to DNA are not so different from each other, except in specific cases, such as with four-stranded G4-DNA [7-13]. Such small difference in the manner of binding of monovalent cations to double-stranded DNA has been well explained under the theoretical framework of 'counterion condensation theory' [35-38]. This theory suggests that, for double-stranded B-DNA, ca. 76% of the intrinsic negative charges or phosphate groups are neutralized in physiological solutions by attracting monovalent cations from the environment in the absence of multivalent counter cations, and that only 24% remain dissociated to provide a negative charge on DNA [39,40]. In other words, the degree of counterion condensation around double-strand DNA is dependent mostly on the valency of counter cations and is almost independent of the species of monovalent cations.

Contrary to the expectation deduced from the theory of 'counter ion condensation', Na^+ and K^+ have dramatically different effects on gene expression as shown in Fig. 3.1. In relation to the effect of monovalent cation on gene expression, Lubin and Ennis reported that, from the experiments by adapting a cell-free system, replace of K^+ by Na^+ caused slowing down of protein synthesis [41]. They argued that such an effect was due to depression of transfer rate of amino acid from aminoacyl soluble ribonucleic acid to polypeptide. However, in their study, it was not considered the effect of the structural change in DNA. In the present study, we showed a clear correlation between DNA structural change and gene expression under different Na^+ and K^+ concentrations. As such a structural change is mainly caused by polyamines even in the presence of monovalent cations, it is regarded that the interaction of DNA with polyamines plays an essential role in the promotion/inhibition of gene expression (Fig. 3.1b,c). Future studies may seek to clarify how polyamines influence RNA and related enzymes, in addition to DNA, during the cell-free luciferase assay to gain a deeper understanding of general kinetic mechanisms in gene expression.

As for the difference between Na^+ and K^+ in the interference on the SPD binding to DNA, the mechanism is attributable to the difference in the ionic radius, i.e., the radius of Na^+ is smaller

than that of K^+ [42]. Studies with NMR measurements have reported that K^+ exhibits a slightly higher binding affinity to DNA [17,43]. Additional studies have argued that K^+ has a slightly higher affinity than Na^+ for binding to the electronegative sites of DNA bases in the minor and/or major grooves [27,28]. A study of electrophoretic mobility indicated that Na^+ exhibits stronger binding to DNA [44]. Other studies have concluded that there is no large difference in the binding constants of Na^+ and K^+ to double-strand DNA [17,27,45]. On the contrary, we found a significant difference between the effects of Na^+ and K^+ on the higher-order structure of DNA in the present and previous studies [23,24]. The small difference in the nature of binding between Na^+ and K^+ may be responsible for the difference in their effects on the higher-order structure of DNA, through competitions of large number of monovalent cations, Na^+/K^+, with number of SPD molecules for DNA binding. If we consider DNA of around the size of 100 kbp, as in Figs. 3.2, 3.3, the number of negative phosphate groups is around $2 \cdot 10^5$. This indicates that the small difference in the nature of binding of Na^+ and K^+ may induce a large difference in the higher-order structural change through the binding of SPD to the larger number of available phosphate groups.

It has been established that giant single DNA molecules above the size of several tens kilo base-pairs (kbp) undergo a large discrete transition between elongated coil and folded compact states, accompanied by a change in density on the order of 10^4-10^5 [29,30]. Thus, we may expect that Na^+ and K^+ will have different effects on both the higher-order structure and biological functions of genomic DNA through competition with polycationic species such as polyamines and histones. Allahverdi et al. reported that Na^+ and K^+ had opposite effects on nucleosome array folding [46] and on the structural integrity of chromosomes [47]. As for effect of polyamine on *in vitro* gene expression, Kanemura et al. reported biphasic effect, acceleration and complete inhibition, depending on the concentration of polyamine [21]. The complete inhibition is caused accompanying by the transition of DNA into a compact state at higher concentration of polyamine. Regarding the acceleration of gene expression at lower concentration of polyamine, a decrease of effective negative charge through the binding of polyamine was suggested to play the major role [21,22]. The surface of RNA polymerase is highly negatively charged under physiological conditions [48]. Thus, it is expected that polyamines will induce favorable conditions for RNA polymerase to get access to DNA by decreasing negative charge of both DNA and RNA polymerase [21,22]. There have been several experimental studies on the effect of monovalent cations on the activity of DNA polymerase isolated from different organisms. It was found that the enzymes from both calf thymus and Landschütz ascites tumor cells are stimulated by low concentrations of K^+ (about 2.5-fold) and Na^+ (about 1.5-fold), and higher salt concentrations had a considerable inhibitory effect [49]. Goulian et al. found that the activity of the enzyme isolated from *E. coli* B infected with bacteriophage $T4^+$ was stimulated optimally (1.5-fold) by 50 mM

KC1 or NaCl, while higher concentrations of these salts (200 mM) were strongly inhibitory, and there seemed to be no remarkable difference between K^+ and Na^+ [50]. However, it was reported that K^+ stimulates DNA polymerase of *E. Coli* B slightly more strongly than Na^+ [51]. The results regarding the effects of monovalent cations on DNA polymerase imply that the difference between the effects of K^+ and Na^+ on gene expression reported here is most probably attributable to the small difference in the binding strength of K^+/Na^+ for the large number of phosphates on giant DNA molecules with respect to competition with polyamine binding.

3.4 Conclusions

More than a half-century ago, Evans and Sorger stated the generalization that a large number of enzymes are activated by K^+ [52]. Since then many studies have focused on how K^+ and Na+ have different effects on the structure and function of individual enzymes [53,54] and negatively-charged polypeptides [55,56]. Here, we clarified that the competitive interaction with polyamines underlies the large difference between the effects of K^+ and Na^+, although there is very little difference in the nature of the interaction of these monovalent cations with DNA. Living organisms on Earth are adapted to a K^+-rich intracellular solution. The significant effect of competition of monovalent cations with other biochemical species as reported in the present study may provide ~~a~~ new insight into the strategy of living organisms to use such a K^+-rich medium, in relation to the longstanding problem of the 'origin of life' [5,57].

In the present study, it has become clear that Na^+ and K^+ have markedly different effects on the binding of a cationic polyamine, SPD, to double-strand DNA and, consequently, also on the higher-order structure of giant DNA. This significant difference between Na^+ and K^+ is expected to be associated with the general trend that living cells on Earth tend to favor K^+-rich intracellular medium. The finding that Na^+ more strongly interferes with the binding of SPD to DNA is attributable to its stronger binding to phosphate groups of DNA because of the smaller ionic radius of Na^+. On the other hand, it has been considered that there is almost no difference between Na^+ and K^+ regarding the degree of counter ion condensation along double-stranded DNA as a strongly charged polyelectrolyte. The large difference in the effects of Na^+ and K^+ on *in vitro* gene expression is attributable to the different interference effects of these monovalent cations on the binding of polyamine to DNA, at least as the main cause. Further studies on the biological effects of the competition between monovalent cations and polyamine will shed light on the longstanding unsolved problem concerning the selectivity between Na^+ and K^+ in living systems.

3.5 Materials and Methods

3.5.1 Materials

Spermidine trihydrochloride (SPD) was purchased from Nacalai Tesque (Kyoto Japan). Sodium chloride (NaCl), potassium chloride (KCl) and the antioxidant 2-mercaptoethanol (2-ME) were purchased from FUJIFILM Wako Pure Chemical Corporation (Osaka, Japan). Plasmid DNA (Luciferase T7 Control DNA: 4,331 bp) containing both the gene encoding luciferase and the promoter region of T7 RNA polymerase was purchased from Promega (Madison, WI, USA). T4 GT7 bacteriophage DNA (166 kbp with a contour length of 57 μm) was purchased from Nippon Gene (Tokyo, Japan). The dimeric cyanine fluorescent dye YOYO-1 (1,10-(4,4,8,8-tetramethyl-4,8-diazaundecamethylene)bis[4-[(3-methylbenzo-1,3-oxazol-2-yl)methylidene]-l,4-dihydroquinolinium] tetraiodide) was obtained from Molecular Probes Inc. (Eugene, OR, USA). Calf thymus DNA (CT DNA: 8-15 kbp) was purchased from Sigma-Aldrich (St. Louis, MO, USA). Other chemical reagents from commercial sources were of analytical grade.

3.5.2 Luciferase assay for gene expression

A cell-free *in vitro* luciferase assay was performed with a TnT T7 Quick Coupled Transcription/Translation System (Promega) according to the manufacturer's instructions and previous reports [21,22]. Plasmid DNA (4331 kbp) was used as the DNA template. The DNA concentration was 0.3 μM in nucleotide units. The reaction mixture containing the DNA template was incubated for 90 min at 30°C on a Dry Thermo Unit (TAITEC, Saitama, Japan). We measured the effects of the addition of various concentrations of spermidine, along with Na^+ or K^+ ions, on the luminescence intensity. The expression of luciferase was evaluated following the addition of luciferin as the luciferase substrate (Luciferase Assay Reagent, Promega) by detecting the emission intensity at around 565 nm using a luminometer (MICROTEC Co., Chiba, Japan).

3.5.3 Fluorescence microscopy (FM) observation

To visualize individual DNA molecules in solution by FM, a large DNA, T4 GT7 DNA (166 kbp), was used as described previously [22]. DNA was dissolved in a 10 mM Tris-HCl buffer solution at pH 7.5 with 4% (v/v) 2-ME. For observation of the DNA conformation in solution, desired concentrations of SPD, NaCl and KCl were added to the sample solutions. Measurements were conducted at a low DNA concentration (0.1 μM in nucleotide units) with the addition of YOYO-1 (0.05 μM). Single-molecule observations were performed with an inverted fluorescence microscope (Axiovert 135, Carl Zeiss, Oberkochen, Germany) equipped with a 100× oil-immersion objective lens. Fluorescent illumination was performed using a mercury lamp (100 W) via a filter set (Zeiss-10, excitation BP 450-490; beam splitter FT 510; emission BP 515-565).

Images were recorded onto a DVD at 30 frames per second through a high-sensitivity EBCCD (Electron Bombarded Charge-Coupled Device) camera (Hamamatsu Photonics, Shizuoka, Japan) and analyzed with the image-processing software ImageJ (National Institute of Mental Health, MD, USA). Based on the observation of time-successive images, the probability distribution of the long-axis length of DNA in solution was evaluated, and 50 DNA molecules were measured under each experimental condition.

3.5.4 NMR titration experiment

The binding abilities of SPD to CT DNA in the presence of Na^+ or K^+ were investigated by ^{1}H-NMR titration experiments. Nuclear magnetic resonance (NMR) spectra were recorded with a Bruker Ascend 400 spectrometer (400 MHz). All experiments were carried out in 10 mM Tris-DCl buffer (pD 7.5) and 3-(trimethylsilyl)-2,2',3,3'-tetradeuteropropionic acid (TMSP-d4) was used as an internal reference both for chemical shift and signal intensity. The titration samples (0.1 mM SPD and 1.6mM CT DNA) were prepared in 10 mM Tris-DCl buffer (pD 7.5). NaCl and KCl stock solutions were prepared at a concentration of 1000 mM in D_2O. The titration sample (0.6 mL) was introduced into the NMR tube, and increasing amounts of the titrant NaCl or KCl solution were added.

3.5.5 Atomic absorption spectroscopy

The concentrations of Na^+ and K^+ contained in the rabbit reticulocyte lysate-based reaction buffer of luciferase assay were measured with an atomic absorption spectrometer, AA-6800 (SHIMADZU, Kyoto, Japan). The measurements were carried out with flame atomization, and a deuterium lamp was used as background correction. The resonance lines of hollow cathode lamps (589.00 nm for Na^+ and 766.49 nm for K^+) were used. Calibration curves of Na^+ and K^+ (2, 4, 6, 8, 10 ppm) were prepared by diluting the standard solution (1,000 ppm) with 0.1 M HCl. Samples were diluted 200 times with 0.1 M HCl. Based on these measurement results, we obtained values of 18 mM and 33 mM, respectively, as the average Na^+ and K^+ concentrations in the reaction buffer.

References

[1] *DOE Handbook of methods for the analysis of the various parameters of the carbon dioxide system in sea water; version 2* (eds A. G. Dickson & C. Goyet) Chapter 5, (1994).

[2] S. H. Wright. Generation of resting membrane potential. *Adv Physiol Educ* **28**, 139-142, (2004).

[3] P. L. Weiden, W. Epstein & S. G. Schultz. Cation Transport in Escherichia coli: VII.

Potassium requirement for phosphate uptake. *J. Gen. Physiol.* **50**, 1641-1661, (1967).

[4] I. R. Booth. Regulation of cytoplasmic pH in bacteria. *Microbiol. Rev.* **49**, 359-378, (1985).

[5] A. Danchin & P. I. Nikel. Why Nature Chose Potassium. *J. Mol. Evol.* **87**, 271-288, (2019).

[6] T. Che *et al.* Natural Alkaloids and Heterocycles as G-Quadruplex Ligands and Potential Anticancer Agents. *Molecules* **23**, 493, (2018).

[7] C. C. Hardin, T. Watson, M. Corregan & C. Bailey. Cation-dependent transition between the quadruplex and Watson-Crick hairpin forms of d (CGCG3GCG). *Biochemistry* **31**, 833-841, (1992).

[8] N. V. Hud, F. W. Smith, F. A. Anet & J. Feigon. The selectivity for K^+ versus Na^+ in DNA quadruplexes is dominated by relative free energies of hydration: a thermodynamic analysis by ^{1}H NMR. *Biochemistry* **35**, 15383-15390, (1996).

[9] N. Korolev, A. P. Lyubartsev, A. Rupprecht & L. Nordenskiöld. Experimental and Monte Carlo simulation studies on the competitive binding of Li^+, Na^+, and K^+ ions to DNA in oriented DNA fibers. *J. Phys. Chem. B* **103**, 9008-9019, (1999).

[10] V. M. Marathias & P. H. Bolton. Determinants of DNA quadruplex structural type: sequence and potassium binding. *Biochemistry* **38**, 4355-4364, (1999).

[11] D. Bhattacharyya, G. Mirihana Arachchilage & S. Basu. Metal cations in G-quadruplex folding and stability. *Front. Chem.* **4**, 38/1-14, (2016).

[12] H. Tateishi-Karimata, K. Kawauchi & N. Sugimoto. Destabilization of DNA G-quadruplexes by chemical environment changes during tumor progression facilitates transcription. *J. Am. Chem. Soc.* **140**, 642-651, (2018).

[13] J. Ida *et al.* G-Quadruplexes as An Alternative Recognition Element in Disease-Related Target Sensing. *Molecules* **24**, 1079/1-30, (2019).

[14] A. Rozov *et al.* Importance of potassium ions for ribosome structure and function revealed by long-wavelength X-ray diffraction. *Nat. Commun* **10**, 2519/1-12, (2019).

[15] A. So, E. Davie, R. Epstein & A. Tissières. Effects of cations on DNA-dependent RNA polymerase. *Proc. Natl. Acad. Sci. USA* **58**, 1739-1746, (1967).

[16] U. P. Strauss, C. Helfgott & H. Pink. Interactions of polyelectrolytes with simple electrolytes. II. Donnan equilibria obtained with DNA in solutions of 1-1 electrolytes. *J. Phys. Chem.* **71**, 2550-2556, (1967).

[17] M. L. Bleam, C. F. Anderson & M. T. Record. Relative binding affinities of monovalent cations for double-stranded DNA. *Proc. Natl. Acad. Sci. USA* **77**, 3085-3089, (1980).

[18] I. Kuznetsov *et al.* Ion-exchange properties of immobilized DNA. *Reactive Polymers, Ion Exchangers, Sorbents* **3**, 37-49, (1984).

[19] P. Auffinger, L. D'ascenzo & E. Ennifar. Sodium and Potassium Interactions with Nucleic

Acids. *The Alkali Metal Ions: Their Role for Life* (eds A. Sigel, H. Sigel & R. K. O. Sigel), in *Metal Ions in Life Sciences* **16**, 167-201 (Springer, 2016).

[20] N. Korolev & L. Nordenskiöld. Influence of alkali cation nature on structural transitions and reactions of biopolyelectrolytes. *Biomacromolecules* **1**, 648-655, (2000).

[21] A. Kanemura *et al.* Opposite effect of polyamines on *In vitro* gene expression: Enhancement at low concentrations but inhibition at high concentrations. *PLoS One* **13**, e0193595/1-11, (2018).

[22] T. Nishio *et al.* Specific effects of antitumor active norspermidine on the structure and function of DNA. *Sci. Rep.* **9**, 14971/1-12, (2019).

[23] A. A. Zinchenko & K. Yoshikawa. Na^+ shows a markedly higher potential than K^+ in DNA compaction in a crowded environment. *Biophys. J.* **88**, 4118-4123, (2005).

[24] K. Hibino *et al.* Na^+ more strongly inhibits DNA compaction by spermidine (3+) than K^+. *Chem. Phys. Lett.* **426**, 405-409, (2006).

[25] K. S. Srivenugopal, D. E. Wemmer & D. R. Morris. Aggregation of DNA by analogs of spermidine: enzymatic and structural studies. *Nucleic Acids Res.* **15**, 2563-2580, (1987).

[26] Y. Yoshikawa *et al.* Effective chiral discrimination of tetravalent polyamines on the compaction of single DNA molecules. *Angew. Chem. Int. Ed. Engl.* **52**, 3712-3716, (2013).

[27] Y. Cheng, N. Korolev & L. Nordenskiöld. Similarities and differences in interaction of K^+ and Na^+ with condensed ordered DNA. A molecular dynamics computer simulation study. *Nucleic Acids Res.* **34**, 686-696, (2006).

[28] A. Savelyev & G. A. Papoian. Electrostatic, steric, and hydration interactions favor Na^+ condensation around DNA compared with K^+. *J. Am. Chem. Soc.* **128**, 14506-14518, (2006).

[29] K. Yoshikawa, M. Takahashi, V. Vasilevskaya & A. Khokhlov. Large discrete transition in a single DNA molecule appears continuous in the ensemble. *Phys. Rev. Lett.* **76**, 3029-3031, (1996).

[30] M. Takahashi, K. Yoshikawa, V. Vasilevskaya & A. Khokhlov. Discrete coil-globule transition of single duplex DNAs induced by polyamines. *J. Phys. Chem. B* **101**, 9396-9401, (1997).

[31] C. B. Post & B. H. Zimm. Internal condensation of a single DNA molecule. *Biopolymers* **18**, 1487-1501, (1979).

[32] A. Y. Grosberg, I. Y. Erukhimovitch & E. Shakhnovitch. On the theory of Ψ-condensation. *Biopolymers* **21**, 2413-2432, (1982).

[33] S. B. Zimmerman. Macromolecular crowding effects on macromolecular interactions: some implications for genome structure and function. *Biochim. Biophys. Acta* **1216**, 175-

185, (1993).

[34] H. Deng, V. A. Bloomfield, J. M. Benevides & G. J. T. Jr. Structural basis of polyamine-DNA recognition: spermidine and spermine interactions with genomic B-DNAs of different GC content probed by Raman spectroscopy. *Nucleic Acids Res.* **28**, 3379-3385, (2000).

[35] G. S. Manning. Limiting laws and counterion condensation in polyelectrolyte solutions I. Colligative properties. *J. Chem. Phys.* **51**, 924-933, (1969).

[36] F. Oosawa. *Polyelectrolytes* Chapter 5, 51-62 (Marcel Dekker, 1971)

[37] M. O. Fenley, G. S. Manning & W. K. Olson. Approach to the limit of counterion condensation. *Biopolymers* **30**, 1191-1203, (1990).

[38] D. H. Turner. in *Nucleic Acids: Structures, Properties and Functions* (eds V. A. Bloomfield, D. M. Crothers, & I. J. Tinoco) Chapter 8, 259-334 (University Science Press, 2000).

[39] G. S. Manning. The molecular theory of polyelectrolyte solutions with applications to the electrostatic properties of polynucleotides. *Q. Rev. Biophys.* **11**, 179-246, (1978).

[40] M. Deserno, C. Holm & S. May. Fraction of condensed counterions around a charged rod: Comparison of Poisson− Boltzmann theory and computer simulations. *Macromolecules* **33**, 199-206, (2000).

[41] M. Lubin & H. L. Ennis. On the role of intracellular potassium in protein synthesis. *Biochimica Et Biophysica Acta (BBA)-Specialized Section on Nucleic Acids and Related Subjects* **80**, 614-631, (1964).

[42] I. Rouzina & V. A. Bloomfield. Competitive electrostatic binding of charged ligands to polyelectrolytes: planar and cylindrical geometries. *J. Phys. Chem.* **100**, 4292-4304, (1996).

[43] V. P. Denisov & B. Halle. Sequence-specific binding of counterions to B-DNA. *Proc. Natl. Acad. Sci. USA* **97**, 629-633, (2000).

[44] E. Stellwagen, Q. Dong & N. C. Stellwagen. Monovalent cations affect the free solution mobility of DNA by perturbing the hydrogen-bonded structure of water. *Biopolymers* **78**, 62-68, (2005).

[45] H. Sigel. Interactions of metal ions with nucleotides and nucleic acids and their constituents. *Chem. Soc. Rev.* **22**, 255-267, (1993).

[46] A. Allahverdi, Q. Chen, N. Korolev & L. Nordenskiöld. Chromatin compaction under mixed salt conditions: opposite effects of sodium and potassium ions on nucleosome array folding. *Sci. Rep.* **5**, 8512/1-7, (2015).

[47] R. Strick, P. L. Strissel, K. Gavrilov & R. Levi-Setti. Cation-chromatin binding as shown by ion microscopy is essential for the structural integrity of chromosomes. *J. Cell Biol.*

155, 899-910, (2001).

[48] P. Cramer, D. A. Bushnell & R. D. Kornberg. Structural basis of transcription: RNA polymerase II at 2.8 Ångstrom resolution. *Science* **292**, 1863-1876, (2001).

[49] H. M. Keir. DNA Polymerases from Mammalian Cells. in *Progress in Nucleic Acid Research and Molecular Biology* **4** (eds J. N. Davidson & W. E. Cohn), 81-128 (Elsevier, 1965).

[50] M. Goulian, Z. J. Lucas & A. Kornberg. Enzymatic Synthesis of Deoxyribonucleic Acid. *J. Biol. Chem.* **243**, 627-638, (1968).

[51] H. Klenow & I. Henningsen. Effect of monovalent cations on the activity of the DNA polymerase of Escherichia coli B. *Eur. J. Biochem.* **9**, 133-141, (1969).

[52] C. Suelter. Enzymes activated by monovalent cations. *Science* **168**, 789-795, (1970).

[53] M. J. Page & E. Di Cera. Role of Na^+ and K^+ in enzyme function. *Physiol. Rev.* **86**, 1049-1092, (2006).

[54] D. W. Gohara & E. Di Cera. Molecular mechanisms of enzyme activation by monovalent cations. *J. Biol. Chem.* **291**, 20840-20848, (2016).

[55] M. V. Fedorov, J. M. Goodman & S. Schumm. To switch or not to switch: the effects of potassium and sodium ions on α-poly-l-glutamate conformations in aqueous solutions. *J. Am. Chem. Soc.* **131**, 10854-10856, (2009).

[56] M. Hasuike, S. Kuroki & M. Satoh. Double conformational transition of alkali metal poly (l-glutamate) s in aqueous ethanol: counterion mixing effect revisited. *Biophys. Chem.* **165**, 48-55, (2012).

[57] G. Ling. The new cell physiology: an outline, presented against its full historical background, beginning from the beginning. *Physiol. Chem. Phys. Med. NMR* **26**, 121-203, (1994).

Chapter 4

Longer DNA exhibits greater potential for cell-free gene expression [v]

4.1 Introduction

Gene expression in living cells is strictly self-regulated to ensure that the correct amounts of proteins are made at the most appropriate timing and location for maintaining cellular homeostasis. Gene regulation can occur at any point in gene expression, from the start of the transcription phase to the translation phase. Due to the complexity of gene regulation, unveiling the complete mechanism of gene regulation has been a long-standing quest. To elucidate the complex mechanism of gene regulation in living cellular systems, it is necessary to closely investigate each phase of gene expression and also to shed light on the cooperative effects between transcription and translation. One of the best methods for such an investigation may be the use of a coupled transcription/translation system which allows artificial control of the experimental conditions *in vitro*[1-3]. The methodology of cell-free gene expression developed during the last couple of decades in molecular biology is expected to provide a useful experimental system for the purpose to gain deeper insights into the coupled transcription/translation dynamics [1-3]. In this regard, cell-free gene expression systems are one of the most widely used techniques in molecular biology [1-3]. The efficiency of cell-free gene expression is known to be affected by various factors such as vector type [4-7], DNA topology [4-7], and reaction components [8-11], as well as the template DNA concentration [12-14]. It is noted that there exists a longstanding controversy regarding the topological effect of supercoiling, or linking number, in circular DNAs on their genomic activity [4-7]. Although these factors have been studied extensively, little is known about how the length of the DNA template influences gene expression. The aforementioned complex factors have made it difficult to investigate the impact of the DNA length on gene regulation, which has been an unexplored topic. In the present study, we evaluated the efficiency of protein translation, focusing on the effect of DNA templates of different lengths on cell-free protein synthesis using a luciferase assay. To exclude the influence of supercoiling, we used linear DNA molecules (PCR amplicons or linearized by restriction enzyme) as a template.

4.2 Results

We compared the levels of gene expression of reporter DNAs encoding the firefly luciferase gene (*luc*-gene) with different lengths of 1,717 bp, 4,331 bp, and 25,690 bp; hereafter we may call as *luc*1.7k, *luc*4.3k and *luc*25.7k, respectively (Fig. 4.1a-c). We used three different conditions: the same *luc*-gene concentration (Fig. 4.1d), the same nucleotide-unit concentration (Fig. 4.1e), and a combination of both (the same *luc*-gene and nucleotide-unit concentration adjusted by the addition of noncoding DNA, *nc*2.6k) (Fig. 4.1f). The expression level from *luc*25.7k is 1,000-times higher than that with *luc*1.7k, indicating that the protein yield per target gene is increased by 1,000-times of magnitude for a longer template, *luc*25.7k (Fig. 4.1d). Under the condition of the same nucleotide-unit concentration, where the concentrations of the targets are inversely proportional to the length of DNA molecules (Fig. 4.1e), the expression level from *luc*25.7k is highest despite the fact that *luc*25.7k has the fewest targets. Interestingly, in a comparison of *luc*1.7k and *luc*4.3k, *luc*4.3k induced a 7-times (Fig. 4.1d) and 2-times (Fig. 4.1e) increase in the gene expression level, respectively. These findings indicate that deletion of a 2.6-kb noncoding region results in a lower protein yield, i.e., the magnitude of gene expression increases when the luciferase-coding region is connected to the noncoding region. To validate this result, the level of gene expression was compared under the condition that both the amount of *luc*-gene and the nucleotide concentration were unified by the addition of extra *nc*2.6k to the reaction buffer (Fig. 4.1f). It is shown that the addition of *nc*2.6k to *luc*1.7k and *luc*4.3k caused an order of magnitude greater protein yields (Fig. 4.1d,f), suggesting the intrinsic effect of nucleotide concentration on gene expression efficiency. Nevertheless, it is clear that the expression efficiency per target is enhanced significantly when the length of the template DNA molecule is longer (Fig. 4.1f).

The above results clearly indicate that the level of gene expression markedly increased in response to an increase in the length of templates, in addition to the effect of nucleotide concentration in the reaction buffer solution. It is revealed that the potency of expression is in the order of *luc*25.7k > *luc*4.3k > *luc*1.7k under all conditions tested here (Fig. 4.1). It depends not on the number of targets, but rather on the length of the template DNA. These results also suggest that the noncoding region in reporter DNAs is involved in the regulation of gene expression.

The design of the linear DNAs shown in Fig. 4.1 may not be convincing enough to investigate the influence of DNA length on gene expression as the non-specific sequences of both up and down streams of the T7 RNA promoter are different in each gene. To address the concern in experimental design, we next designed an *in vitro* translation assay with four kinds of reporter genes of different nucleotide lengths. The four reporter DNAs encoding firefly luciferase with a T7 promoter were obtained from an identical 25.7-kbp plasmid DNA cleaved with restriction

enzyme Sal I, Afl II, Aat II, or ApaL I, respectively (Fig. 4.2a). Sal I yields a single 25.7-kbp linear reporter gene, and the other enzymes generate reporter genes of different lengths with non-coding DNA fragments (Fig. 4.2b). The resulting DNA mixtures with reporter genes of different lengths (ApaLI 2.8k, AatII 3.3k, AflII 11.2k and *luc*25.7k) were used to evaluate their translational efficiency as DNA templates for continuous coupled transcription/translation. As expected, reporter gene expression increased in a nucleotide-length-dependent manner on the DNA templates while the amount and composition of nucleotides remained identical in each reaction (Fig. 4.2c,d). These results strongly suggest that DNA length positively affects gene activities in a cell-free gene expression system.

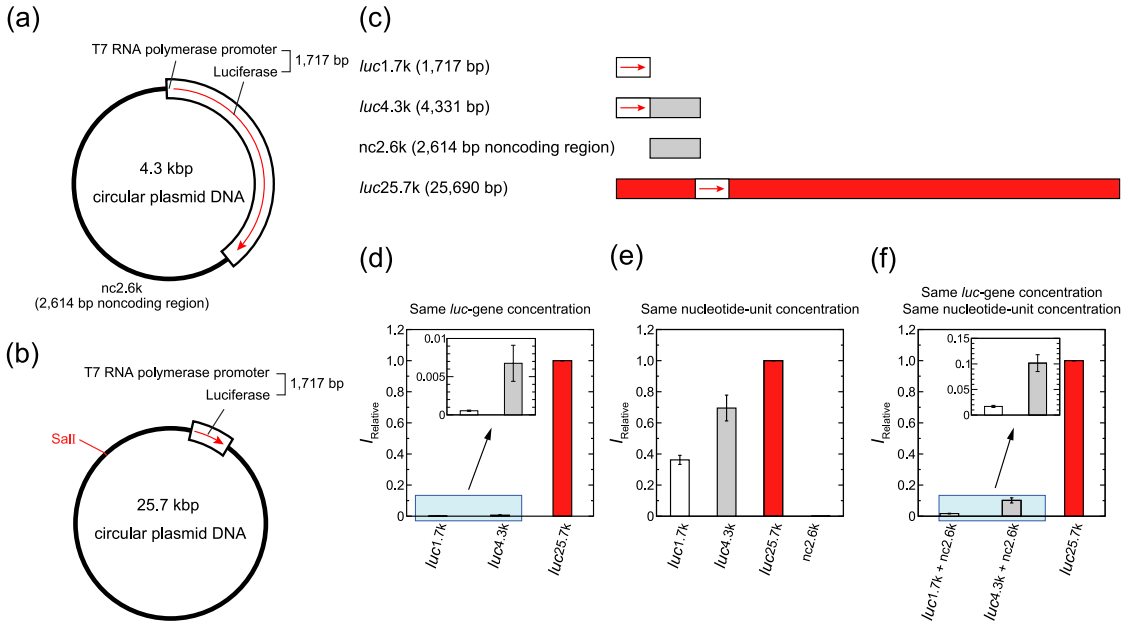

Figure 4.1 Effects of various factors on the efficiency of gene expression. (a)(b) Schematic diagram of the parental 4.3-kbp and 25.7-kbp plasmid DNAs. The white box on the plasmid DNA represents a firefly luciferase reporter gene with a T7 promoter. The red arrow in the white box shows the direction of reporter gene transcription. (c) DNA fragments resulting from Sal I digestion of the parental 25.7-kbp plasmid or PCR amplification. Sal I yields a single 25.7-kbp linear reporter gene. A 1.7-kbp reporter gene, a 4.3-kbp reporter gene, and a 2.6-kbp non-coding DNA fragment were prepared by standard PCR. The 25.7-kbp linear reporter gene and the 2.6-kbp non-coding DNA region are colored in red and gray, respectively. (d)(e)(f) Efficiency, *I*, of the coupled transcription/translation reaction of *luc*-gene, as evaluated from the change of luminescence intensity. The same *luc*-gene concentration (0.12 μM, (d)), the same nucleotide-unit concentration (1.8 μM, (e)), or a combination of both (the same *luc*-gene and nucleotide-unit concentration) (0.12 μM and 1.8 μM, (f)) of reporter genes. In (d)-(f), the longitudinal axis shows the relative luminescence intensity normalized to that of *luc*25.7k. The relative protein expression levels with *luc*25.7k are presented as means ± SD of at least five independent experiments.

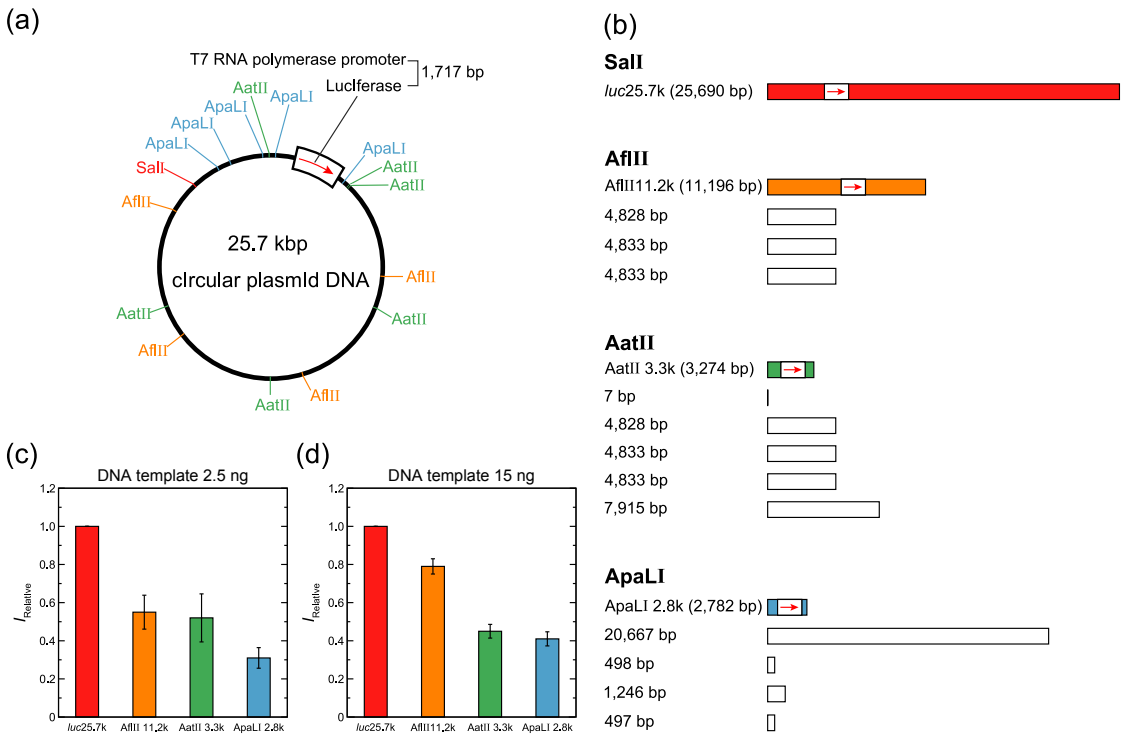

Figure 4.2 Nucleotide-length dependency of the coupled transcription/translation of the *luc*-gene. (a) Schematic diagram of the parental 25.7-kbp plasmid DNA with restriction enzyme digestion sites. The white box on the plasmid DNA represents a firefly luciferase reporter gene with a T7 promoter. The red arrow in the white box shows the direction of reporter gene transcription. (b) DNA fragments resulting from enzyme digestion reactions of the parental plasmid. Sal I yields a single 25.7-kbp linear reporter gene. Afl II, Aat II and ApaL I generate a 11.2-kbp reporter gene and three kinds of 4.8-kbp non-coding DNA fragments, a 3.3-kbp reporter gene and five kinds of non-coding DNA fragments (7-bp, three 4.8-kbp and 7.9-kbp lengths), and a 2.8-kbp reporter gene and four kinds of non-coding DNA fragments (20.7-kbp, 1.2-kbp and two 0.5-kbp lengths), respectively. The reporter genes in the DNA fragments are colored red for Sal I, orange for Afl II, green for Aat II and light blue for ApaL I treatments, respectively. (c)(d) Efficiency, *I*, of the coupled transcription/translation reaction of *luc*-gene, as evaluated from the luminescence intensity. 2.5 ng (c) and 15 ng (d) of digested DNA mixtures were used as DNA templates for the reaction. In (c), (d), the longitudinal axis shows the relative luminescence intensity normalized to that of *luc*25.7k. The relative protein expression levels with *luc*25.7k are presented as means ± SD of at least five independent experiments.

To determine the effect of reporter gene size on gene expression activity, single-molecule observations of each linear reporter gene were performed by AFM. The AFM images of each DNA in 10 mM Tris-HCl buffer (pH7.5) revealed a linearized structure, indicating that DNA molecules tend to exhibit a more winding structure as their length increases (Fig. 4.3a). Notably,

in a 0.05% reaction mixture for *in vitro* gene expression, *luc*25.7k formed a shrunken structure with a higher density of DNA segments than that of *luc*4.3k and *luc*1.7k (Fig. 4.3b). Based on these observations, we consider that the sliding and hopping behaviors of RNA polymerase, which have been studied extensively, is enhanced with longer DNA. In addition, proteins coexisting in the gene expression reaction buffer tend to localize onto the shrunken conformation for the larger DNA molecules, suggesting that the effective affinity of RNA polymerase for DNA is enhanced in longer DNA (see the schematic representations on the lower pictures in Fig. 4.3b). In the following discussion, we may argue the mechanism on the promotion of gene expression in relation to the physico-chemical characteristics of longer DNA molecules.

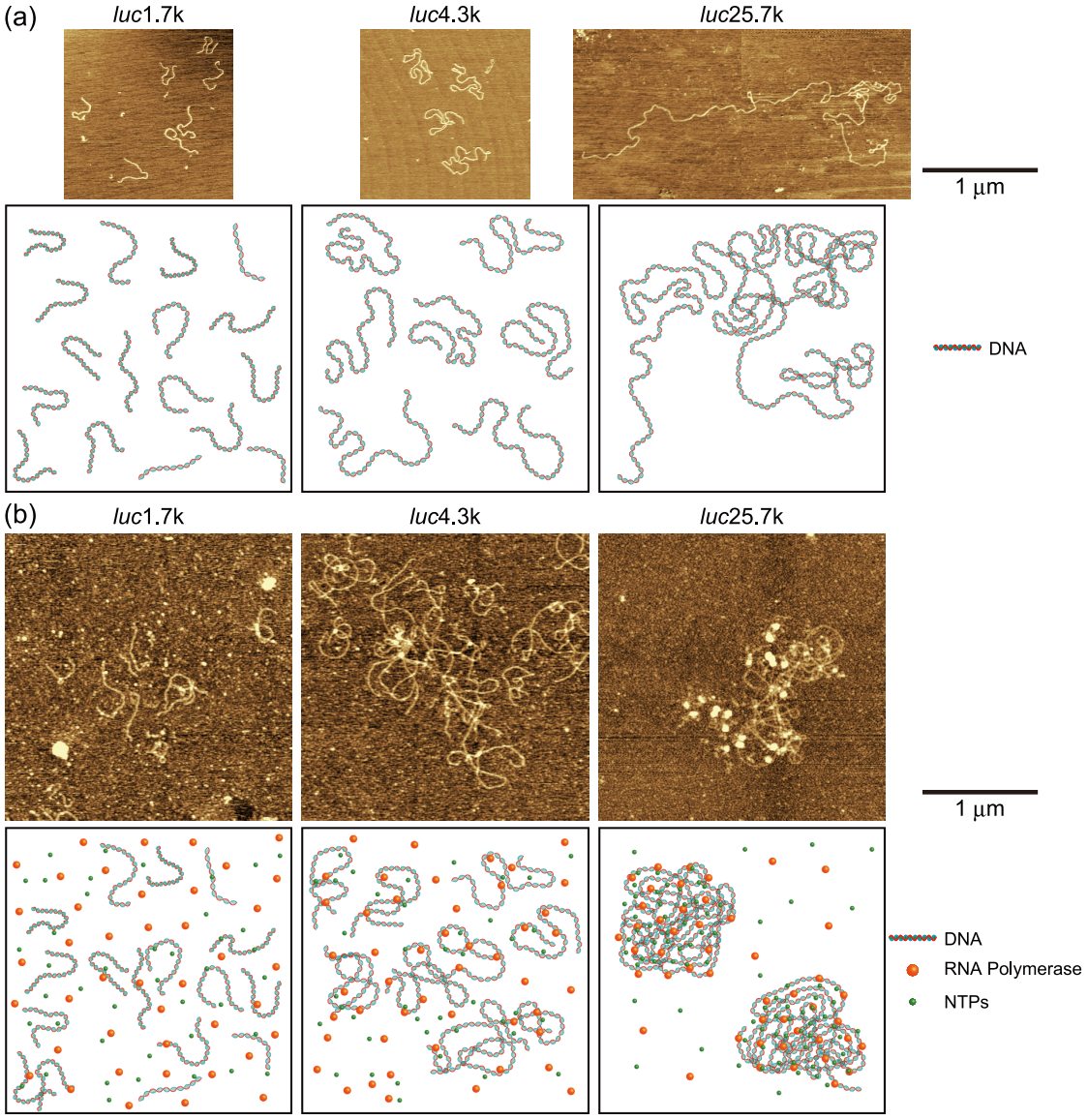

Figure 4.3 AFM images of reporter DNAs with different lengths together with the schematic representations. (a) AFM images of each linear reporter DNAs in 10 mM Tris-HCl buffer (pH7.5). (b) AFM images of each linear reporter DNA in a 0.05% reaction mixture for *in vitro* gene expression.

Cells regulate gene expression to maintain cellular functions. Gene expression starts with transcription and is continuously followed by translation events. Hence, the initiation of transcription is an efficient point for controlling protein production. In the present study, we demonstrated that DNA length is a crucial factor for gene expression by using a coupled transcription/translation system. The positive effects of DNA length on gene expression efficiency can mainly be explained by increased transcription activity, while mRNA stability, nucleases' activity, and template degradation should also be taken into account. In fact, it appeared that mRNA was slightly less stable than ribosomal RNA when the stability of mRNA in reticulocyte cell lysates was examined by RT-qPCR (Table. 4.1). Meanwhile, it is noted that the lengths and stabilities of transcripts from each reporter gene in Fig. 4.2 are the same as those of nucleotide from the T7 promoter to its terminator. It is thus regarded that the translation phase is not involved in controlling gene expression in the present experiments in a cell-free system.

Table 4.1 RT-qPCR quantification of mRNA stability. Time course mRNA measurement for quantification of mRNA stability in cell lysates was performed by RT-qPCR. The amount of luciferase mRNA and 18S rRNA in each sample was normalized to no incubated samples, respectively: $\Delta C_T = C_T$ (30, 60, and 90 min) - C_T (0 min). $\Delta\Delta C_T$ values were determined by subtracting the ΔC_T values for S18S rRNA from the ΔC_T values for luciferase mRNA. Results are for two independent experiments.

Templates	Time (min)	C_T	ΔC_T*	$\Delta\Delta C_T$**
Luc mRNA	0	12.1 ± 0.7	–	–
	30	11.7 ± 0.0	-0.4	-0.1
	60	12.3 ± 0.1	0.2	0.5
	90	12.8 ± 0.1	0.7	1.0
18S rRNA	0	17.2 ± 0.5	–	–
	30	16.7 ± 0.1	-0.3	–
	60	16.9 ± 0.1	-0.3	–
	90	16.9 ± 0.2	-0.3	–

*$\Delta C_T = C_T$ (incubate time (min)) - C_T (0 min)

*$\Delta\Delta C_T = \Delta C_T$ (Luc mRNA) - ΔC_T (18S rRNA)

4.3 Discussion

A plausible mechanism for the promoting effect of DNA length on transcriptional efficiency may be represented by the difference in the conformation of DNA molecules. It is getting clearer that the higher-order structure of the template DNA molecule plays an important role as a

controlling factor on the activity of gene expression. To date, not a number of studies have reported that transcriptional condensates with genomic DNA serve as regulatory hubs in gene expression [15-24]. As for the characteristic property of the high-order structure on DNA, it has been established that giant DNA above the size of several tens kbp undergoes a large discrete transition from an elongate coil state into a tightly compact state, accompanied by the increase of concentration of various polycationic species such as polyamines [25,26]. It is known that transcriptional activity is completely inhibited in the tightly compact state [27,28]. Recently, it has been found that gene expression is promoted at the lower concentrations of polyamines than the concentration that causes compaction [9]. That is, maximum expression is generated in the shrunken state where the density of DNA segments is higher than in the elongated coil state by avoiding tight packing. Inspection for the actual structure of the shrunken conformation has indicated enhancement of parallel orientation between DNA segments in a shrunken state of long DNA [9,10,29]. In other words, the basic property of the alignment of DNA segments resembles that of liquid crystals, where rod-like elements prefer to be arranged in parallel under weak repulsive interactions [9].

If we consider the above-mentioned effect of the shrunken conformation in the reaction mixture on gene expression, we can expect that formation of the shrunken conformation with a preference for parallel alignment accelerates gene expression and that such a promoting effect would be caused by the greater ability of RNA polymerase to access shrunken DNA. We denote the length of template DNA as L, corresponding to the 'contour length' in the definition of polymer physics[30]. For simplicity, if we assume that the average distance between DNA segments is nearly constant, the volume, v, of a DNA molecule in the shrunken state would exhibit a scaling relationship with L as $v \sim L$, which is different from a polymer chain in a good solvent, $v \sim L^{\frac{9}{5}}$, and an ideal chain, $v \sim L^{\frac{3}{2}}$ [30]. The preferential binding of RNA polymerase together with the enhanced location of NTPs would be effective in the inner volume of the shrunken state. Thus, we may consider that the effective volume of the active region of translation is given by subtracting the infectivity on the surface region: $v_E \sim (L - \alpha L^{\frac{2}{3}})$, where we used an approximation of scaling relationships; $v \sim L$, $[\text{Surface Area}] \sim L^{\frac{2}{3}}$, and α is a positive constant. Now, we may evaluate the relative activity of gene expression as in the case of Fig. 4.1e. By taking the variables n (number density of DNA) and C (density of DNA in base pair units), the relationship is obtained as in $nL = C$. From these relationships, the total active volume of DNA molecules is deduced to be $V_E \sim nv_E \sim \frac{C}{L}\left(L - \alpha L^{\frac{2}{3}}\right) = C(1 - \alpha L^{-\frac{1}{3}})$. Thus, the value $L^{-\frac{1}{3}}$

corresponds to the degree of the decrease in gene expression, which is 2.5, 2.0 and 1.0 for template DNAs of *luc*1.7k, *luc*4.3k and *luc*25.7k, respectively. By taking the gene expression of *luc*1.7k as a control, the increase in activity is estimated from the calculations of "2.5 - 2.0 = 0.5" and "2.5 - 1.0 = 1.5", i.e., 0.5 and 1.5, for *luc*4.3k and *luc*25.7k, respectively. These expected values of the increase in genetic activities correspond to the observed experimental trend, despite the simplicity of the theoretical argument.

4.4 Conclusions

In the present article, we found that longer DNA enhances the efficiency of gene expression. It is known that DNA molecules much larger than the persistence length (150-200 bp) behave as semiflexible polymer chains [31-33]. Here, it has become clear that such relatively long DNA molecules exhibit a shrunken conformation in reaction buffer, which increases the opportunity for encountering RNA polymerase and NTPs due to an increase in their effective concentration around DNA. Although the discovery of the size effect of DNA on gene expression is still in a preliminary stage, it would be promising to extend this insight by shedding light on the actual mechanisms of gene regulation in living cells through extensive studies for longer DNA molecules with the sizes of Mbp-Gbp. It would also be interesting to examine the effect of DNA length on the activity of other enzymes, such as restriction enzymes, DNA repair enzymes, DNA polymerase, etc.

4.5 Materials and Methods

4.5.1 Preparation of linear reporter genes by PCR

A 4.3-kbp plasmid DNA (Luciferase T7 Control DNA: 4,331 bp) was purchased from Promega (Madison, WI, USA). A 1.7-kbp linear reporter DNA, a 4.3-kbp linear reporter DNA and a 2.6-kbp linear non-coding DNA were amplified by PCR using the following primers: for the 1.7-kbp linear DNA (forward 5′-TAATACGACTCACTATAGGGAGACC-3′; reverse 5′-CAATTTGGACTTTCCGCCCTTC-3′); for the 4.3-kbp linear DNA (forward 5′-TAATACGACTCACTATAGGGAGACC-3′; reverse 5′-ATTTCGATAAGCCAGCTGC-3′); and for the 2.6-kbp non-coding DNA (forward 5′-CTGTATTCAGCGATGACGAAATTC-3′; reverse 5′-ATTTCGATAAGCCAGCTGC-3′). 1 ng of the 4.3-kbp parental plasmid was used as a template for PCR. PCR was performed with KOD FX neo (Toyobo, Tokyo, Japan) using a Thermal Cycler Dice (TP600) (Takara Bio Inc, Shiga, Japan), according to the manufacturer's protocol. The PCR products were precipitated with 0.3 M sodium acetate/ethanol, washed with 70% ethanol, and dried. The DNA pellets were dissolved in 50 μL of TE buffer (pH 8.0) and

stored at -20°C until use. Each template DNA was analyzed using a DNA ladder marker (1kbp DNA Ladder One, Nacalai Tesque, Kyoto, Japan) by standard 1% agarose gel electrophoresis (Fig. 4.4a).

4.5.2 Preparation of linear reporter genes by restriction enzyme treatment

A parental 25.7-kbp plasmid DNA was purchased from Kazusa Genome Technologies (Chiba, Japan). Restriction enzymes Sal I, Afl II, Aat II and ApaL I were purchased from Takara Bio Inc. 2 μg of the 25.7-kbp plasmid was cleaved with 30 U of each restriction enzyme in 100 μL of T buffer (Takara Bio Inc) containing 0.1% BSA. The reaction mixtures were incubated for 120 min at 37°C. After enzymatic digestion, the DNA mixtures were precipitated with 0.3 M sodium acetate/ethanol, washed with 70% ethanol, and dried. The DNA pellets were dissolved in 50 μL of TE buffer (pH 8.0) and stored at -20°C until use. Each digested DNA was analyzed using a DNA ladder marker (1kbp DNA Ladder One, Nacalai Tesque, Kyoto, Japan) by standard 1% agarose gel electrophoresis (Fig. 4.4b).

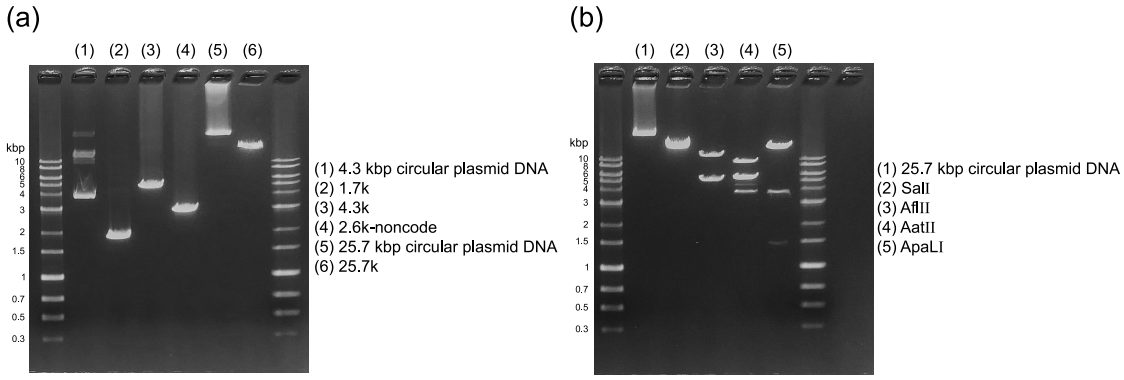

Figure 4.4 Gel electrophoresis analysis. (a) Parental 4.3 kbp and 25.7 kbp plasmid DNAs and linearized DNAs obtained from each of these circular plasmid DNAs. (b) Reporter genes of different lengths with non-coding DNA fragments generated by each restriction enzyme.

4.5.3 AFM observation

For AFM imaging using an SPM-9700 (Shimadzu, Kyoto, Japan) with a High-Throughput Scanner (Shimadzu, Kyoto, Japan), 0.3 μM DNA was dissolved in 10 mM Tris-HCl buffer (pH 7.5) including 10 μM spermidine or in 0.05% TnT Quick Master Mix (*in vitro* gene expressions reaction mixture). The DNA solutions were transferred onto a freshly cleaved mica surface and then incubated for 10-30 min at room temperature (24°C). Subsequently, the samples were rinsed with ultra-pure water, dried with nitrogen gas and imaged by AFM. All measurements were performed in air using the tapping mode. The cantilever, OMCL-AC200TS-C3 (Olympus, Tokyo, Japan), was 200 μm long with a spring constant of 9-20 N/m. The scanning rate was 2 Hz and

images were captured using the height mode in a 512 × 512 pixel format. The obtained images were plane-fitted and flattened by the computer program supplied with the imaging module.

4.5.4 Luciferase reporter assay

Cell-free *in vitro* transcription/translation of *Luc*-gene was performed with a TnT T7 Quick Coupled Transcription/Translation System (Promega) according to the manufacturer's instructions and previous reports [9-11]. Reaction mixtures containing the reporter DNAs were incubated for 90 min at 30°C on a Dry Thermo Unit (TAITEC, Saitama, Japan). The expression levels of luciferase were evaluated following the addition of luciferin as a luciferase substrate (Luciferase Assay Reagent, Promega) by detecting the emission intensity at around 565 nm using a luminometer (MICROTEC Co., Chiba, Japan).

4.5.5 Evaluation of mRNA stability

A 1.7 kb luciferase mRNA was mixed with reticulocyte cell lysates in a TnT T7 Quick Coupled Transcription/Translation System (Promega). After 0, 30, 60 and 90 mins incubation at 30°C, the total RNAs were isolated using ISOGEN (Nippon Gene Co., Ltd.), according to the manufacturer's protocol. First strand cDNAs were reverse-transcribed from 200 ng of the RNA samples, using a random primer and PrimeScript™ II 1st strand cDNA Synthesis Kit (Takara Bio Inc.), according to the manufacturer's protocol. The cDNAs were subjected to qPCR using a pair of luciferase primers for quantification of luciferase mRNA [5'-GCG CGG AGG AGT TGT GTT-3' and 5'-TCT GAT TTT TCT TGC GTC GAG TT-3'], and a primer pair for quantification of S18 rRNA [5'-AAA CGG CCA CCA CAT CCA AG-3' and 5'-CAA TTG CAG GGC TCT CGA AG-3'].

References

[1] F. Katzen, G. Chang & W. Kudlicki. The past, present and future of cell-free protein synthesis. *Trends Biotechnol.* **23**, 150-156, (2005).

[2] E. D. Carlson, R. Gan, C. E. Hodgman & M. C. Jewett. Cell-free protein synthesis: applications come of age. *Biotechnol. Adv.* **30**, 1185-1194, (2012).

[3] A. D. Silverman, A. S. Karim & M. C. Jewett. Cell-free gene expression: an expanded repertoire of applications. *Nat. Rev. Genet.* **21**, 151-170, (2020).

[4] N. Ballas, N. Zakai, D. Friedberg & A. Loyter. Linear forms of plasmid DNA are superior to supercoiled structures as active templates for gene expression in plant protoplasts. *Plant Mol. Biol.* **11**, 517-527, (1988).

[5] J.-H. Ahn *et al.* Cell-free synthesis of recombinant proteins from PCR-amplified genes at

a comparable productivity to that of plasmid-based reactions. *Biochem. Biophys. Res. Commun.* **338**, 1346-1352, (2005).

[6] S. Youn Jun, S. Hyeon Kang & K.-H. Lee. Continuous-exchange cell-free protein synthesis using PCR-generated DNA and an RNase E-deficient extract. *BioTechniques* **44**, 387-391, (2008).

[7] R. N. Irobalieva *et al.* Structural diversity of supercoiled DNA. *Nat. Commun* **6**, 1-11, (2015).

[8] D. M. Kim & J. R. Swartz. Prolonging cell-free protein synthesis by selective reagent additions. *Biotechnol. Prog.* **16**, 385-390, (2000).

[9] A. Kanemura *et al.* Opposite effect of polyamines on *In vitro* gene expression: Enhancement at low concentrations but inhibition at high concentrations. *PLoS One* **13**, e0193595/1-11, (2018).

[10] T. Nishio *et al.* Specific effects of antitumor active norspermidine on the structure and function of DNA. *Sci. Rep.* **9**, 14971/1-12, (2019).

[11] T. Nishio *et al.* K^+ promotes the favorable effect of polyamine on gene expression better than Na^+. *PloS one* **15**, e0238447/1-13, (2020).

[12] D. Siegal-Gaskins, Z. A. Tuza, J. Kim, V. Noireaux & R. M. Murray. Gene circuit performance characterization and resource usage in a cell-free "breadboard". *ACS Synth. Biol.* **3**, 416-425, (2014).

[13] S. J. Moore *et al.* Rapid acquisition and model-based analysis of cell-free transcription-translation reactions from nonmodel bacteria. *Proc. Natl. Acad. Sci. U. S. A.* **115**, E4340-E4349, (2018).

[14] R. Marshall & V. Noireaux. Quantitative modeling of transcription and translation of an all-E. coli cell-free system. *Sci. Rep.* **9**, 11980/1-12, (2019).

[15] M. Golkaram, S. Hellander, B. Drawert & L. R. Petzold. Macromolecular crowding regulates the gene expression profile by limiting diffusion. *PLoS Comp. Biol.* **12**, e1005122/1-16, (2016).

[16] K. M. Harlen & L. S. Churchman. The code and beyond: transcription regulation by the RNA polymerase II carboxy-terminal domain. *Nat. Rev. Mol. Cell Biol.* **18**, 263-273, (2017).

[17] D. Hnisz, K. Shrinivas, R. A. Young, A. K. Chakraborty & P. A. Sharp. A phase separation model for transcriptional control. *Cell* **169**, 13-23, (2017).

[18] Z. Hu & W.-W. Tee. Enhancers and chromatin structures: regulatory hubs in gene expression and diseases. *Biosci. Rep.* **37**, BSR20160183/1-13, (2017).

[19] M. Boehning *et al.* RNA polymerase II clustering through carboxy-terminal domain phase separation. *Nat. Struct. Mol. Biol.* **25**, 833-840, (2018).

[20] A. Boija *et al.* Transcription factors activate genes through the phase-separation capacity of their activation domains. *Cell* **175**, 1842-1855. e1816, (2018).

[21] S. Chong *et al.* Imaging dynamic and selective low-complexity domain interactions that control gene transcription. *Science* **361**, eaar2555/1-9, (2018).

[22] B. R. Sabari *et al.* Coactivator condensation at super-enhancers links phase separation and gene control. *Science* **361**, eaar3958/1-11, (2018).

[23] P. Cramer. Organization and regulation of gene transcription. *Nature* **573**, 45-54, (2019).

[24] S. Ide, R. Imai, H. Ochi & K. Maeshima. Transcriptional suppression of ribosomal DNA with phase separation. *Science Advances* **6**, eabb5953/1-15, (2020).

[25] K. Yoshikawa, Y. Yoshikawa & T. Kanbe. All-or-none folding transition in giant mammalian DNA. *Chem. Phys. Lett.* **354**, 354-359, (2002).

[26] A. Estévez-Torres & D. Baigl. DNA compaction: fundamentals and applications. *Soft Matter* **7**, 6746-6756, (2011).

[27] K. Tsumoto, F. Luckel & K. Yoshikawa. Giant DNA molecules exhibit on/off switching of transcriptional activity through conformational transition. *Biophys. Chem.* **106**, 23-29, (2003).

[28] A. Estevez-Torres *et al.* Sequence-independent and reversible photocontrol of transcription/expression systems using a photosensitive nucleic acid binder. *Proc. Natl. Acad. Sci. U. S. A.* **106**, 12219-12223, (2009).

[29] T. Nishio *et al.* Branched-Chain Polyamine Found in Hyperthermophiles Induces Unique Temperature-Dependent Structural Changes in Genome-Size DNA. *ChemPhysChem* **19**, 2299-2304, (2018).

[30] P.-G. De Gennes. *Scaling Concepts in Polymer Physics*, (Cornell University Press, 1979).

[31] G. S. Manning. The persistence length of DNA is reached from the persistence length of its null isomer through an internal electrostatic stretching force. *Biophys. J.* **91**, 3607-3616, (2006).

[32] Y. Yoshikawa *et al.* Critical behavior of megabase-size DNA toward the transition into a compact state. *J. Chem. Phys.* **135**, 225101, (2011).

[33] S. Sazer & H. Schiessel. The biology and polymer physics underlying large-scale chromosome organization. *Traffic* **19**, 87-104, (2018).

Chapter 5

Branched-chain polyamine found in hyperthermophiles induces unique temperature-dependent structural changes in genome-size DNA [i]

5.1 Introduction

Polyamines are found in all living organisms, where they play important roles in many cellular processes including cell growth and proliferation [1-3]. The most commonly occurring natural polyamines are putrescine (2+), spermidine (3+) and spermine (4+), all of which have a linear chain structure. Linear analogues of these polyamines, such as norspermidine (3+), norspermine (4+), thermospermine (4+) and homocaldopentamine (5+), which differ with regard to the length and arrangement of CH_2 spacers and valency, are also found in various organisms [4,5]. It is known that polyamines induce DNA condensation/compaction because of their polycationic nature at physiological pH [6]. A number of *in vitro* studies have investigated the physicochemical mechanism of polyamine-induced DNA condensation/compaction [7-25]. These *in vitro* studies shed some light on the manner of packing of DNA in living systems [26,27].

Recently, it was reported that a hyperthermophilic archaeon microorganism, *Thermococcus kodakarensis*, synthesizes a unique branched-chain polyamine N^4-bis(aminopropyl)spermidine 3(3)(3)4 that has not been found in other microorganisms [28,29]. *T. kodakarensis* grows at temperatures between 60 and 100°C, with an optimum growth temperature of 85°C [30]. Interestingly, synthesis of the branched-chain polyamine 3(3)(3)4 increases with an increase in the growth temperature [28]. Therefore, this branched-chain polyamine may be a key molecule for survival in high-temperature environments [28].

We previously investigated the effects of branched- and linear-chain polyamines on the higher-order structure of genome-size DNA at room temperature by the use of fluorescence microscopy and atomic force microscopy (AFM) [31]. We found that branched-chain polyamines tend to induce a meshwork assembly of randomly oriented DNA fibers, whereas linear-chain polyamines cause a parallel alignment between DNA segments [31]. Circular dichroism (CD) measurements revealed that branched-chain polyamines induce the A-like form in the secondary structure of

DNA, while linear-chain polyamines have only a minimal effect [31].

Here we extended this work by focusing on the temperature-dependence of the interactions of polyamines with DNA. We evaluated the temperature-dependent effect of a pentavalent branched-chain polyamine, 3(3)(3)4, on DNA structure. The results were compared to those obtained with linear-chain polyamines, spermidine SPD and homocaldopentamine 3334 which is a structural isomer of 3(3)(3)4. Their chemical structures are shown in Fig. 5.1. We used a genome-size DNA, T4 GT7 DNA (166 kbp), to monitor the change in conformation by AFM observation. It has been shown that the size or length of DNA molecules is a critical determinant governing their overall morphological features [32-36]. Teif reported that long enough DNA molecules can collapse into compact globules with various shapes such as a toroid or rod, while DNA fragments shorter than the persistence length do not form such ordered structures [34].

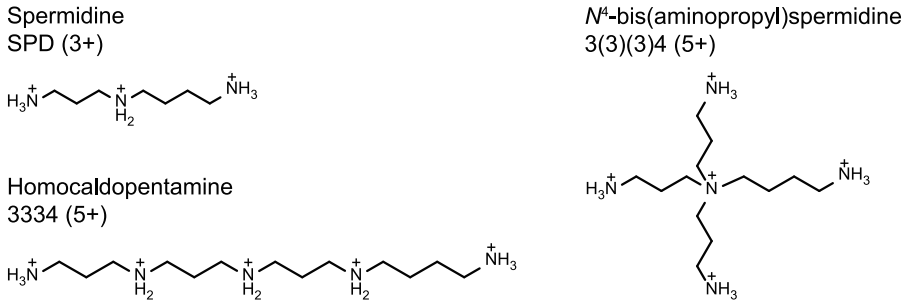

Figure 5.1 Chemical formulas of linear- and branched-chain polyamines examined in the present study.

5.2 Results and Discussion

5.2.1 AFM observation of the higher-order structure of DNA at room temperature

Figure 5.2 shows typical AFM images of T4 GT7 DNA in the presence of linear- or branched-chain polyamines on a mica surface at 24°C. The mica surface was not pretreated with any polycations such as magnesium or SPD before the application of a droplet of sample. In this experiment, we adopted 200 μM SPD, 5 μM 3334 and 3 μM 3(3)(3)4 as the polyamine concentrations based on the results obtained through a single molecule observation by fluorescence microscopy (Fig. 5.3). The average long-axis length of DNA was ca. 0.4 μm for all polyamines. We have confirmed that the degree of shrinking on the higher-order structure of DNA molecules are essentially the same under the conditions of 200 μM SPD, 5 μM 3334 and 3 μM 3(3)(3)4. Figure 5.2a shows an elongated conformation of DNA in the presence of a low concentration of SPD (10 μM) as a control observation. In the presence of a linear-chain polyamine, SPD (200 μM) or 3334 (5 μM), DNA molecules with multiple loops tend to crossover at the same point and produce flower-like structures (Fig. 5.2b-e). Similar DNA conformations

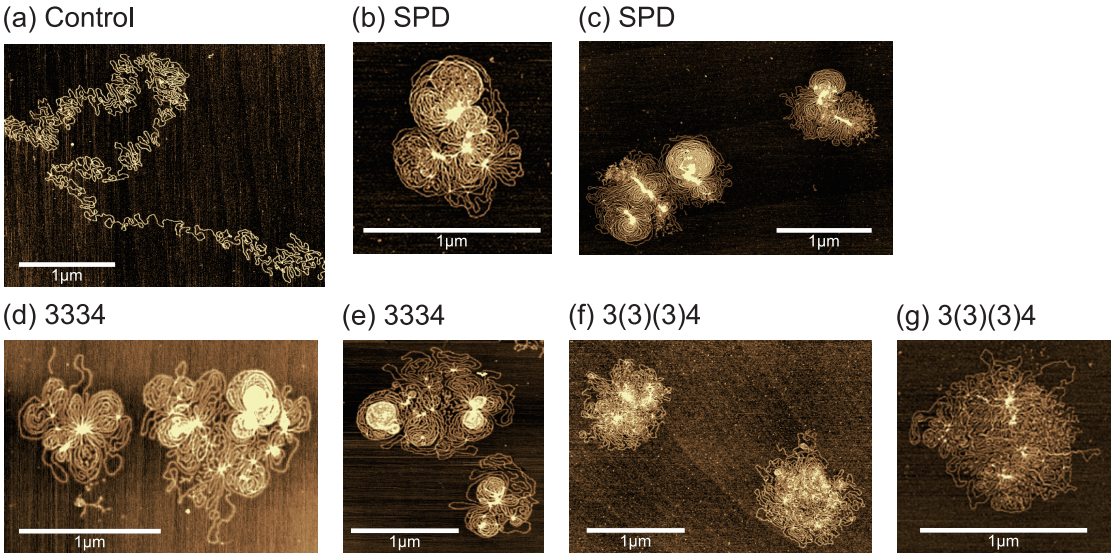

Figure 5.2 AFM images of T4 DNA in the presence of polyamines at 24°C: (a) control image at a low concentration, 10μM SPD.; (b) and (c) 200 μM SPD; (d) and (e) 5 μM 3334; (f) and (g) 3 μM 3(3)(3)4. Scale bar: 1 μm. The DNA concentration is 0.5 μM in nucleotide units.

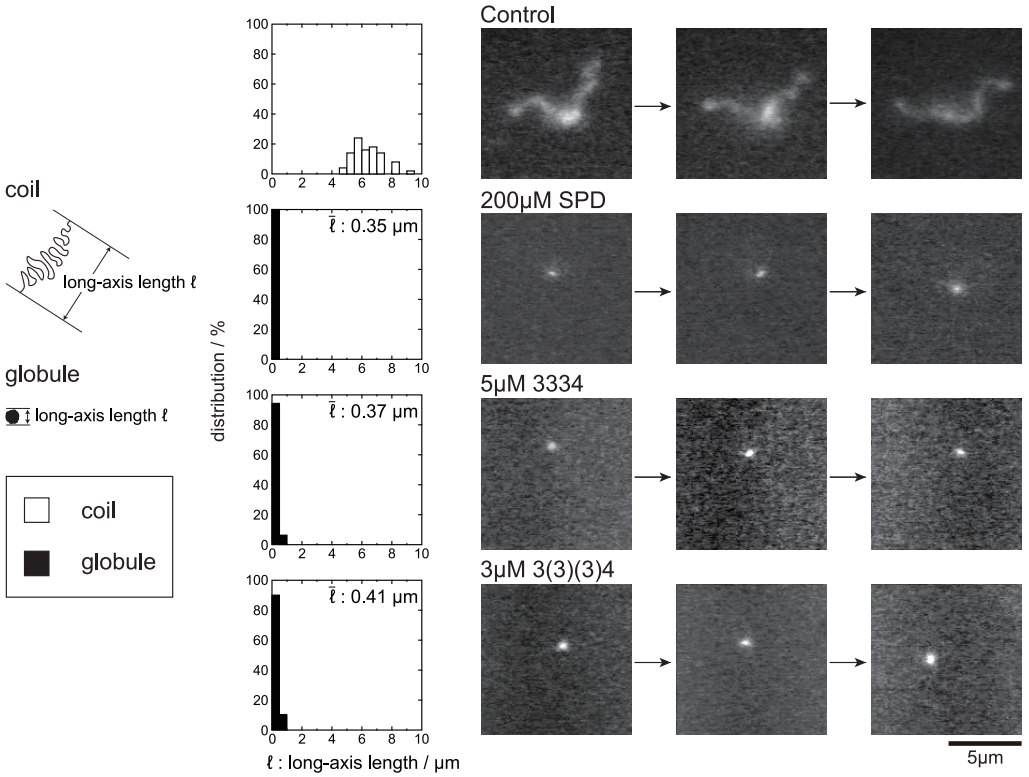

Figure 5.3 Change of the higher-order structure of T4 DNA in the presence of polyamines: (a) control image without polyamine.; (b) 200 μM SPD; (c) 5 μM 3334; (d) 3 μM 3(3)(3)4. (left) Distribution of the long-axis length ℓ. (right) Fluorescence microscopy images of single DNA molecules moving freely in bulk solution. The time interval between successive images is 0.2-0.3 s.

induced by SPD were reported by Fang and Hoh [37]. On the other hand, in the presence of 3 μM 3(3)(3)4, a mesh-like structure with a number of crossings or bridges appears. In other words, DNA segments are aligned parallel to each other in the presence of a linear-chain polyamine but are randomly-oriented in the presence of a branched-chain polyamine. This difference between linear- and branched-chain polyamines is in good agreement with our previous result [31]. To compare the frequency of crossings in the presence of linear- and branched-chain polyamines, we calculated the number of crossings per 1 μm, ξ, from AFM images based on the method of analysis depicted in Fig. 5.4. We counted the number of crossings N for the total length L of DNA for the region where the density of DNA segments is not so high and is similar among AFM images with different polyamines. The number of crossings per 1 μm is thus obtained as $\xi = N/L$. From the data shown in Fig. 5.4, the degree of crossing for 3(3)(3)4 is more than twice those for SPD and 3334.

Polyamine	ξ [μm^{-1}]	L/S [μm^{-1}]
SPD	5.8 ± 0.2	62.7 ± 2.2
3334	5.7 ± 0.4	59.4 ± 5.8
3(3)(3)4	11.5 ± 0.3	63.7 ± 4.0

ξ : number of crossings per 1 μm, N : number of crossings,
L : total length [μm], S : area [μm^2]

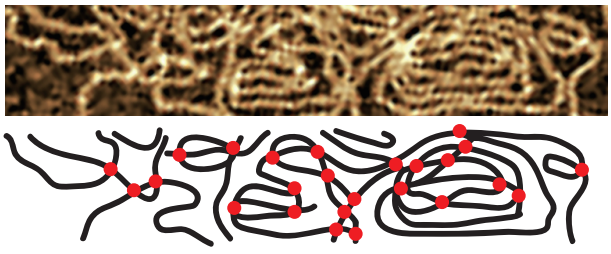

Figure 5.4 Degree of entanglement, ξ, for a DNA chain evaluated from AFM images, where ξ represents the number of crossings per 1 μm of DNA chain as depicted schematically in the lower part.

5.2.2 Temperature-dependent changes in the higher-order structure of DNA observed by AFM

Figure 5.5 shows AFM images of DNA in the presence of polyamines on a mica surface at 50°C; DNA molecules tend to unwind with increasing temperature. As the temperature rose to 80°C, there was a marked difference between DNA structures induced by linear- and branched-chain polyamines (Figs. 5.6-5.8). Especially, the unwounded parts in 3(3)(3)4-induced structure are noted (Fig. 5.8b,c). The high-magnification AFM image in Fig. 5.8d clearly indicates that multiple nano-loop structures with diameters of 10 - 50 nm are formed along the DNA strand in the presence of 3(3)(3)4. Such structural features at 80°C generated by 3(3)(3)4 may be related to its ability to enhance the thermal stability of DNA. The observed nano-looping conformation is similar in size to the inner diameter of a toroid in the tightly folded state of DNA, where the

outer diameter is 50-80 nm [32-36]. Here, we will roughly estimate the energy cost for the formation of such a nano-loop structure. It has been well established that the persistence length, L_p, of double-stranded DNA is around 50 nm [38]. Under the Hooke's law, the bending elastic constant, B, has the following relationship with L_p [39].

$$B = k_B T L_p \tag{5.1}$$

where k_B is Boltzmann constant and T is absolute temperature. Thus, the energy cost, ΔE, to form a loop with diameter D is given as in Eq. (5.2).

$$\Delta E = 2\pi B/D = 2\pi k_B T L_p/D \tag{5.2}$$

From this relationship, the energy cost to form a loop of D = 10 nm (with ca. 100 bp DNA or with ca. 200 phosphate groups) is estimated to be $10\pi k_B T$ (≈ 80 kJ/mol). It is considered that stabilization energy caused by the binding of a single polyamine to phosphate groups is in the order of 10 kJ/mol or more. Thus, an energy cost of $10\pi k_B T$ to form a 10 nm loop is regarded to be within the range of stabilization energy that can be afforded through the binding of plural number of branched-chain polyamine to the nano-loop.

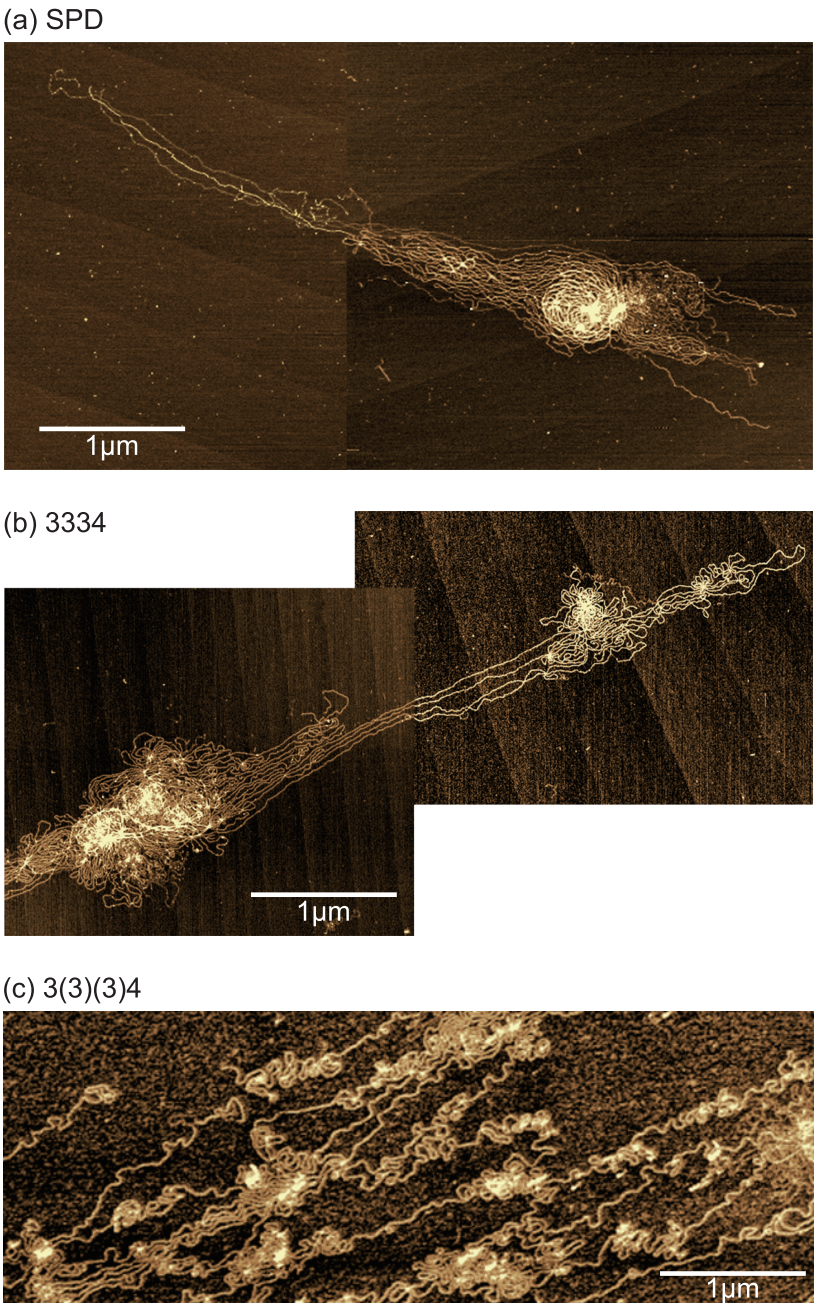

Figure 5.5 AFM images of T4 DNA in the presence of polyamines at 50°C: (a) 200 μM SPD; (b) 5 μM 3334; (c) 3 μM 3(3)(3)4.

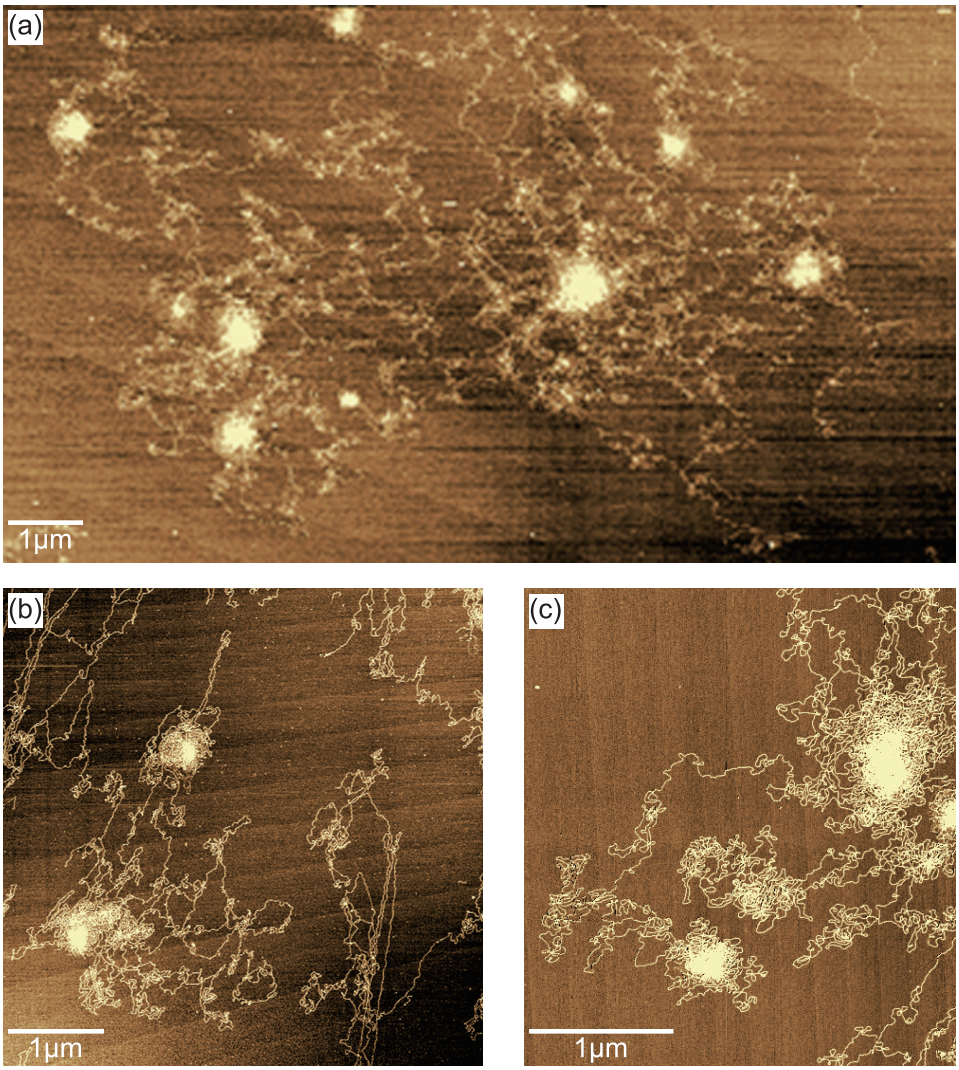

Figure 5.6 AFM images of T4 DNA in the presence of 200 μM SPD at 80°C: (a) wide scan image; (b) and (c) enlarged images.

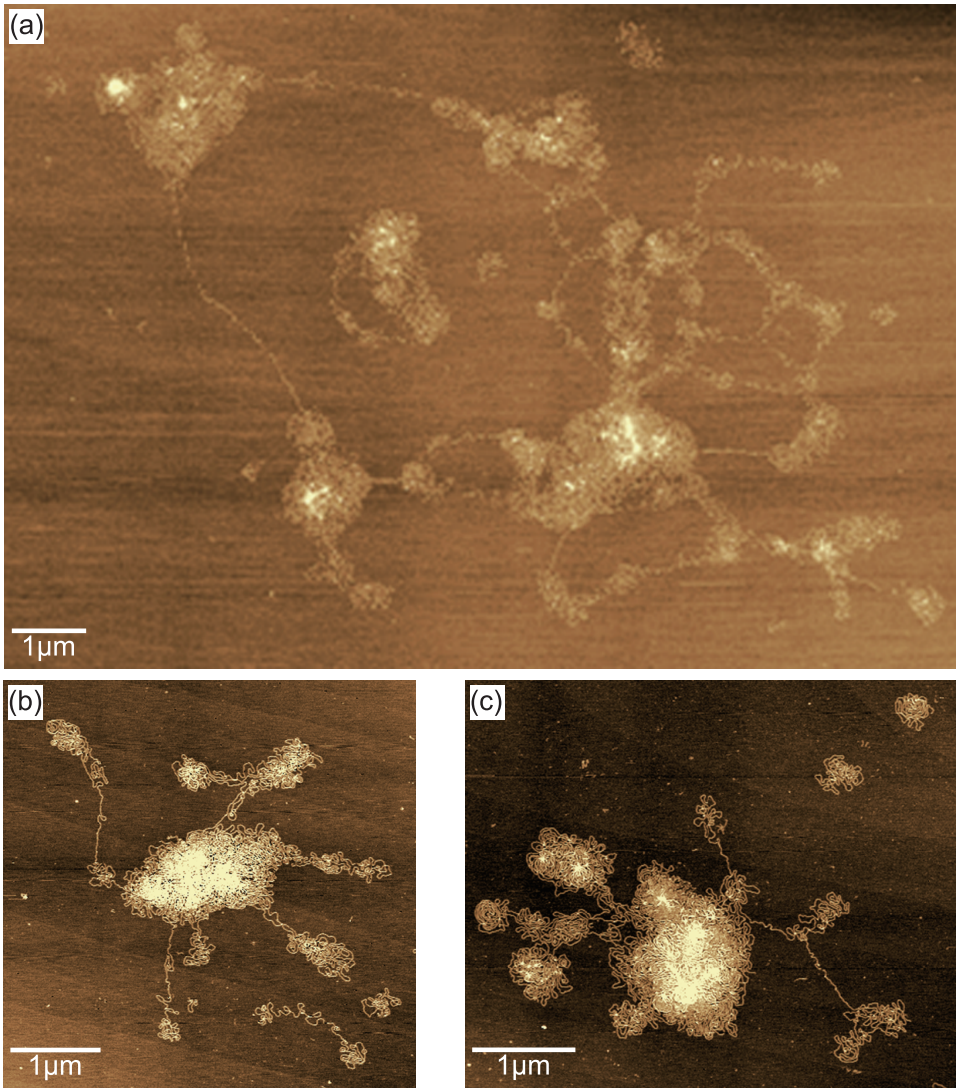

Figure 5.7 AFM images of T4 DNA in the presence of 5 μM 3334 at 80°C: (a) wide scan image; (b) and (c) enlarged images.

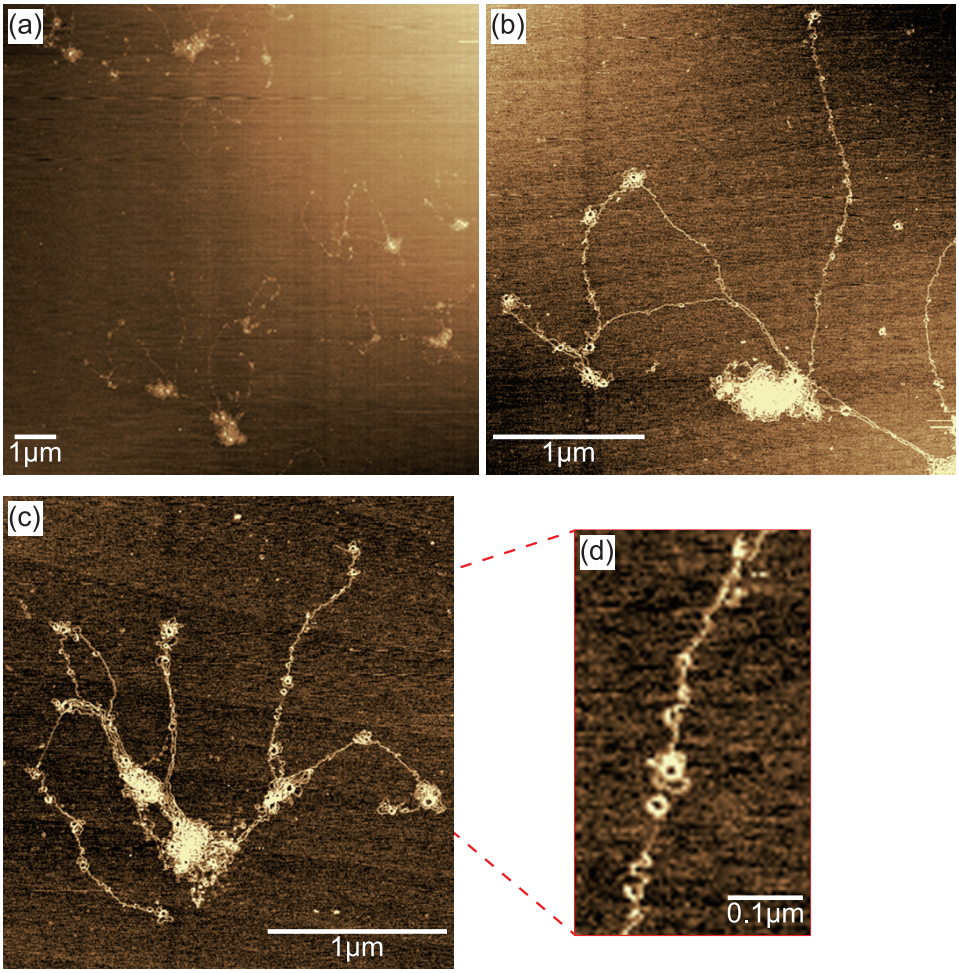

Figure 5.8 AFM images of T4 DNA in the presence of 3 μM 3(3)(3)4 at 80°C: (a) wide scan image; (b) and (c) enlarged images; (d) magnified image of the red square in (c), where arrows indicate the appearance of nano-loops.

5.2.3 Effect of temperature on the secondary structure of DNA as evaluated by CD measurements

Figure 5.9 shows the effect of temperature on CD spectra of calf thymus DNA in the presence of linear- and branched-chain polyamines. The CD spectra with different polyamine concentrations were given in Fig. 5.10. Without polyamine, the CD signals at 240 nm and 275 nm decreased with an increase in temperature to 80°C, indicating the occurrence of a helix-coil transition (Fig. 5.9a). In the presence of the linear-chain polyamine, SPD, the profiles of CD spectra remained essentially the same from 20°C to 80°C, indicating that the secondary structure retains the B-form even at 80°C. (Fig. 5.9b). This is due to the protective effect of polyamines against the thermal helix-coil transition. The linear-chain polyamine, 3334, was also associated with minimal changes in the CD spectra (Fig. 5.9c). On the other hand, the branched-chain polyamine, 3(3)(3)4, induced a transition from B-form to A-like form DNA characterized by a higher intensity of the positive band at 275 nm over a wide range of temperatures (Fig. 5.9d) [40]. To better understand the changes in the CD spectrum induced by an increase in temperature, we calculated the difference in ellipticities at 275 nm, $\Delta\theta$, between ellipticities obtained in the absence of polyamine, θ_0 and those obtained in the presence of polyamines, θ_r as defined by the following equation:

$$\Delta\theta = (\theta_r - \theta_0) \tag{5.3}$$

The change in $\Delta\theta$ at 275 nm depending on the temperature is depicted in Fig. 5.9e, which shows a marked change in CD with the addition of 3(3)(3)4 even at 20°C. The value $\Delta\theta$ tends to increase slightly with an increase of temperature in the presence of 3(3)(3)4. In contrast, the minimal effect of the linear polyamines, SPD and 3334, indicates that the secondary structure retains the B-form even under high temperatures. It was reported that a virus that infects a hyperthermophile, which lives at 80°C and pH 3, encapsidates A-form DNA [41,42]. Whelan et al. suggested that the A-form is prevalent in cells under stress based on observations of live bacteria by FTIR spectroscopy [43]. At present, the mechanisms underlying the change from the B- form to A-like form of DNA induced by the branched-chain polyamine 3(3)(3)4 remain unclear, but the preference for the A-like form over the B-form at higher temperatures suggests that the A-like form is associated with thermal resistance.

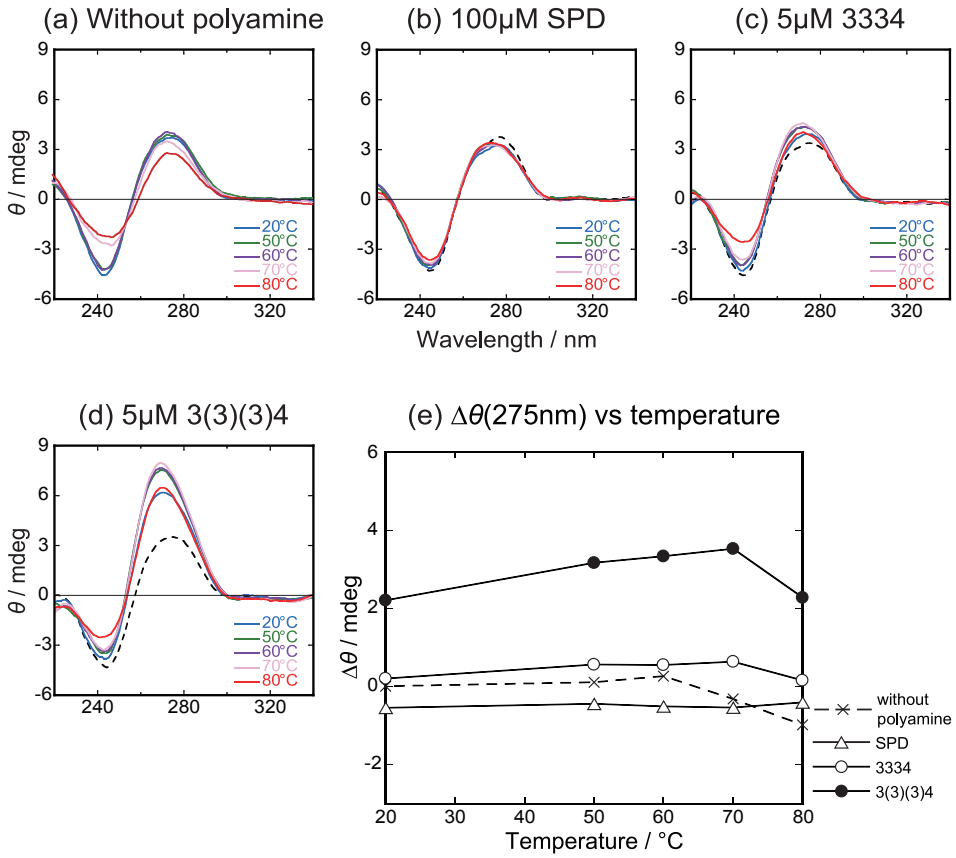

Figure 5.9 CD spectra of calf thymus (CT) DNA at different temperatures in the presence of polyamines. The black broken line in (b), (c) and (d) indicates the CD spectrum at 20°C in the absence of polyamine. The concentration of CT DNA is 30 μM in nucleotide units.

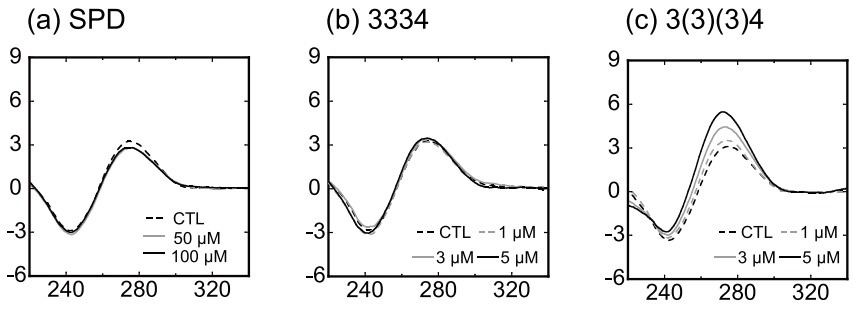

Figure 5.10 CD spectra of calf thymus (CT) DNA at different concentrations of polyamines: (a) SPD (b) 3334 and (c) 3(3)(3)4. The concentration of CT DNA is 30 μM in nucleotide units.

5.3 Conclusions

Past studies showed the effect of various polyamines on thermal stability of DNA oligonucleotides [44,45]. Here we used a large genome-size DNA (166 kbp) and showed that the branched-chain polyamine induces a unique temperature-dependent structural change. To the best of our knowledge, this is the first report to investigate the effect of polyamines on the higher-order structure of large DNA with increasing temperature up to 80°C. In addition, the branched-chain polyamine induces the secondary structural change from B-form to A-like form that is more marked at higher temperatures. These effects are specific to the branched-chain polyamine and are clearly different from the effects of linear-chain polyamines. These findings in the present study will provide additional insights not only on thermo-adaptation but also on understanding the mechanism how hyperthermophiles maintain their genetic activity under high temperature environments.

5.4 Materials and Methods

5.4.1 Materials

Spermidine trihydrochloride (SPD) was purchased from Nacalai Tesque (Kyoto, Japan). Homocaldopentamine (3334) and N^4-bis(aminopropyl)spermidine (3(3)(3)4) were synthesized according to a previous report [31]. Calf Thymus DNA (CT DNA: 8-15 kbp) was purchased from Wako Pure Chemical Industries (Osaka, Japan). T4 GT7 phage DNA was purchased from Nippon Gene (Toyama, Japan). Other chemicals were analytical grade and obtained from Nacalai Tesque.

5.4.2 AFM observations

AFM measurements were performed with an SPM-9700 (Shimadzu, Kyoto, Japan). For the preparation of sample specimens, 0.5 μM T4 DNA was dissolved in 1 mM Tris-HCl buffer solution at pH 7.5. Polyamines were then added to the solution. The resulting DNA solution was incubated at the target temperature for 3 min. Freshly cleaved mica was also incubated at the same target temperature. The DNA solution was then transferred onto the mica surface and was stood for 10 min at room temperature (24°C). Subsequently, the sample was rinsed with ultra-pure water, dried with nitrogen gas and imaged by AFM. All measurements were performed in air using the tapping mode. The cantilever, OMCL-AC200TS-C3 (Olympus, Tokyo, Japan), was 200 μm long with a spring constant of 9-20 N/m. The scanning rate was 0.4 Hz and images were captured using the height mode in a 512 × 512 pixel format. The obtained images were plane-fitted and flattened by the computer program supplied with the imaging module.

5.4.3 CD measurements

CD spectra of CT DNA upon heating were measured in the presence of each polyamine in 1 mM Tris-HCl buffer (pH 7.5) on a J-720W spectropolarimeter (JASCO, Tokyo, Japan). The DNA concentration was 30 μM in nucleotide units for all of the CD measurements. The cell path length was 1 cm. Data were collected every 1 nm between 220 and 340 nm at a scan rate of 100 nm/min, and were accumulated 3 times.

References

[1] C. W. Tabor & H. Tabor. Polyamines. *Annual Review of Biochemistry* **53**, 749-790, (1984).

[2] L. Miller-Fleming, V. Olin-Sandoval, K. Campbell & M. Ralser. Remaining Mysteries of Molecular Biology: The Role of Polyamines in the Cell. *J. Mol. Biol.* **427**, 3389-3406, (2015).

[3] A. O. Gevrekci. The roles of polyamines in microorganisms. *World J. Microbiol. Biotechnol.* **33**, 204/1-7, (2017).

[4] N. Nishibori *et al.* Occurrence of the polyamines caldopentamine and homocaldopentamine in axenic cultures of the red tide flagellates Chattonella antiqua and Heterosigma akashiwo (Raphidophyceae). *FEMS Microbiol. Lett.* **298**, 74-78, (2009).

[5] S. Finger, C. Schwieger, A. Arouri, A. Kerth & A. Blume. Interaction of linear polyamines with negatively charged phospholipids: the effect of polyamine charge distance. *Biol. Chem.* **395**, 769-778, (2014).

[6] A. M. Katz *et al.* Spermine Condenses DNA, but Not RNA Duplexes. *Biophys. J.* **112**, 22-30, (2017).

[7] T. H. Eickbush, D. K. Watson & E. N. Moudrianakis. A chromatin-bound proteolytic activity with unique specificity for histone H2A. *Cell* **9**, 785-792, (1976).

[8] E. C. Ong, C. Snell & G. D. Fasman. Chromatin models. The ionic strength dependence of model histone-DNA interactions: circular dichroism studies of lysine-leucine polypeptide-DNA complexes. *Biochemistry* **15**, 468-477, (1976).

[9] D. K. Chattoraj, L. C. Gosule & A. Schellman. DNA condensation with polyamines. II. Electron microscopic studies. *J. Mol. Biol.* **121**, 327-337, (1978).

[10] S. A. Allison, J. C. Herr & J. M. Schurr. Structure of viral φ29 DNA condensed by simple triamines: A light-scattering and electron-microscopy study. *Biopolymers* **20**, 469-488, (1981).

[11] R. E. Dickerson & H. R. Drew. Structure of a B-DNA dodecamer: II. Influence of base sequence on helix structure. *J. Mol. Biol.* **149**, 761-786, (1981).

[12] B. G. Feuerstein, N. Pattabiraman & L. J. Marton. Spermine-DNA interactions: a

theoretical study. *Proc. Natl. Acad. Sci. USA* **83**, 5948-5952, (1986).

[13] K. S. Srivenugopal, D. E. Wemmer & D. R. Morris. Aggregation of DNA by analogs of spermidine: enzymatic and structural studies. *Nucleic Acids Res.* **15**, 2563-2580, (1987).

[14] T. Thomas & R. P. Messner. Structural specificity of polyamines in left-handed Z-DNA formation: immunological and spectroscopic studies. *J. Mol. Biol.* **201**, 463-467, (1988).

[15] R. Gessner, C. A. Frederick, G. Quigley, A. Rich & A. Wang. The molecular structure of the left-handed Z-DNA double helix at 1.0-A atomic resolution. Geometry, conformation, and ionic interactions of d (CGCGCG). *J. Biol. Chem.* **264**, 7921-7935, (1989).

[16] S. Jain, G. Zon & M. Sundaralingam. Base only binding of spermine in the deep groove of the A-DNA octamer d (GTGTACAC). *Biochemistry* **28**, 2360-2364, (1989).

[17] P. G. Arscott, A. Z. Li & V. A. Bloomfield. Condensation of DNA by trivalent cations. 1. Effects of DNA length and topology on the size and shape of condensed particles. *Biopolymers* **30**, 619-630, (1990).

[18] V. A. Bloomfield. Condensation of DNA by multivalent cations: considerations on mechanism. *Biopolymers* **31**, 1471-1481, (1991).

[19] T. Thomas & T. Thomas. Selectivity of polyamines in triplex DNA stabilization. *Biochemistry* **32**, 14068-14074, (1993).

[20] L. W. Tari & A. S. Secco. Base-pair opening and spermine binding—B-DNA features displayed in the crystal structure of a gal operon fragment: implications for protein-DNA recognition. *Nucleic Acids Res.* **23**, 2065-2073, (1995).

[21] R. Golan, L. I. Pietrasanta, W. Hsieh & H. G. Hansma. DNA toroids: stages in condensation. *Biochemistry* **38**, 14069-14076, (1999).

[22] V. S. Trubetskoy *et al.* Caged DNA does not aggregate in high ionic strength solutions. *Bioconjugate Chem.* **10**, 624-628, (1999).

[23] H. Deng, V. A. Bloomfield, J. M. Benevides & G. J. T. Jr. Structural basis of polyamine-DNA recognition: spermidine and spermine interactions with genomic B-DNAs of different GC content probed by Raman spectroscopy. *Nucleic Acids Res.* **28**, 3379-3385, (2000).

[24] V. Vijayanathan, T. Thomas, A. Shirahata & T. J. Thomas. DNA condensation by polyamines: a laser light scattering study of structural effects. *Biochemistry* **40**, 13644-13651, (2001).

[25] A. Venancio-Marques, A. Bergen, C. Rossi-Gendron, S. Rudiuk & D. Baigl. Photosensitive polyamines for high-performance photocontrol of DNA higher-order structure. *ACS Nano* **8**, 3654-3663, (2014).

[26] R. Everaers & H. Schiessel. The physics of chromatin. *J. Phys.: Condens. Matter* **27**, 060301/1-2, (2015).

[27] T. Nozaki *et al.* Dynamic Organization of Chromatin Domains Revealed by Super-Resolution Live-Cell Imaging. *Mol. Cell* **67**, 282-293 e287, (2017).

[28] K. Okada *et al.* Identification of a novel aminopropyltransferase involved in the synthesis of branched-chain polyamines in hyperthermophiles. *J. Bacteriol.* **196**, 1866-1876, (2014).

[29] R. Hidese *et al.* Identification of a novel acetylated form of branched-chain polyamine from a hyperthermophilic archaeon Thermococcus kodakarensis. *Biosci., Biotechnol., Biochem.* **81**, 1845-1849, (2017).

[30] H. Atomi, T. Fukui, T. Kanai, M. Morikawa & T. Imanaka. Description of Thermococcus kodakaraensis sp. nov., a well studied hyperthermophilic archaeon previously reported as Pyrococcus sp. KOD1. *Archaea* **1**, 263-267, (2004).

[31] A. Muramatsu *et al.* Naturally occurring branched-chain polyamines induce a crosslinked meshwork structure in a giant DNA. *J. Chem. Phys.* **145**, 235103/1-7, (2016).

[32] B. I. Kankia, V. Buckin & V. A. Bloomfield. Hexamminecobalt(III)-induced condensation of calf thymus DNA: circular dichroism and hydration measurements. *Nucleic Acids Res.* **29**, 2795-2801, (2001).

[33] K. Yoshikawa & Y. Yoshikawa. Compaction and condensation of DNA. *Pharmaceutical perspectives of nucleic acid-based therapeutics*, 137-163, (2002).

[34] V. B. Teif. Ligand-induced DNA condensation: choosing the model. *Biophys. J.* **89**, 2574-2587, (2005).

[35] A. C. Toma, M. de Frutos, F. Livolant & E. Raspaud. DNA condensed by protamine: a "short" or "long" polycation behavior. *Biomacromolecules* **10**, 2129-2134, (2009).

[36] Y. Yoshikawa *et al.* Critical behavior of megabase-size DNA toward the transition into a compact state. *J. Chem. Phys.* **135**, 225101/1-7, (2011).

[37] Y. Fang & J. H. Hoh. Early intermediates in spermidine-induced DNA condensation on the surface of mica. *Journal of the American Chemical Society* **120**, 8903-8909, (1998).

[38] G. S. Manning. The persistence length of DNA is reached from the persistence length of its null isomer through an internal electrostatic stretching force. *Biophys. J.* **91**, 3607-3616, (2006).

[39] A. Y. Grosberg & A. R. Khokhlov. *Statistical Physics of Macromolecules*, in *Polymers and Complex Materials*, (AIP Press, 1994).

[40] V. I. Ivanov, L. E. Minchenkova, A. K. Schyolkina & A. I. Poletayev. Different conformations of double-stranded nucleic acid in solution as revealed by circular dichroism. *Biopolymers* **12**, 89-110, (1973).

[41] F. DiMaio *et al.* A virus that infects a hyperthermophile encapsidates A-form DNA. *Science* **348**, 914-917, (2015).

[42] B. R. Wood. Correction: The importance of hydration and DNA conformation in interpreting infrared spectra of cells and tissues. *Chem. Soc. Rev.* **45**, 1999-1999, (2016).

[43] D. R. Whelan *et al.* Detection of an en masse and reversible B- to A-DNA conformational transition in prokaryotes in response to desiccation. *J. R. Soc., Interface* **11**, 20140454, (2014).

[44] M. H. Hou *et al.* Effects of polyamines on the thermal stability and formation kinetics of DNA duplexes with abnormal structure. *Nucleic Acids Res.* **29**, 5121-5128, (2001).

[45] Y. Terui, M. Ohnuma, K. Hiraga, E. Kawashima & T. Oshima. Stabilization of nucleic acids by unusual polyamines produced by an extreme thermophile, Thermus thermophilus. *Biochem J* **388**, 427-433, (2005).

Chapter 6

Repulsive/attractive interaction among compact DNA molecules as judged through laser trapping: Difference between linear- and branched-chain polyamines [ii]

6.1 Introduction

Polyamines are polycations with two or more amino groups that are ubiquitously found in all living cells [1,2]. Under physiological conditions, polyamines interact with various anionic biomolecules such as DNA, RNA, and proteins, and play essential roles in many cellular functions [1,3-6]. Recently, it was found that a hyperthermophilic archaeon microorganism, *Thermococcus kodakarensis*, produces a specific pentavalent branched-chain polyamine, N^4-bis(aminopropyl)spermidine 3(3)(3)4 (Fig. 6.1) [7,8]. *T. kodakarensis* grows at temperatures between 60 and 100°C, with an optimum growth temperature of 85°C [9]. The amount of 3(3)(3)4 produced in this thermophile increases with an increase in the temperature of the medium [7]. Thus, it is strongly suspected that the branched-chain polyamine 3(3)(3)4 plays a crucial role in the ability of hyperthermophilic microorganisms to survive at higher temperatures near the boiling point of water.

Several previous studies reported that DNA condensation was caused through the highly cooperative binding of polyamines, which was considered to be a combination of aggregation, shrinkage, compaction and precipitation [10-15]. About two decades ago, it was revealed that individual DNA molecules undergo a transition between elongated coil and folded compact states through single-molecule observations with fluorescence microscopy [16-23]. Recently, we studied the effects of a linear-chain polyamine, homocaldopentamine 3334 (Fig. 6.1), and a branched-chain polyamine, 3(3)(3)4, which are structural isomers of each other, on genome-size DNA [24,25]. The experiments revealed that 3(3)(3)4 tends to induce a meshwork assembly of randomly oriented DNA segments. On the other hand, 3334 causes a parallel alignment among DNA segments [24,25]. Regarding the secondary structure of DNA, it was shown that 3(3)(3)4 induces an A-like form, whereas 3334 causes no marked change [24,25]. In the present study, we extended the previous works by clarifying the differences in the physico-chemical properties of

compacted DNA induced by these two isomers using optical manipulation. It has been reported that effective laser trapping/manipulation on individual compact DNA molecules can be performed without any chemical modifications of DNA, such as attachment to a polymer bead [26-29].

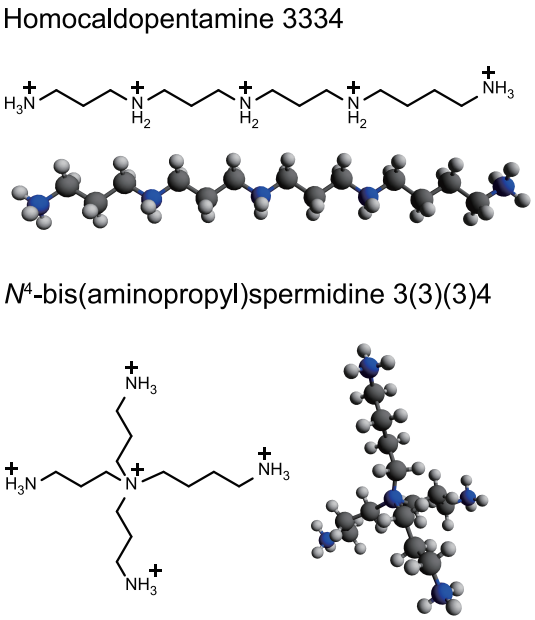

Figure 6.1 Chemical structures of 3334 and 3(3)(3)4.

6.2 Results and Discussion

Figure 6.2 exemplifies the fluorescence microscopic images of individual T4 DNA molecules in the presence of 3334 and 3(3)(3)4. In these images, single DNA molecules undergo translational and intramolecular Brownian motion in bulk solution under FM observation. In the absence of polyamine, an elongated random coil conformation is observed (Fig. 6.2a). The compact globule states caused by 3334, and 3(3)(3)4 are shown in Fig. 6.2b,c, respectively.

Figure 6.3 summarizes the distribution of the long-axis length L of DNA molecules as a function of the concentrations of 3334 and 3(3)(3)4 together with an assignment of the conformational characteristics in FM images, where L values exhibit uncertainty or experimental error on the order of 0.5-1.0 μm due to the blurring effect. Both 3334 and 3(3)(3)4 cause shrinkage/compaction of the DNA conformation with an increase in the polyamine concentration. The results indicate that the potency of 3(3)(3)4 for DNA shrinkage is slightly higher than that of 3334, i.e., the average length $\bar{L}$ at 3 μM is 0.96 μm for 3334 and 0.71 μm for 3(3)(3)4. At 7 μM, the $\bar{L}$ values for 3334 and 3(3)(3)4 are almost the same. We previously confirmed that, under the condition that polyamine concentration is slightly larger than the threshold concentration to cause

the compaction, compact DNA molecules do not aggregate with each other even through collision under Brownian motion, indicating that compact DNA molecules have a charged colloidal nature [30]. Based on these experimental results, we compared the physicochemical properties of compact DNA molecules at a polyamine concentration of 7 μM for both 3334 and 3(3)(3)4.

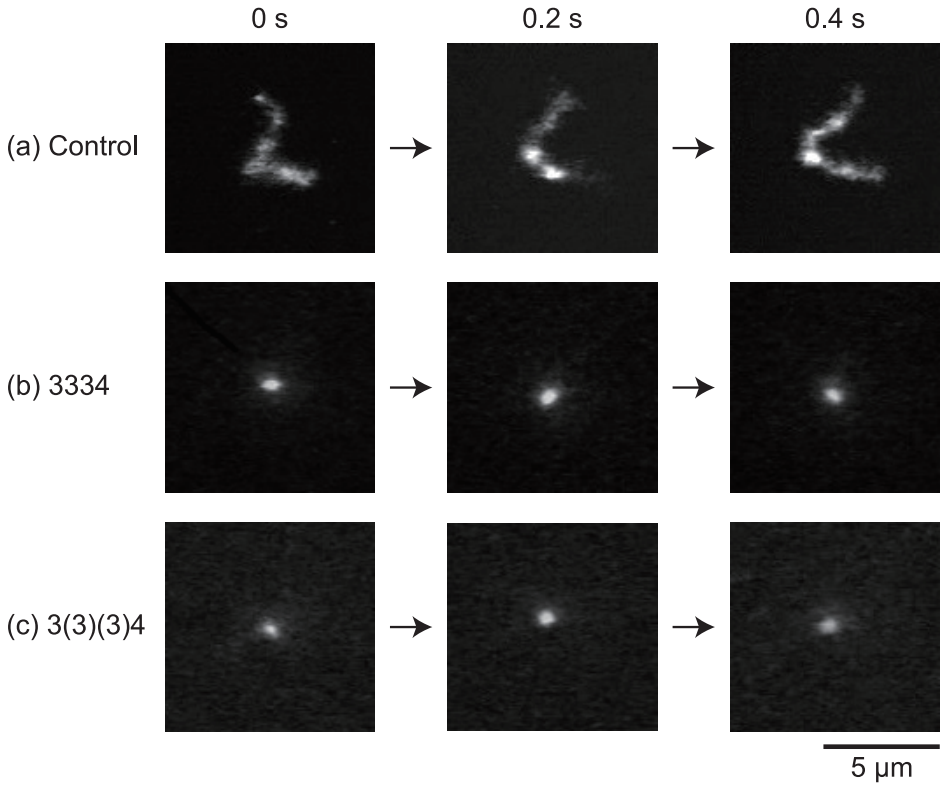

Figure 6.2 Fluorescence microscopic images of single T4 DNA molecules in solution at different concentrations of polyamines. (a) control image without polyamine, (b) 7 μM 3334, (c) 7 μM 3(3)(3)4. The time interval between successive images is 0.2 s.

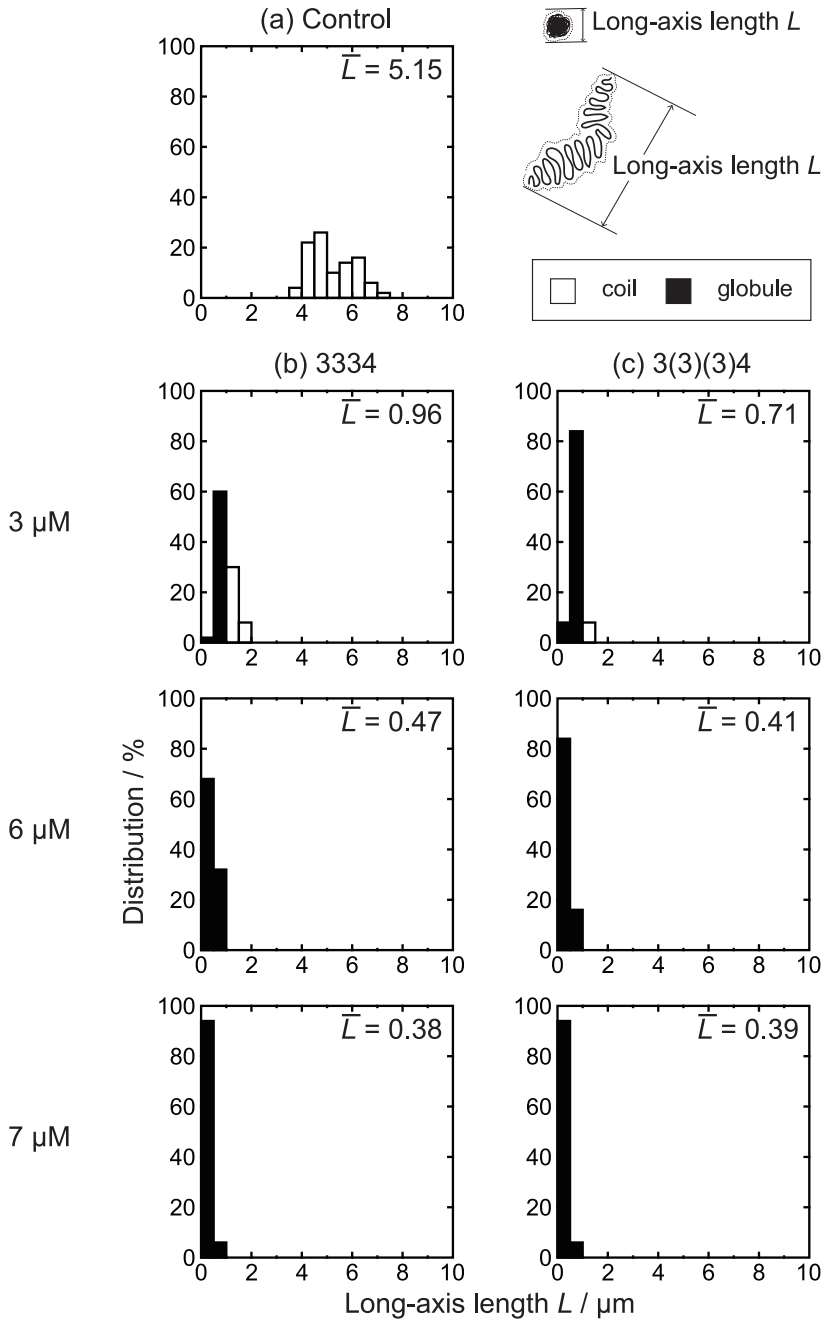

Figure 6.3 Distribution of the long-axis length L of T4 DNA at various concentrations of 3334 and 3(3)(3)4, as evaluated from single-DNA measurements with fluorescence microscopy. $\bar{L}$ (μm) is the ensemble average for 40-50 DNA molecules.

Figure 6.4a exemplified the experimental result of trapping DNA molecules by manipulating focused laser. Where the time dependent changes are also shown on the stability of the DNA assembly after switching off the laser. Figure 6.4b shows a schematic representation of the trapping and assembly of DNA molecules by the YAG laser in the presence of 7 μM of the polyamines, either 3334 or 3(3)(3)4. The focused laser, with a power of about 700 mW, can achieve steady trapping of a desired folded compact DNA molecule [26] for solutions with 3334 and 3(3)(3)4. When individual DNA molecules are trapped by a laser, 12 DNA molecules are assembled onto the laser focus (A-2 and B-2 in Fig. 6.4a). It is noted that, for 3334, a rod-shaped assembly is formed through the collection of multiple DNA molecules. Spontaneous formation of such rod like structure with DNA molecules by use of laser trapping has been reported in a past study [29]. When the laser light is turned off, the DNA assembly begins random Brownian motion while maintaining its shape (a-3 and a-4). In contrast, the DNA assembly generated in the presence of 3(3)(3)4 tend to dissociate (b-3 and b-4). The instability of the DNA/3(3)(3)4 assembly suggests a repulsive interaction between the compact DNA molecules. On the other hand, the stable assembly of DNA/3334 is attributed to the attractive interaction between the compact DNAs. Thus, although compact DNA behaves as a negatively charged colloid, DNA molecules compacted by 3334 exhibit attraction when they are in direct contact, which is similar to the potential profile under the DLVO theory of relatively large van der Waals attraction with long-range electric repulsion [31]. Actually, it was reported that electrophoretic mobility of compact DNA caused by the addition of a linear polyamine, spermidine, decreases to ca. 1/10 accompanied by the folding transition [32]. In contrast, DNA molecules compacted by 3(3)(3)4 remain repulsive when in direct contact, suggesting larger surviving negative charge.

Figure 6.5 shows a schematic representation of the interaction of double-stranded DNA with 3334 or 3(3)(3)4. Here, Avogadro software was used to prepare the schematics to account for the interplay between DNA and polyamines [33]. As shown, it is expected that the linear-chain polyamine 3334 can interact with the arrayed phosphate negative groups on DNA in an effective manner, suggesting effective charge neutralization on the negative DNA molecule. This may explain the stability of the DNA assembly in the presence of 3334, as in Fig. 6.4. In contrast, the branched-chain polyamine interacts with the negatively charged phosphate groups in an incommensurate manner, which may cause repulsive contact interaction with 3(3)(3)4.

Figure 6.6a shows the coarse-grained DNA model adapted in the present Monte Carlo simulation. By using such kind of simple model, it becomes possible to explore the effect of different manner of binding of the polyamine isomers on the manner of charge neutralization/reduction of negatively charged DNA molecule in a semi-quantitative fashion. Figure 6.6b compares the reduced density distribution of charged beads (charged ammonium cations) between linear (circles) and branched (squares) polyamine when Γ =1.02 nm (solid symbols) and 1.70 nm (open

symbols). For both Γ values, the $\rho(r)$ of linear polyamine displays a greater density distribution at near DNA surface compared to its counterpart of branched polyamine. The peak in the $\rho(r)$ of linear polyamine at about (but smaller than) r = 1.0 nm arises from the close contact between the oppositely charged ammonium and a phosphate group with some penetration of polyamine into the soft cylindrical DNA. This peak is enhanced as Γ is increased from 1.02 to 1.70 nm. Actually, there is another peak in the $\rho(r)$ of linear polyamine at around r = 1.4 nm. The peak is perceivable in the case of Γ = 1.02 nm, but diminishes for Γ = 1.70 nm, indicating that the weaker electrostatic attraction between ammonium group and DNA increases the degrees of freedom for a polyamine to move around DNA. The snapshot in Fig. 6.6c shows the typical configuration for Γ = 1.70 nm in that a linear polyamine tilts about 40° from the axis of DNA to maximize its electrostatic attraction with DNA. Note that the two chain ends have a greater chance to distribute away from the DNA surface as Γ is decreased.

The branched polyamine displays similar behavior as its linear counterpart, in that the corresponding $\rho(r)$ shifts towards smaller r and the density of ammonium groups increases near the DNA surface as Γ is increased from 1.02 to 1.70 nm. In contrast to the linear polyamine with more dispersed charge density along the chain and a greater contact area, a branched polyamine creates a higher charge density concentrated within its more spherical-like shape and a smaller contact area. To increase its attraction with DNA, part of the charged groups in a branched polyamine tend to penetrate into DNA (the region r < 0.732 nm in Fig. 6.6b). Nevertheless, the central ammonium group is unable to make direct contact with DNA, which is partially manifested in the peak of $\rho(r)$ located at near 1.4 nm for both Γ values. The typical snapshot in Fig. 6.6c for a branched polyamine around a DNA when Γ = 1.7 nm shows that some ammonium groups are located away from the DNA surface due to the geometric constraints within a branched polyamine molecule.

The charge distribution of ammonium groups as indicated in our simulation model may also contribute to the van der Waals attraction among compact DNA molecules in aggregates under optical trapping. In the branched polyamine, it is noticeable that the charged ammonium cations display a greater chance to distribute away from the DNA compared to the linear polyamine. In Fig. 6.6b, the wider spatial distribution of branched polyamine at large r suggests that separation between positively charged ammonium groups and negatively charge phosphate groups is a common structural feature in the complex of 3(3)(3)4 polyamine and DNA Such a spatial arrangement can be an origin of dipole-dipole force between DNA segments. As such the branched polyamine may induce stronger van der Waals interaction than the linear one. This argument coincides with the higher potency of a branched polyamine on DNA shrinkage.

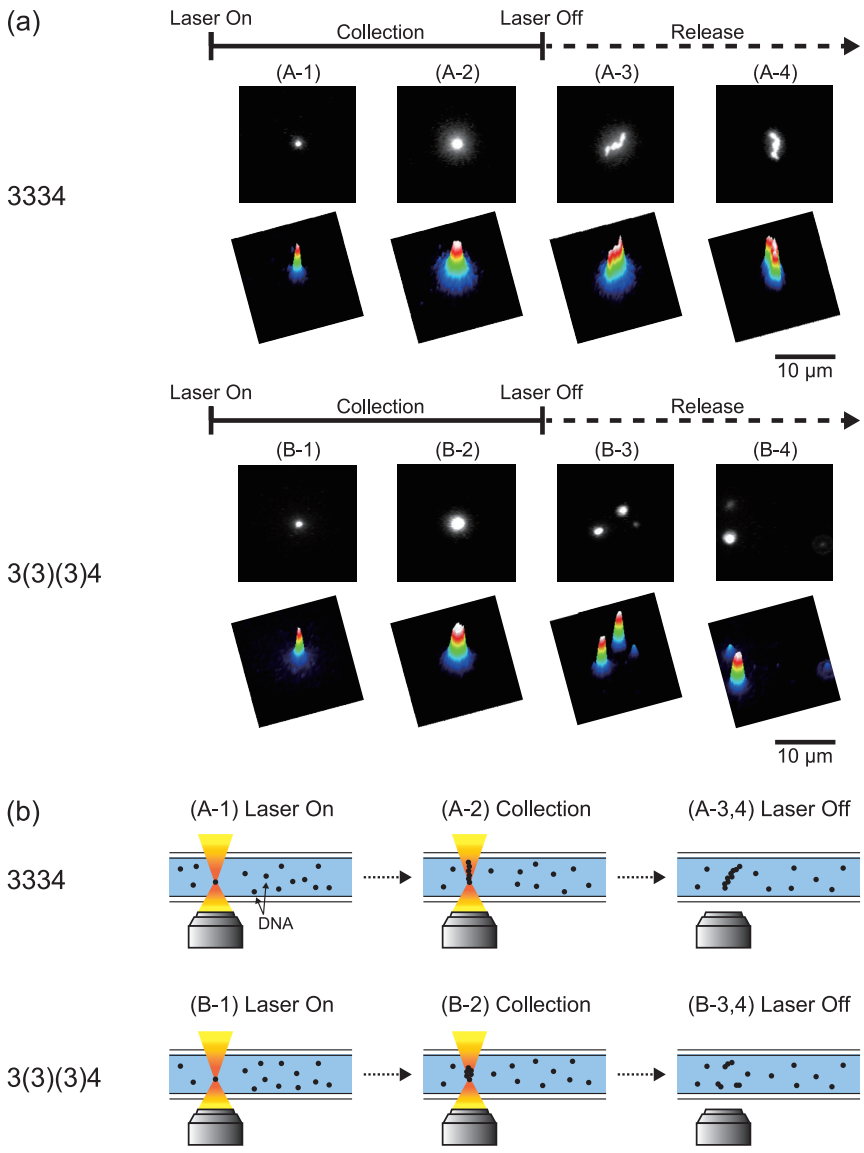

Figure 6.4 (a) Trapping and assembly of compact DNA molecules by optical tweezers, showing the fluorescent microscopic images and corresponding quasi-3D profiles of the fluorescence intensities, respectively. (A-1), (B-1) Individual DNA molecules folded by 7μM of 3334 or 3(3)(3)4 are optically trapped at the beam focus. (A-2), (B-2) Through the operation to move the focus point in the solution, 12 compact DNA molecules are collected, respectively. (A-3,4) When the laser is turned off, the assembly of DNA complexed with 3334 retains its shape and undergoes the Brownian motion. (B-3,4) The assembly of DNA complexed with 3(3)(3)4 tends to separate into individual DNA molecules. The time difference between the neighboring frames in (A) and (B) is 180 sec, corresponding to the period of laser irradiation. The time differences after the laser switch-off are 120, and 30 sec in (A), respectively, and those in (B) are 5, and 5 sec, respectively. (b) Schematic representation on the experimental operation of laser tweezers for the observation shown in (a). Polyamines are depicted as black objects.

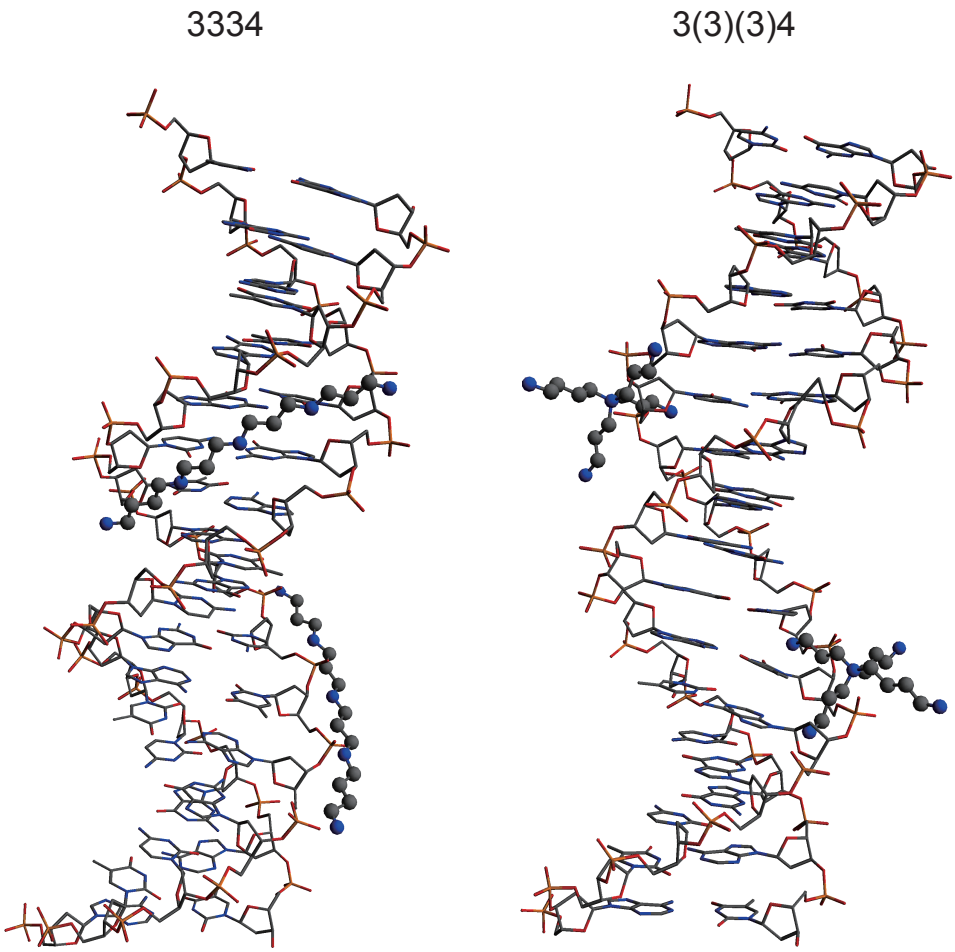

Figure 6.5 Schematic representation of the interaction of double-stranded DNA with (a) 3334 and (b) 3(3)(3)4 for double-strand DNA. Polyamines are shown as ball-and-stick model with nitrogen atoms denoted by blue beads.

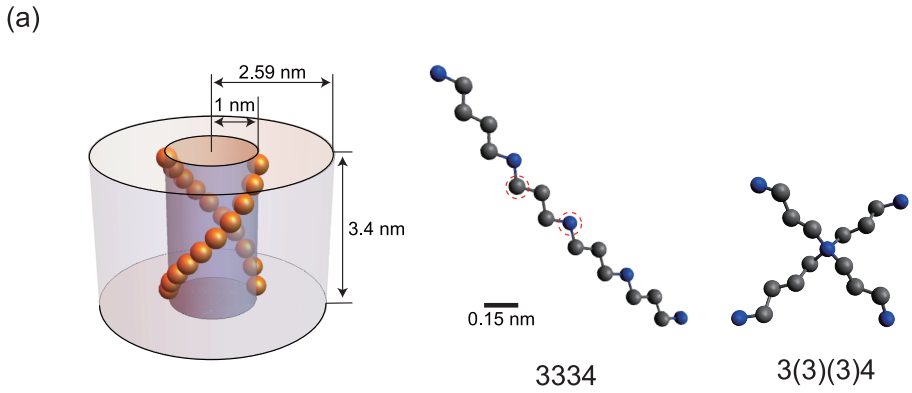
(a)
2.59 nm
1 nm
3.4 nm
0.15 nm
3334
3(3)(3)4

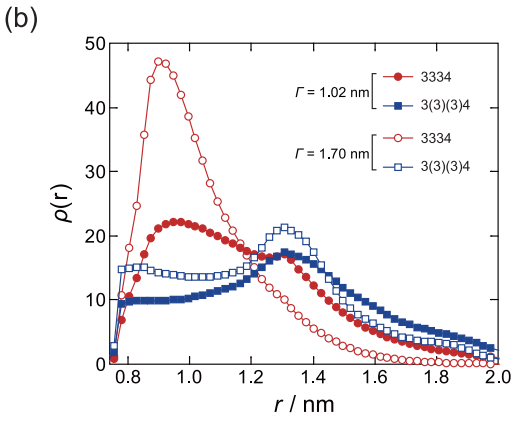
(b)
ρ(r)
r / nm
Γ = 1.02 nm
3334
3(3)(3)4
Γ = 1.70 nm
3334
3(3)(3)4

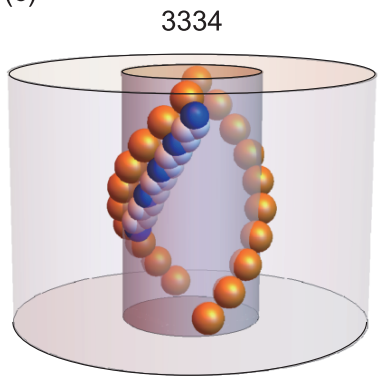
(c)
3334

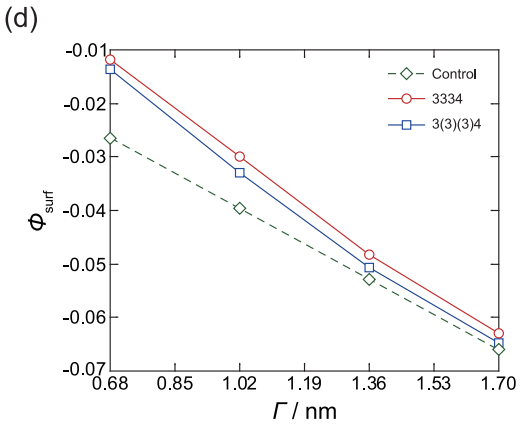
(d)
Φsurf
Γ / nm
Control
3334
3(3)(3)4

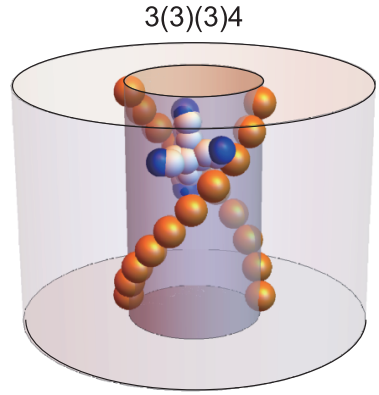
3(3)(3)4

Figure 6.6 (a) DNA model adapted in the present Monte Carlo simulation. The DNA is modeled as a soft cylinder of 1 nm, which allows polyamines to penetrate the DNA with a depth equal to the radius of a phosphate group. Simple modeling with 20 charged spheres representing phosphate ions in DNA constitute the structure similar to one pitch about 3.4 nm long in DNA. The radius of phosphate group is about 0.238 nm. The surrounding aqueous solution is assumed as a cylindrical cell with the length and radius of 3.40 nm and 2.59 nm, respectively under the boundary condition of a hard cylindrical wall. The periodic boundary condition is applied along the DNA axis. The two pictures on right are the lowest energy conformations for linear polyamine (left), 3334, and branched polyamine (right), 3(3)(3)4, respectively, which were obtained from the energy minimization, and all methyl, methylene and ammonium groups are then coarse-grained into beads of the same radius. Blue beads denote nitrogen atoms, and gray beads denote carbon atoms. Note that the scale bar denotes 0.15 nm, the average bond length between two neighboring atoms in a polyamine. These beads interacting with phosphate charged spheres through screened Coulomb potential if their separation is above 0.31 nm (cf.: Eq. (1)). Below this distance, the potential becomes infinity. These beads are allowed to penetrate the soft DNA cylinder to mimic the space in DNA major and minor grooves. (b) Plot of the reduced charge density distribution along the radius direction (r) for linear (circles) and branched polyamine (squares) when Γ = 1.02 nm (solid symbols) and 1.70 nm (open symbols). Lines are for eye guide, and the error bars are smaller than the symbols. (c) Typical snapshots for linear polyamine and branched polyamine interacting with DNA when Γ = 1.7 nm. Note that blue beads denote ammonium groups, and white beads denote methyl and methylene groups. (d) Plot of the average surface potential Φ_{surf} with Γ in the presence of linear (circles) polyamine and branched (square) polyamine, and in the absence of polyamine (diamond with dashed line). The error bars are smaller than the size of symbols. Lines are for eye guide.

To investigate the electrostatic shielding of polyamines on DNA, the average surface potential Φ_{surf} at the boundary of the simulation cell is computed. The calculated Φ_{surf} is corresponding to the electrostatic potential experienced by a point unit charge located at any point of the cylindrical boundary under thermal fluctuation of polyamine around DNA. Figure 6.6d plots Φ_{surf} as a function of Γ in the presence of linear (circles) and branched (squares) polyamine as well as in the absence of polyamine as a control (diamond with dashed line). The difference of Φ_{surf} between the case without polyamine and the case with polyamine (either linear or branched) decreases from Γ = 0.68 to 1.7 nm, suggesting that the polyamine induced charge shielding becomes less effective at high Γ. At the lower Γ, the electrostatic interaction is weaker, and the polyamine gains more freedom to move around. Such a process can be one possible mechanism to shield DNA charge. Meanwhile, our finding shows that a linear polyamine is more effective to increase Φ_{surf} (less negative) than a branched one. Since some ammonium groups in the branched polyamine tends to distribute away from DNA more than the linear polyamine as shown in Fig. 6.6b, suggesting that the direct polyamine/DNA binding (formation of ion pairs) may provide the second pathway to neutralize the DNA charge. By considering the polyamine topology, a linear polyamine is more elongated and has a greater contact area with DNA, so it may bind with more phosphate groups in DNA. One may argue that the branched polyamine carries a higher charge density which leads to a stronger local interaction with DNA. Nevertheless, the overall coverage of a branched polyamine onto the DNA phosphate groups may not be high due to the smaller contact area arising from its spherical-like shape (with a higher survival charge in DNA). In other words, the branched polyamine can bind to DNA more locally, but the linear polyamine with more dispersed charge density (weaker local attraction with DNA) may facilitate its coverage over more phosphate groups via thermal fluctuation (lowering the survival charge in DNA). Furthermore, it is noted that the difference between the two types of polyamine decreases from 13% to 3% as Γ is increased from 0.68 to 1.7 nm. This is an indication that strong polyamine/DNA binding may impede the polyamine capacity in shielding DNA charge because both types of polyamine bind to DNA locally and tightly at high Γ. In those cases, more polyamines are needed to shield the DNA charge.

These simulation results are consistent with the experimental observation reported in this work. The branched polyamine (3(3)(3)4) carries a higher charge density per unit volume because all of its charged ammonium cations are concentrated within a more compact molecular structure. The higher charge density in a branched polyamine sustains its electrostatic attraction with DNA even though not all ammonium groups can directly contact with charged phosphate groups in DNA, as shown in the simulation snapshot in Fig. 6.6c. There are two significant effects due to the branched molecular topology. First, the charged ammonium cations show a wider distribution away from the soft DNA cylindrical surface compared to that of linear polyamine in Fig. 6.6b. The longer

tail of positive charge distribution in space facilitates bridging between two DNA segments, a pathway to compact a long chain DNA. Such a bridging process can be viewed as a short-range attraction requiring two DNA segments in close contact with a branched polyamine. Secondly, since the branched polyamine has a smaller contact area with DNA, which causes a greater survival charge on a DNA segment and a more negative electrostatic potential at a longer distance, for example, at the boundary of the polyamine/DNA complex set in our simulation cell, as shown in Fig. 6.6d.

In contrast, a linear polyamine (3334) has a lower charge density due to the dispersion of ammonium groups along its elongated chain, but the linear chain induces a larger contact area to interact with DNA. Though one expects that both branched and linear polyamines play the same role to neutralize the total DNA charge and bridging neighboring DNA segments, locally, the linear polyamine has more direct contact with those phosphate groups in DNA. As a result, the linear polyamine distributes more closely to DNA as shown in Fig. 6.6b,c. Meanwhile, the lower but more dispersed linear charge density of polyamine allows the linear polyamine to induce multiple ways to interact with DNA, which links with the lower surface potential in Fig. 6.6d, an indication that the DNA charge is neutralized more by the linear polyamine (with a lower DNA survival charge) than the branched counterpart.

It is to be noted that the conclusion drawn from this work is quite general, and the distinct behavior between linear and branched polyamine can be primarily attributed to their different molecular topologies. Our additional tests (data not shown) further suggest that the qualitative finding in this work is insensitive to the chosen parameters of the simulation model, such as diameter of cylindrical DNA, chain stiffness of polyamine, width of simulation cell, size of charged groups etc. The quantitative roles of these secondary effects will be further studied in our future work.

6.3 Conclusions

The present study clearly shows a difference in physicochemical properties between compact DNAs induced by linear- and branched-chain polyamines. Single-DNA observations in solution by fluorescence microscopy revealed that the branched-chain polyamine 3(3)(3)4 is slightly more likely to cause shrinkage of the higher-order structure of DNA than the linear-chain polyamine 3334. Experiments on the assemblies of compact DNA molecules collected by laser trapping revealed that 3334 induces attractive interactions between compact DNA molecules. Under the same polyamine concentration, an assembly of compact DNA molecules in the presence of 3(3)(3)4 tends to dissociate, suggesting repulsive interactions between DNAs. This difference in the effects of linear- and branched-chain polyamines on DNA is due to the difference in their

steric interactions with negatively charged phosphate moieties of double-strand DNA.

By using Monte Carlo simulation, we investigate a simple model at the coarse-grained level to address the electrostatic interaction between phosphate groups in DNA and a polyamine. Our finding indicates that in contrast to linear polyamines, branched polyamines can be an effective reagent to bridge adjacent DNA segments through their branches, which leads to enhancement of DNA compaction. However, the smaller contact area in a branched polyamine causes a higher survival charge in DNA, a mechanism to induce stronger repulsion among compact DNA molecules. The theoretical simulation, thus, provides useful insights into the experimental observation in this work regarding the distinct behavior between linear and branched polyamine in general. Our future work will focus on the quantitative aspect of the simulation parameters. Also, the future dynamical studies of polyamines within the aggregate to mimic the condition with and without optical tweezer can be useful to reveal the role of polyamine on the stability of aggregates of compact DNA molecules.

6.4 Materials and Methods

6.4.1 Materials

T4 GT7 phage DNA (166 kbp, contour length 57 μm) was purchased from Nippon Gene (Toyama, Japan). The fluorescent cyanine dye YOYO-1 (1,1'-(4,4,8,8-tetramethyl-4,8-diazaundecamethylene)bis[4-[(3-methylbenzo-1,3-oxazol-2-yl)methylidene]-l,4-dihydroquinolinium] tetraiodide) was purchased from Molecular Probes Inc. (Eugene, OR). The antioxidant 2-mercaptoethanol (2-ME) was purchased from Wako Pure Chemical Industries (Osaka, Japan). Homocaldopentamine 3334 and N^4-bis(aminopropyl)spermidine 3(3)(3)4 were synthesized as described previously [24]. Other chemicals were analytical grade and obtained from commercial sources.

6.4.2 Fluorescence microscopy (FM) observation and optical trapping of DNA molecules

T4 phage DNA was dissolved in a 10 mM Tris-HCl buffer and 4% (v/v) 2-ME at pH 7.5 in the presence of various concentrations of polyamines (0-7 μM). Measurements were conducted at a low DNA concentration (0.1 μM in nucleotide units). To visualize individual DNA molecules by FM, 0.05 μM of YOYO-1 (Excitation/Emission 491/509 nm) was added to the DNA solution. Experimental observations and optical trapping were performed using a fluorescent microscope (OLYMPUS) with a large-aperture oil-immersion objective lens (Plan Fluor ×100, NA =1.40, OLYMPUS). A Nd:YAG laser (TEM_{00}, CW 1064 nm, JPK Instruments) for optical trapping was introduced into the objective lens by a dichroic mirror and focused to a point of about 1 μm on the observation field oriented to give a convergent angle of about 90-120°. We used an output

laser power of between 700 and 1,000 mW. Microscopic fluorescent images were detected by a high-sensitivity SIT video camera and recorded through an image processor (HAMAMATSU Photonics). The observations were carried out at a room temperature of about 24°C.

6.4.3 Model and Monte Carlo simulation

To better understand the charge effect arising from complexation of DNA and polyamine, we resort to a simple coarse-grained model motivated by a charged DNA segment, corresponding to one pitch of a long chain DNA with length around 3.4 nm, interacting with a charged polyamine of different topologies: linear and branched one (see e.g.: Fig. 6.6a). In the DNA segment, 20 charged spheres (+1 unit charge for each sphere) to mimic phosphate groups are placed around a soft cylinder of length 3.4 nm. The soft cylinder is chosen due to the fact that some empty space is present in the major and minor grooves of a DNA, which allows polyamines to partially penetrate into the interior of a cylindrical DNA segment. In our DNA model, 20 charged sites on the DNA segment are grouped into 10 pairs. The two charged spheres in each pair is separated by 180° around the cylinder and their separation is set 2 nm, close to the width of a DNA molecule. These 10 pairs of charged groups are arranged from the bottom to the top of cylinder by rotating 36° for each pair, and any two adjacent pairs are separated by 0.34 nm. The top and bottom pairs are 0.17 nm away from the end of the cylinder. This greatly simplified model exhibits some basic structural features similar to the charged groups in DNA, and renders an opportunity to elucidate how polyamines shield the charge of a DNA.

In Monte Carlo simulation, the hard simulation cell takes the cylindrical shape with 3.40 nm long and 2.59 nm in radius. The length of the simulation cell is thus chosen so that under the periodic boundary condition, the DNA will replicate itself from the central simulation cell to form an infinite long DNA similar to the conventional cell model in DNA simulation as the zero-th order approximation [34]. Here, we consider the most basic stoichiometric ratio with one polyamine and one DNA segment. The charged groups in DNA are modeled as charged spheres of radius 0.238 nm (around the size of a phosphate ion), and are fixed on the cylindrical DNA. Based on the recent atomistic simulation of the mixture of spermine and DNA [35], we notice that charged polyamines are actually quite rigid with little conformational change even in the presence of highly charged DNA. Namely the conformational fluctuation of polyamines is basically a secondary effect. The polyamine chain can be quite elongated because of the electrostatic repulsion from the charged ammonium groups within the polyamine chain along with high bending energy and the energy barrier of torsional motion. To this end, in our simulation, we consider linear and branched polyamines as rigid molecules. Their conformations are first obtained from energy minimization under UFF (Universal force field) in Avogadro software [33]. After the conformation of minimal energy is obtained, the methylene and ammonium groups are

replaced by beads of 0.195 nm in radius [36], and each type of polyamine has 18 beads as shown in Fig. 6.6a where they are interacting with DNA. The beads representing methylene groups are neutral but the 5 beads modeling charged ammonium groups carry +1 unit charge each. Note that the bond length of minimum-energy polyamines is about 0.15 nm (as the length of the scale bar) and the bond angle is near 109.4°.

The one-dimensional periodic boundary condition and minimum image convention are applied along the DNA axis [34]. The bead of a polyamine is allowed to move between 0.762 nm (partially penetrating the DNA segment) and 2.396 nm (due to the cylindrical hard wall of the simulation cell interacting with the hard sphere of polyamine bead) along the radial direction within the cylindrical simulation cell. To account for water, smaller counterions and coions from electrolytes, the screened coulomb potential is adapted to depict the effective interaction potential between a bead in polyamine and a charged group in DNA given by

$$\begin{aligned} V(r)/k_{\mathrm{B}}T &= \infty && \text{if } r_{ij} < r_{\mathrm{c}} \\ &= \Gamma Q_i Q_j \exp(-\kappa r)/r && \text{if } r_{ij} \geq r_{\mathrm{c}} \end{aligned} \tag{6.1}$$

where i is the i-th bead in the polyamine with charge Q_i; j is the j-th charged sphere in DNA with charge Q_j; r_c is the shortest distance between a bead in polyamine and a charged sphere in DNA without hard core repulsion; Γ is the interaction strength; κ is the inverse Debye screening length. In the calculation, r_c is approximated to be 0.31 nm, a typically closest distance between charged ammonium and phosphate group in DNA [37]. We vary interaction strength Γ ranging from Γ = 0.68 to 1.7 nm, roughly about 1 to 2.5 times of Bjerrum length at 25°C, and κ is set 0.024 nm^{-1} by assuming weak electrostatic screening near DNA. Since the model is developed to investigate the proximity where a polyamine is very close to a DNA segment, the dielectric constant, water and small ion distribution may not follow the traditional picture of a bulk solution. In the study of varying the magnitude of electrostatic interaction by adapting a simple physico-chemical parameter, such as Γ in this work, it may enable a better understanding about the charge effect on the polyamine/DNA interaction. Note that the one-dimensional Ewald summation is applied to compute the above screened Coulomb potential energy [38].

In our Monte Carlo simulation, the rigid polyamine is randomly moved by translation and rotation motions, and the step sizes for the above motions are adjusted so that the acceptance ratio is around 50% for each type of motion under the Metropolis algorithm [39]. We conduct 2-5 × 10^8 moves in the simulation, and discard the first 10^8 moves to assure the simulation converges. Two properties are calculated including the density distribution function and the surface potential at the boundary of the simulation cell.

The distribution function of charged beads (i.e., ammonium groups) in polyamine and the average surface electrostatic potential of any point at the boundary of the simulation cell. The reduced dentistry distribution function $\rho(r)$ is computed by dividing the cylindrical simulation into 100 layers along the radial direction, and then the average number of charged beads in the i-th layer $H_i(r)$ is counted. The $\rho(r)$ is computed by

$$\rho(r) = V_{\mathrm{cyl}} H_i(r)/V_i(r) \tag{6.2}$$

where $H_i(r)$ is the histogram to compute the average number of charged ammonium in the i-th layer of radial distance r; $V_i(r)$ is the volume of the i-th layer, and V_{cyl}, the volume of the cylindrical simulation cell, is introduced to make density distribution function dimensionless. To calculate the reduced surface electrostatic potential Φ_{surf}, we compute the electrostatic potential of a test charged point with +1 unit charge at the boundary of the simulation cell, and its location on the boundary is randomly chosen. The total potential of the test point particle at that point is determined based on the screened Coulomb potential in Eq. (6.1). Note that both charged groups in polyamine and DNA contribute to the surface potential. For each configuration, we randomly choose 5 locations for the test point particle, and average over all the configurations sampled in the simulation.

References

[1] C. W. Tabor & H. Tabor. Polyamines. *Annual Review of Biochemistry* **53**, 749-790, (1984).

[2] *Polyamines* (eds R. Alcázar & A. F. Tiburcio), in *Methods in Molecular Biology* **1694**, (Humana Press, 2018).

[3] T. Thomas & T. J. Thomas. Polyamines in cell growth and cell death: molecular mechanisms and therapeutic applications. *Cell. Mol. Life Sci.* **58**, 244-258, (2001).

[4] A. C. Childs, D. J. Mehta & E. W. Gerner. Polyamine-dependent gene expression. *Cell. Mol. Life Sci.* **60**, 1394-1406, (2003).

[5] K. Igarashi & K. Kashiwagi. Modulation of cellular function by polyamines. *International Journal of Biochemistry & Cell Biology* **42**, 39-51, (2010).

[6] A. K. Handa, T. Fatima & A. K. Mattoo. Polyamines: Bio-Molecules with Diverse Functions in Plant and Human Health and Disease. *Front Chem* **6**, 10/1-18, (2018).

[7] K. Okada *et al.* Identification of a novel aminopropyltransferase involved in the synthesis of branched-chain polyamines in hyperthermophiles. *J. Bacteriol.* **196**, 1866-1876, (2014).

[8] R. Hidese *et al.* Identification of a novel acetylated form of branched-chain polyamine

from a hyperthermophilic archaeon Thermococcus kodakarensis. *Biosci., Biotechnol., Biochem.* **81**, 1845-1849, (2017).

[9] H. Atomi, T. Fukui, T. Kanai, M. Morikawa & T. Imanaka. Description of Thermococcus kodakaraensis sp. nov., a well studied hyperthermophilic archaeon previously reported as Pyrococcus sp. KOD1. *Archaea* **1**, 263-267, (2004).

[10] L. C. Gosule & J. A. Schellman. Compact form of DNA induced by spermidine. *Nature* **259**, 333-335, (1976).

[11] D. K. Chattoraj, L. C. Gosule & A. Schellman. DNA condensation with polyamines. II. Electron microscopic studies. *J. Mol. Biol.* **121**, 327-337, (1978).

[12] I. Baeza *et al.* Electron microscopy and biochemical properties of polyamine-compacted DNA. *Biochemistry* **26**, 6387-6392, (1987).

[13] V. A. Bloomfield. Condensation of DNA by multivalent cations: considerations on mechanism. *Biopolymers* **31**, 1471-1481, (1991).

[14] J. Pelta, F. Livolant & J. L. Sikorav. DNA aggregation induced by polyamines and cobalthexamine. *J. Biol. Chem.* **271**, 5656-5662, (1996).

[15] M. Saminathan, T. Thomas, A. Shirahata, C. K. Pillai & T. J. Thomas. Polyamine structural effects on the induction and stabilization of liquid crystalline DNA: potential applications to DNA packaging, gene therapy and polyamine therapeutics. *Nucleic Acids Res.* **30**, 3722-3731, (2002).

[16] S. M. Mel'nikov, V. G. Sergeyev & K. Yoshikawa. Discrete coil-globule transition of large DNA induced by cationic surfactant. *J. Am. Chem. Soc.* **117**, 2401-2408, (1995).

[17] K. Yoshikawa & Y. Matsuzawa. Discrete phase transition of giant DNA dynamics of globule formation from a single molecular chain. *Physica D: Nonlinear Phenomena* **84**, 220-227, (1995).

[18] M. Takahashi, K. Yoshikawa, V. Vasilevskaya & A. Khokhlov. Discrete coil－ globule transition of single duplex DNAs induced by polyamines. *J. Phys. Chem. B* **101**, 9396-9401, (1997).

[19] K. Yoshikawa, H. Noguchi & Y. Yoshikawa. Folding transition in single long duplex DNA chain. *Formation and Dynamics of Self-Organized Structures in Surfactants and Polymer Solutions* (eds K. Kawasaki, B. Lindman & H. Okabayashi), in *Progress in Colloid & Polymer Science* **106**, 204-208 (Springer, 1997).

[20] Y. Yoshikawa, K. Yoshikawa & T. Kanbe. Formation of a giant toroid from long duplex DNA. *Langmuir* **15**, 4085-4088, (1999).

[21] S. V. Mikhailenko *et al.* Interplay between folding/unfolding and helix/coil transitions in giant DNA. *Biomacromolecules* **1**, 597-603, (2000).

[22] A. A. Zinchenko, O. A. Pyshkina, A. V. Lezov, V. G. Sergeyev & K. Yoshikawa. Single

DNA Molecules: Compaction and Decompaction. *DNA Interactions with Polymers and Surfactants* (eds R. Disa & B. Lindman) Chapter 3, 59-88 (John Wiley & Sons, 2008).

[23] A. Venancio-Marques, A. Bergen, C. Rossi-Gendron, S. Rudiuk & D. Baigl. Photosensitive polyamines for high-performance photocontrol of DNA higher-order structure. *ACS Nano* **8**, 3654-3663, (2014).

[24] A. Muramatsu *et al.* Naturally occurring branched-chain polyamines induce a crosslinked meshwork structure in a giant DNA. *J. Chem. Phys.* **145**, 235103, (2016).

[25] T. Nishio *et al.* Branched-Chain Polyamine Found in Hyperthermophiles Induces Unique Temperature-Dependent Structural Changes in Genome-Size DNA. *ChemPhysChem* **19**, 2299-2304, (2018).

[26] Y. Matsuzawa *et al.* Laser trapping of an individual DNA molecule folded using various condensing agents. *J. Am. Chem. Soc.* **121**, 11581-11582, (1999).

[27] Y. Yoshikawa, M. N. Shin-ichirou, T. Kanbe & K. Yoshikawa. Controlling the folding/unfolding transition of the DNA-histone H1 complex by direct optical manipulation. *Chem. Phys. Lett.* **330**, 77-82, (2000).

[28] Y. Matsuzawa, K. Hirano, A. Mizuno, M. Ichikawa & K. Yoshikawa. Geometric manipulation of DNA molecules with a laser. *Appl. Phys. Lett.* **81**, 3494-3496, (2002).

[29] M. Ichikawa, Y. Matsuzawa, Y. Koyama & K. Yoshikawa. Molecular fabrication: aligning DNA molecules as building blocks. *Langmuir* **19**, 5444-5447, (2003).

[30] K. Yoshikawa & Y. Yoshikawa. Compaction and condensation of DNA. *Pharmaceutical perspectives of nucleic acid-based therapeutics* (eds R. I. Mahato & S. W. Kim) Chapter 8, 137-163 (CRC Press, 2002).

[31] J. N. Israelachvili. *Intermolecular and surface forces*, (Academic press, 2011).

[32] Y. Yamasaki, Y. Teramoto & K. Yoshikawa. Disappearance of the Negative Charge in Giant DNA witha Folding Transition. *Biophys. J.* **80**, 2823-2832, (2001).

[33] M. D. Hanwell *et al.* Avogadro: an advanced semantic chemical editor, visualization, and analysis platform. *J. Cheminformatics* **4**, 17/1-17, (2012).

[34] C. F. Anderson & M. T. Record. Ion distributions around DNA and other cylindrical polyions: theoretical descriptions and physical implications. *Annu. Rev. Biophys. Biophys. Chem.* **19**, 423-463, (1990).

[35] J. Yoo & A. Aksimentiev. The structure and intermolecular forces of DNA condensates. *Nucleic Acids Res.* **44**, 2036-2046, (2016).

[36] K. Schweizer & J. Curro. PRISM theory of the structure, thermodynamics, and phase transitions of polymer liquids and alloys. *Atomistic Modeling of Physical Properties* (eds L. Moonnerie & U. W. Suter), in *Advanced in Polymer Science* **116**, 319-377 (Springer, 1994).

[37] J. Yoo & A. Aksimentiev. Improved Parameterization of Amine-Carboxylate and Amine-Phosphate Interactions for Molecular Dynamics Simulations Using the CHARMM and AMBER Force Fields. *Journal of Chemical Theory and Computation* **12**, 430-443, (2016).

[38] H. Takemoto, T. Ohyama & A. Tohsaki. Direct sum of Coulomb potential without ambiguities of conditionally convergent series. *Progress of theoretical physics* **109**, 563-573, (2003).

[39] M. P. Allen & D. J. Tildesley. *Computer simulation of liquids*, (Oxford university press, 2017).

Chapter 7

General Conclusion

To summarize the findings presented in Chapters 2–6, I will describe the conclusion with reference to my publications [i–v].

Chapter 2 showed that the polyamines SPD and NSPD each had biphasic effects, enhancement and inhibition, on gene expression. The results showed that SPD is significantly more potent at promoting gene expression than NSPD, while NSPD suppresses gene expression at a lower concentration than SPD. Through single-DNA molecule observation, it became clear that SPD tends to induce a larger flower-like structure than NSPD, while NSPD induces shrinkage/compaction with a higher potency than SPD. This flower-like structure, in which DNA is loosely packed and has parallel ordering of DNA segments, enhances gene expression due to a decrease in the negative charge of double-stranded DNA. On the other hand, gene expression is completely inhibited in tightly packed DNA. Therefore, it is considered that these biphasic effects on gene expression are related to the changes in the higher-order structure of DNA induced by polyamines. Both experimental and theoretical results clearly showed that the difference of only one methylene group between SPD and NSPD causes marked differences in the binding affinity for the DNA structure, which leads to significant differences in the gene expression profile *in vitro* [i].

Chapter 3 extended the work in Chapter 2 and investigated the interaction of polyamines with DNA in the presence of K^+ or Na^+. As a result, K^+ enhanced gene expression in the presence of SPD much more strongly than Na^+, through cell-free gene expression. Single-DNA observation by fluorescence microscopy showed that Na^+ prevents the folding transition of DNA into a compact state more strongly than K^+. ^{1}H NMR measurement revealed that Na^+ inhibits the binding of SPD to DNA more strongly than K^+. Thus, SPD binds to DNA more favorably in K^+-rich medium than in Na^+-rich medium, which leads to favorable conditions for RNA polymerase to access DNA by decreasing the negative charge. Further studies on the biological effects of the competition between monovalent cations and polyamine will shed light on the longstanding unsolved problem concerning the selectivity between Na^+ and K^+ in living systems [ii].

Chapter 4 showed that longer DNA molecules exhibit significantly greater potency in gene expression; for example, the expression level for DNA of 25.7 kbp is 1000-times higher than that for DNA of 1.7 kbp. AFM observation of the DNA conformation indicates that longer DNA takes

a shrunken conformation with a higher segment density in the reaction mixture for gene expression, in contrast to the stiff conformation of shorter DNA. I proposed an underlying mechanism for the favorable effect of longer DNA on gene expression in terms of an increase in the access of RNA polymerase to the shrunken conformation. In relation to this, I found that the shrunken conformation, or flower-like structure, of DNA caused by polyamine enhances gene expression. Therefore, it is expected that the enhancement of the efficiency of gene expression with a shrunken DNA conformation would also be a rather general mechanism in living cells [iii].

Chapter 5 presented the results of AFM, which showed that DNA molecules which were folded by a polyamine tended to unwind with an increase in temperature. Interestingly, the results demonstrated that DNA molecules generate multiple nano-loops with a diameter of 10–50 nm along the DNA strand at 80°C only in the presence of the branched-chain polyamine 3(3)(3)4. 3(3)(3)4 induces DNA to a mesh-like structure with several crossings or bridges of DNA segments at room temperature (24°C). This means that DNA segments are aligned parallel to each other in the flower-like structure in the presence of a linear-chain polyamine, but are randomly oriented in the presence of a branched-chain polyamine. It is considered that a mesh-like structure that exhibits highly entangled DNA segments is an important factor for inducing the unique nano-loop structure of DNA at 80°C.

In Chapter 6, a Monte Carlo simulation was carried out to compare the effects of branched- and linear-chain polyamines on the electrostatic interaction between phosphate groups in DNA and the polyamine. The results showed that branched-chain polyamines can be an effective reagent for bridging adjacent DNA segments in contrast to linear-chain polyamines. In addition, branched-chain polyamines induce changes in the secondary structure, from B-form to an A-like form that is more marked at higher temperatures (Chapter 5). These effects are specific to branched-chain polyamines and are clearly different from those of linear-chain polyamines. These findings should provide additional insights not only into thermo-adaptation, but also into understanding the mechanism of how hyperthermophiles maintain genetic activity in high-temperature environments [iv, v].

The above results demonstrate the close relationship between the higher-order structure of DNA and gene function such as gene expression. These newly suggested gene-regulation mechanisms are independent of the nucleotide sequence and depend on the non-specific interaction between DNA and cationic biomolecules such as polyamines. Therefore, our proposal that the higher-order structure of DNA regulates gene function may be an essential mechanism of gene regulation in all living organisms. Further extension of this study may help to clarify the underlying mechanisms of canceration, cell differentiation and so on, in the near future.

References from the author's publications

[i] **T. Nishio**, Y. Yoshikawa, W. Fukuda, N. Umezawa, T. Higuchi, S. Fujiwara, T. Imanaka, K. Yoshikawa, "Branched-Chain Polyamine Found in Hyperthermophiles Induces Unique Temperature-Dependent Structural Changes in Genome-Size DNA", *ChemPhysChem*, **19**, 2299-2304 (2018).

[ii] Y. Kashiwagi, **T. Nishio**, M. Ichikawa, C-Y. Shew, N. Umezawa, T. Higuchi, K. Sadakane, Y. Yoshikawa, K. Yoshikawa, "Repulsive/attractive interaction among compact DNA molecules as judged through laser trapping: difference between linear- and branched-chain polyamines", *Colloid and Polymer Sci.*, **297**, 397-407 (2018).

[iii] **T. Nishio**, Y. Yoshikawa, C-Y. Shew, N. Umezawa, T. Higuchi, K. Yoshikawa, "Specific effects of antitumor active norspermidine on the structure and function of DNA", *Sci. Rep.*, **9**, 14971/1–12 (2019).

[iv] **T. Nishio**, K. Sugino, Y. Yoshikawa, M. Matsumoto, Y. Oe, K. Sadakane, K. Yoshikawa, "K^+ promotes the favorable effect of polyamine on gene expression better than Na^+", *PLOS ONE.*, **15**, e0238447/1–13 (2020).

[v] **T. Nishio**, Y. Yoshikawa, K. Yoshikawa, S. Sato, "Longer DNA exhibits greater potential for cell-free gene expression", *Sci. Rep.*, **11**, 11739/1–7 (2021).